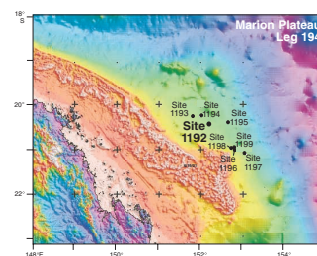# 3. SITE 1192[1]

Shipboard Scientific Party[2]

INTRODUCTION

Site 1192 (proposed Site CS-13A; Fig. F1) is located in 375 m of water on regional seismic line MAR20 (shotpoint 4126; see Fig. F7, p. 67, in the "Leg 194 Summary" chapter). The site is located in marginal slope sediments ~40 km east from the margin of the Northern Marion Platform (NMP) drilled during Leg 194. The total sediment thickness at this site was estimated to be ~520 m. Holes 1192A and 1192B penetrated 242.5 and 355.5 m of hemipelagic sediments, respectively.

The main objective at Site 1192 was a feasibility test of the Hydrate Autoclave Coring Equipment (HYACE), including the HYACE Rotary Pressure Core Sampler (H-PCS) developed at the Technische Universität Berlin, and the HYACE/Fugro Vibracore Sampler (HF-VS) developed by Fugro Geotechnical Engineering. The Ocean Drilling Program (ODP) has been working with the Technische Universität Berlin to develop an improved gas hydrate sampling and monitoring tool capable of retrieving samples at in situ formation pressure. The H-PCS development was based on the pressure core sampler developed by ODP. Both the H-PCS and the HF-VS are compatible with the advanced piston corer (APC)/extended core barrel (XCB) bottom-hole assembly (BHA) and are being considered for upcoming gas hydrate legs (e.g., Leg 201).

In July 2000, the HYACE team was awarded 72 hr of testing time at the beginning of Leg 194. The developer parties did not specify a particular test site, so ODP chose proposed Site CS-13A, a contingency site of the Leg 194 scientific program. The H-PCS team members were Hans-Jürgen Hohnberg, Michael Koppe, and Karl Eduard Winter. The HF-VS team members were Peter Looijen and Roeland Baas. The ODP observers were Leon Holloway and Eddie Wright. Greg Meyers represented Lamont-Doherty Earth Observatory (LDEO). At the conclusion of the HYACE test, all of those mentioned above departed the vessel and returned to Mackay.

F1. Bathymetry map, p. 27.

In addition to the engineering test, Site 1192 provided essential information on the facies and age range of Marion Plateau Megasequences B–D, the age and facies of marginal slope sediments shed from the northern carbonate platform, the lithologic signature of basinward unconformities adjacent to the northern platform, and a calibration of regional seismic sequence stratigraphy. Basement was not reached at this site.

OPERATIONS

Leg 194 began with an early port call in Townsville, Australia, at 2200 hr on 4 January 2001. At 0700 hr on 8 January, 3 days ahead of schedule, the vessel began the transit to Site 1192 (proposed Site CS-13A). The 399-nmi voyage was accomplished at an average speed of 12.0 kt. A beacon was dropped at 1720 hr on 9 January 2001. The precision depth recorder depth referenced to the dual elevator stool (DES) indicated a water depth of 390.4 m.

During the initial fit testing of the HYACE tools in the BHA, it was discovered that the outside diameter of the top 1 m of the H-PCS tool was several thousandths of an in too large to pass through the latch sleeve. It was assumed that this would not cause problems because pump pressure and flow rate between the landing sleeve and the H-PCS would generate sufficient resistance to offset the rotation and torque caused by the rotation of the small bit. Consequently, the latch sleeve was left out of the BHA.

Hole 1192A

Hole 1192A was spudded with the APC at 0205 hr on 10 January and established the seafloor depth at 385.0 m relative to the top of the DES on the rig floor (water depth of 374.4 m). The HF-VS was deployed three times, and the H-PCS was run twice in this hole. During the H-PCS tests, the LDEO drill string accelerometer was also deployed and provided downhole pressure and accelerations that will be used in a post deployment analysis of the instrument.

The first HF-VS run, designated as Core 4M, cored the interval from 28.5 to 29.5 meters below seafloor (mbsf) (Tables T1, T2). The internal shear pin parted as designed at 525 psi. As the pump pressure was decreased to 250 psi to start the hammer, no clear indication was obtained that the hammer was active, which could be attributed to the soft formation. The tool recovered only 0.19 m (19% of the cored interval). After retrieval, it was noted that the flapper was not completely closed, which prevented recovery of a sample at in situ formation pressure. The Fugro engineers concluded that the speed of bit retraction may have been too fast to allow establishment of a seal.

Piston coring resumed and advanced to 86.5 mbsf, where the HF-VS was deployed a second time (Core 11M; 86.5 to 87.5 mbsf). This time, the HF-VS tool was landed before the bit was placed on bottom. The shear pin parted at 525 psi. The pump pressure was decreased to 250 psi to activate the hammer, which appeared to operate for ~20 s. The bit was lifted off bottom very slowly for the first 3 m before the tool was carefully retrieved by wireline. The tool momentarily stuck in the pipe at 5 m above the landing seat, but came free after several strong pulls on the wireline with tension as high as 9000 lb. After retrieval, the tool was placed horizontally on the pipe racker platform, and it was con-

firmed that the flapper had closed. The autoclave section was disassembled, and a pressure gauge was connected to the autoclave. The gauge indicated an in situ pressure of 42 bar (609 psi) that roughly corresponded to the expected pressure at 473 m (total drill string length at 87.5 mbsf). The pressure was bled off, and the 0.91-m-long sample (97% recovery) was removed.

Piston coring again resumed to a depth of 192.0 mbsf. The third HF-VS (Core 23M) cored the interval from 192.0 to 193.0 mbsf. The tool was deployed as in the second run. After the shear pin did not appear to part at 600 psi or at the increased pressure of 800 psi, pressure was decreased to 250 psi to see if the hammer would start. Hammering was detected for a few seconds after which the tool was retracted with minimum speed. Once again, the tool became stuck in the drill string during the extraction process but was pulled free by the wireline. When the tool was recovered, it was observed that the latching pawls were jammed, which prevented full retraction of the liner into the inner barrel. In addition, the flapper did not close. The barrel was full, but only 0.77 m (77%) of the sample was recovered because of the difficulties with the polyvinyl chloride liner.

Once again, piston coring resumed and advanced to 231.0 mbsf, where coring was stopped for the initial test of the rotary pressure core sampling test with the H-PCS tool. This tool is designed to operate in more indurated sediments than the HF-VS tool. The first run of the H-PCS (Core 28M) attempted to core the interval from 231.0 to 232.0 mbsf. During this deployment, the expected pressure peaked at ~650 psi, indicating that activation of the positive displacement motor was not observed and that there was not any indication of the end of stroke. After the instrument was recovered, the inner barrel was still retracted in the autoclave and the flapper valve was not properly seated. It is possible that the lack of a latch sleeve in the BHA allowed the upper part of the tool to rotate instead of the lower section.

Piston coring resumed with Core 29H and advanced from 232.0 to 241.5 m. The core barrel had to be drilled over and extracted from the formation with 80 klb of overpull. This interval was considered to be the piston coring refusal depth.

The H-PCS was deployed for the second time (Core 30M) in an attempt to core the interval from 241.5 to 242.5 mbsf. No core was recovered in this attempt. Prior to deployment, the tool was marked with paint on the upper and lower sections in order to ascertain if there was slippage and if the tool was properly seated. After deployment, the marking was reviewed. Abrasions of the paint suggested that the upper section had rotated and that the bottom section had not seated properly. It was decided to recover the drill string and add the latch sleeve. The rig mechanic machined the top 1 m of the tool containing the upper latch body, upper sub, and latch dogs to the same diameter as the tool body.

Twenty-five APC cores were retrieved from Hole 1192A. The cored interval was 237.5 m with 241.59 m recovered (101.7% average recovery). The cores were oriented, starting with Core 3H. The drill string was recovered, and the bit was at the rotary table at 0855 hr.

Hole 1192B

After the latch sleeve was installed in the BHA and the H-PCS tool was modified, the drill string was deployed again with the vessel offset 10 m from the previous hole. Hole 1192B was spudded at 1145 hr on 11

January. Following a single mudline core that established the seafloor depth at 387.1 m (water depth of 376.5 m), the hole was drilled ahead to 179.9 mbsf (Table T1).

The fourth deployment of the HF-VS (Core 1M) cored the interval from 179.9 to 180.9 mbsf. The results of this test were similar to the Core 23M experiment. There was no positive indication of the parting of the shear pin at 600 psi. The pressure was increased to 800 psi with still no indication of release. The pressure was decreased to 250 psi to see if the hammer would start. Hammering was detected for a few seconds. The tool was retracted with minimum speed. When the tool was recovered, it was observed that the latching pawls were jammed, which prevented full retraction of the liner into the inner barrel. The flapper was not closed. The barrel recovered 0.84 m of sediment (84% recovery).

Immediately following this last HF-VS deployment, the H-PCS tool was run for the third time (Core 2M), attempting to core the interval from 180.9 to 180.9 mbsf. This time, the tool inner barrel did stroke out and rotate, but no sediment sample was obtained.

Coring resumed with hopes of finding more indurated sediment before time on site expired. APC coring advanced to 229.4 mbsf, and XCB boring deepened the hole to 335.2 mbsf. Coring operations were delayed during the retrieval of Cores 18X and 19X (316.0 to 335.2 mbsf) when the core barrels had to be "fished" with the wireline.

The fourth run of the H-PCS, Core 3M, attempted to core the interval from 335.2 to 336.2 mbsf. The tool inner barrel stroked out, rotated, and recovered ~0.27 m of sediment. The formation was too soft for the type of core catcher available, and it was believed that some sediment was lost in the recovery process. The retraction mechanism was not released, so the core was not under pressure.

This run concluded the downhole experiments that preceded the Leg 194 science program as nearly all of the 72 hr allocated for the tests had expired. While the tool was cleaned and dressed, an additional two XCB cores were obtained. In total, six APC cores were retrieved with 43.6 m recovery (87.3%), and 13 XCB cores were retrieved with 60.43 m recovery (48.3%), for a total depth of 355.5 mbsf. Total recovery in Hole 1192B, including test cores, was 105.1 m, representing 59.1% of the cored interval. In addition, a 177.5-m interval was drilled without coring.

Operations at Site 1192 ended at 1440 hr on 12 January, and the vessel proceeded to the first high-priority site of the Leg 194 science program.

LITHOSTRATIGRAPHY AND SEDIMENTOLOGY

The lithostratigraphy of Site 1192 comprises five main units (Table T3; Fig. F2) defined by variations in carbonate content, texture, and the presence or absence of quartz, glauconite, and phosphate grains. Unit definition depended upon changes in sediment characteristics as described below. The entire succession ranges from unlithified at the top to lithified at the base, indicating continued induration and late cementation after burial. These sediments are generally heavily bioturbated and reveal distinctive ichnofossils such as *Chondrites, Planolites, Skolithos, Palaeophycus,* and *Teichichnus* (Fig. F3). Color variations are generally subtle with most of the succession being light to dark green-gray or olive-green in color. The greenish color indicates the presence of

T3. Table defining major lithologic units, p. 67.

F2. Lithologic summary, p. 28.
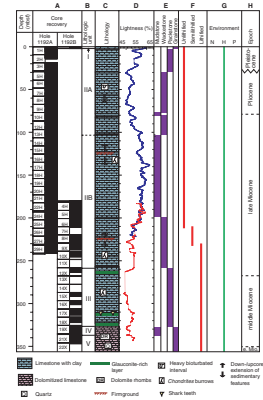
F3. Close-up photograph of *Teichichnus* ichnofossil, *Chondrites* ichnofossil, and firmground, p. 29.
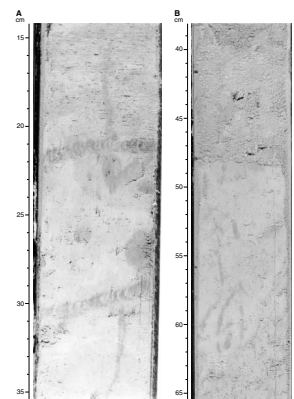
terrigenous clay, which is reflected in decreased lightness and increased calcium carbonate content (Fig. F4). Because of the presence of clay, sediments and rocks have been classified as foraminifer grainstone, packstone, or wackestone with clay (see "Lithostratigraphy and Sedimentology," p. 5, in the "Explanatory Notes" chapter for principal lithology definitions). Planktonic foraminifers dominate the sand-sized fraction of sediments in Units I–III, whereas benthic foraminifers were more dominant in Units IV–V. Collectively, the succession of these units indicates a range of physical energy conditions representing a deepening-upward trend.

Lithologic Units

Unit I (0–2.4 mbsf; Holocene to Pleistocene)

Unit I is a 2.4-m-thick light yellow, tan to brown, poorly sorted, planktonic foraminifer grainstone containing gravel-sized cemented intraclasts (Fig. F2). These intraclasts are dominantly cemented planktonic foraminifers. Other allochems include echinoderm fragments and spines, as well as gastropod and bivalve shells. Bedding is indicated by gradual color changes. Little to no terrigenous material is present. Bioturbation is rare. Thin section analysis indicates mixing of grains with different types of intraparticle infilling (Fig. F5). The lower boundary between Units I and II is sharp.

Unit II (2.4–258.1 mbsf; Pleistocene to Late Miocene)

Unit II is characterized by a heavily bioturbated, planktonic foraminifer mudstone to packstone with clay (Fig. F2). The sediments are mostly light greenish gray with variations in color resulting from variations in clay content. This unit also has centimeter-sized, black framboidal pyritic stains scattered throughout. Commonly, these stains are associated with burrows. Core catcher descriptions from the >63-µm fraction of Unit II indicate that benthic foraminifers, bryozoans, pteropods, ostracodes, arthropod spines, and mollusk fragments are rare relative to the planktonic foraminifers.

Unit II is divided into two subunits based upon color reflectance data (Fig. F4) and textural changes occurring at 103 mbsf. Significantly, geochemical and core physical properties data record changes at this depth as well (see "Geochemistry," p. 14, and "Core Physical Properties," p. 18).

Subunit IIA (2.4–103.1 mbsf; Pleistocene to Late Miocene)

Subunit IIA is essentially a skeletal packstone to wackestone with clay and is light olive-gray to light gray (Fig. F6). Planktonic foraminifers are the dominant skeletal component. The upper portion of Subunit IIA is a packstone, which grades downward to a wackestone at the base of this subunit. Several meter-scale to submeter-scale mudstone units appear near the base of Subunit IIA. Significant bioturbation with distinct ichnofossils (e.g., *Scolicia, Thalassinoides,* and *Taenidium*) begins at ~39 mbsf extending downcore. Color reflectance values indicate greater clay content as compared to Subunit IIB. These data also clearly indicate significant lithologic variations at a scale of meters to tens of meters.

F4. Color reflectance and calcium carbonate content data, p. 30.
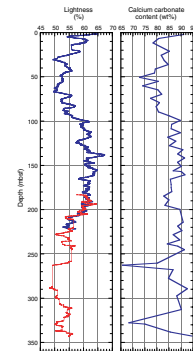
F5. Unit I microfacies, p. 31.
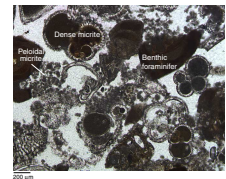
F6. Subunit IIA microfacies, p. 32.
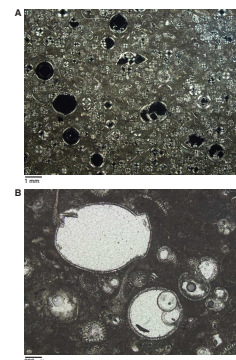
Subunit IIB (103.1–258.2 mbsf; Late Miocene)

Subunit IIB consists of mudstone that begins to coarsen downcore at 203 mbsf with small units of mudstone, wackestone, and packstone extending to the base of the subunit. Light greenish gray is the most persistent color. Below 135 mbsf, *Chondrites* are distinctly recognizable. Portions of Subunit IIB are characterized by meter-scale lithologic variations showing variations in texture and degree of bioturbation (Fig. F3). A typical lithologic variation begins with a sharp base (sometimes topographically irregular) interpreted to be a firmground or distal turbidites. Above this contact is a moderately sorted, unburrowed, foraminifer packstone several tens of centimeters thick. This grades upward into a burrowed wackestone and mudstone forming a complete fining-upward sequence, which is capped by another firmground. The mudstone beneath the firmground contains distinct, large (1–2 cm diameter) burrows, which have been infilled by the overlying packstone. These burrows crosscut earlier, smaller diameter (3–5 mm) mud-filled burrows of *Chondrites*. The cyclic lithologic variations described above can be found from 116 to 135 and from 203 to 246 mbsf in Subunit IIB, but not between 184 and 203 mbsf, which is a section of monolithic, heavily bioturbated mudstone with clay.

Unit III (258.2–325.6 mbsf; Middle to Late Miocene)

The top of Unit III (Fig. F2) is defined by the appearance of more abundant quartz, glauconite, and phosphate grains set within the foraminifer packstone with clay that dominates the unit (Fig. F7). These distinctive greenish black and black grains become more common downsection. Additionally, *Amphistegina* sp. and *Lepidocyclina howchini,* both shallow-water benthic foraminifers, appear near the top of this unit (Fig. F7). Drilling disturbance resulting from XCB coring and expressed as biscuiting is common and is partially the result of increased lithification. Unit III is bioturbated with *Skolithos*(?) ichnofossils.

At ~307–313 mbsf, another dark, greenish gray banded glauconite-rich packstone to grainstone unit, which contains shark teeth, occurs. This interval also contains dolomitic rhombs and coccoliths as seen in smear slides.

The base of Unit III contains a thin (<1 m) bed of coarse, glauconitic and bioclastic grains. The contact between Units III and IV is sharp.

Unit IV (325.6–336.2 mbsf; Early Middle Miocene)

Unit IV (Fig. F2) consists of alternating units of planktonic foraminifer mudstone and packstone with clay (Fig. F8). The dark olive-green to dark greenish gray color of this unit is darker than the color of Unit III. Glauconite and quartz grains are present. Together, Units III and IV show an overall upward increase in grain size, with Unit III having less mud. Dolomitic rhombs appear at the base of this unit, as well as possibly quartz silt.

Unit V (336.2–347 mbsf; Early Middle Miocene to Early Miocene)

Unit V consists of a silt-sized dolomitic grainstone with clay that becomes coarser toward the bottom of the hole (Fig. F2). Smear slide and thin section analyses show that silt-sized dolomitic rhombs and angular

F7. Unit III microfacies, p. 33.
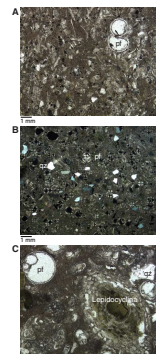
F8. Unit IV microfacies, p. 34.
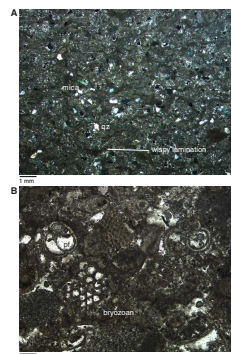
quartz are common. Based on its well-sorted character and its low matrix content, this sediment is classified as a grainstone because particles can be individually recognized in macroscopic examination and they are generally in grain contact. At the base of this unit, a coarse grainstone was recovered with planktonic foraminifers being the dominant particles. Even though only 9 m of Unit V was recovered, its distinctive lithology dictates its recognition as a separate lithologic unit.

Discussion

The periplatform sediments in the lower portion of this site (Units V–III) have been reworked and transported from a neritic environment as suggested by the presence of shallow-water benthic foraminifers. Seismic data show that this portion of the sedimentary section occurs within the distal slope facies of the NMP (see "Seismic Stratigraphy," p. 23). Thus, these sediments probably were transported down a very low gradient slope within density underflows (hyperpycnal flows) and turbidity currents. The well-sorted nature of these sediments, as well as the extensive bioturbation, precludes any recognition of primary sedimentary structures and thus more detailed interpretation of depositional processes.

The upper portion of Unit III may correlate with the drowning and/or exposure phase of the NMP. The shutdown of this carbonate factory resulted in sediment starvation on the upper slopes of the platform, thus favoring glauconite formation and the development of a phosphate hardground, which may be the source of the distinct, dark grains seen at the top of this unit. The quartz grains admixed with the platform carbonates probably originate from the northeast Australian margin.

Sediments in the upper portion of this site (Units II–I) reflect deposition in an open-platform, hemipelagic environment with variations in energy level at and near the seafloor. The firmground and fining-upward beds between 116–135 and 203–246 mbsf in Unit II indicate discrete sedimentation events that could be either turbidity currents or distinct periods of contourite deposition. The latter interpretation is supported by the fact that Unit II lies within the seismic facies that is interpreted to be a sediment drift complex (see "Seismic Stratigraphy," p. 23). However, the extensive bioturbation observed has removed most, if not all, of the primary sedimentary structures that might confirm either interpretation.

Magnetic susceptibility and grain density data show greater variations above ~100 mbsf than below (see "Core Physical Properties," p. 18). This is consistent with the abrupt onset of terrigenous clay deposition from the northeast Australian margin, which is transported out to the Marion Plateau through hyperpycnal flows. Physical properties data also show small-scale variations supporting this interpretation, as do the color reflectance data (Fig. F4).

Sedimentation rates based on the age model (see "Age Model," p. 13) indicate a maximum rate (~75 m/m.y.) occurring within the late Miocene Subunit IIB. This rate decreased to a minimum (~10 m/m.y.) near the Pliocene/late Miocene boundary or at ~80 mbsf, in the lower part of Subunit IIA. These data suggest that in addition to the increase in clay content expressed by geochemical and physical properties data, there must have been a corresponding decrease in carbonate productivity as well. However, the overall pattern in sedimentation within Unit II

probably reflects lateral shifts in the positions of the drift deposit centers.

Unit I includes the modern seafloor, which has undergone disturbances allowing cementation and reworking, as indicated by the intraclasts with brownish iron oxide stains on these sediments. Site survey data indicate that portions of the modern seafloor are characterized by current-swept hardgrounds representing various stages of lithification. The depth at which modern physical processes rework Unit I sediments is unknown.

BIOSTRATIGRAPHY AND PALEOENVIRONMENTS

Biostratigraphic control at Site 1192 was provided by shipboard analyses of calcareous nannoplankton and planktonic foraminifers from core catcher samples. Faunal assemblage changes in benthic foraminifers were also studied. The biostratigraphic results and zonal assignments of Holes 1192A and 1192B indicate a Pleistocene to middle lower Miocene sequence.

Calcareous Nannofossils

Calcareous nannofossils are generally abundant and moderately well preserved at Site 1192. No significant reworking of nannofossils was apparent, and all nannofossil events recognized occur in normal stratigraphic sequence in these sediments. Over a dozen nannofossil datums were determined based on examination of core catcher samples, providing modest biostratigraphic resolution for the Pleistocene through middle early Miocene.

Samples 194-1192A-1H-CC and 2H-CC contain abundant, well-preserved nannofossils, including common *Reticulofenestra asanoi* (Table **T4**). The presence of this species in the absence of *Calcidiscus macintyrei* indicates an age range of 0.88–1.7 Ma (Pleistocene) for these two samples.

Samples 194-1192A-3H-CC through 6H-CC contain late Pliocene index species. *Reticulofenestra pseudoumbilica* and *Sphenolithus* spp. were found in Samples 194-1192A-7H-CC through 9H-CC, and they allow the assignment of nannofossil Zones CN10–CN11 (early Pliocene) to this interval.

The Pliocene/Miocene boundary is drawn between Samples 194-1192A-9H-CC and 10H-CC based on the presence of *Discoaster quinqueramus* in the latter, whereas planktonic foraminifers place the boundary between Samples 1194-1192A-12H-CC and 13H-CC. Samples 194-1192A-10H-CC through 15H-CC also contain *Discoaster surculus;* thus, an age range of 5.6–7.5 Ma (Zone CN9) can be assigned to this interval. Samples 194-1192A-16H-CC and 17H-CC contain *D. quinqueramus* but no *D. surculus* and can be assigned to the lower part of Subzone CN9a with an age range of 7.5–8.5 Ma. Neither *D. quinqueramus* nor *Discoaster neohamatus* is present in Sample 194-1192A-19H-CC, and this absence suggests an age of CN8 (8.5–9.4 Ma). *D. neohamatus* was found in Samples 194-1192A-20H-CC and 21H-CC, indicating an age range of 9.4–11.9 Ma. Samples 194-1192A-24H-CC through 29H-CC contain *Cyclicargolithus floridanus* but no *Sphenolithus heteromorphus,* and thus can be assigned an age range between 11.9 and 13.6 Ma (Zone CN5, middle Miocene).

T4. Biostratigraphic datums, p. 68.

Samples 194-1192B-4H-CC and 5H-CC contain *D. neohamatus* but no *D. quinqueramus* or *Discoaster hamatus,* indicating these samples are within the lower part of Zone CN8. *D. hamatus* occurs in Samples 194-1192B-6H-CC through 8H-CC, and the range of this species defines Zone CN7 (9.5–10.5 Ma). Neither *D. hamatus* nor *C. floridanus* is present in Samples 194-1192B-9H-CC through 11H-CC, and this suggests an age range of 10.5–11.9 Ma for the interval. Samples 194-1192B-17X-CC through 2X-CC contain *S. heteromorphus,* resulting in an age range assignment of 13.8–18.2 Ma for this interval.

Planktonic Foraminifers

Hole 1192A (Cores 194-1192A-1H through 29H) represents an incomplete sequence ranging in age from the Pleistocene to the late Miocene; Zones N23–N18 and N16 were identified. Hole 1192B (Cores 194-1192B-1H through 22X) also represents an incomplete sequence of Pleistocene to early Miocene age; Zones N23–N22, N17–N16, N14, and N8–N7 were identified. A list of foraminifer datums from Holes 1192A and 1192B are given in Table **T4.**

Samples from Holes 1192A and 1192B, in general, contain good to moderate planktonic foraminifer preservation from the Pleistocene to late Miocene. Poor preservation is encountered at the base of the hemipelagic sequence (see **"Lithostratigraphy and Sedimentology,"** p. 4) in Sample 194-1192B-22X-CC, which affects the age assignment in these samples. Three of the samples, 194-1192B-13X-CC, 16X-CC, and 18X-CC, were barren of index fossils with low abundances of all planktonic foraminifers and high levels of siliciclastics. The first of these samples is coincident with the onset of significant lithification in the sediments.

Hole 1192A

In this hole, the Pleistocene is a relatively straightforward interval for planktonic foraminifer biostratigraphy. The base of Zone N22 is marked by the first appearance of *Globorotalia truncatulinoides* overlapping in range with its ancestral form *Globorotalia tosaensis*. *G. truncatulinoides* occurs in Samples 194-1192A-1H-CC and 2H-CC but not in 3H-CC, thus placing the base of the Pleistocene between Samples 2H-CC and 3H-CC.

Several planktonic foraminifer datums occur in the Pliocene section of Hole 1192A, and there are a number of index fossils defining the Pliocene in this hole, although they are not particularly abundant. *G. tosaensis* clearly defines Zone N21 with its first occurrence (FO). This zone fossil is present up to and including Sample 194-1192A-7H-CC, indicating that the cores down to this point are Zone N21 or younger. The last occurrence (LO) of *Globigerinoides fistulosus* coincides with the Zones N21/N22 boundary and occurs between Samples 194-1192A-2H-CC and 3H-CC. However, *G. fistulosus* does not occur in the other Zone N21 samples (i.e., 194-1192A-6H-CC and 7H-CC). The *Dentoglobigerina altispira* LO datum marks the Zone N20/N21 boundary and provides a useful marker in this hole. This zone fossil first occurs in Sample 194-1192A-7H-CC and is common throughout the rest of the section. The FO of *Globorotalia miocenica,* which defines the base of Zone N20, could not be identified with certainty, as this species is not clearly distinct from its ancestor *Globorotalia pseudomiocenica* at this site. The LO of *Globigerina nepenthes* marks the top of Zone N19 and is present in Samples 194-1192A-9H-1, 80–82 cm, and older.

The zone fossil *Sphaeroidinella dehiscens* is absent from Samples 194-1192A-13H-CC and older and generally infrequent from the Pliocene and Pleistocene samples. The FO of this species marks the base of Zone N18 and thus the Miocene/Pliocene boundary. It is possible to assign the Pliocene/Miocene boundary between Samples 194-1192A-12H-CC and 13H-CC, based on the overlap of the LO datum of *Globorotalia plesiotumida* near the base of Zone N19 and the FO datum of *Globorotalia tumida* near the base of Zone N18. The LO datum of *G. dehiscens* also clearly defines the top of Zone N18 as between Samples 194-1192A-12H-CC and 13H-CC. This must be compared with the nannofossil Miocene/Pliocene boundary between Samples 194-1192A-9H-CC and 10H-CC.

The LO of *G. dehiscens* occurs in Sample 194-1192A-13H-CC, which marks the Zones N18/N19 boundary. Samples 194-1192A-14H-CC through 24H-CC are assigned to Zones N17–N16, based on the absence of *G. tumida* and the consistent presence of *G. plesiotumida* and *Neogloboquadrina acostaensis* (FO datum marks the base of Zone N16).

Samples 194-1192A-25H-CC through 29H-CC occur in Zone N16 based on the LO datum of *Globorotalia paralenguanensis* (between 25H-CC and 26H-CC), which marks the Zone N16/N17 boundary. In these samples, *G. plesiotumida* and its ancestor *Globorotalia merotumida* become indistinguishable and are unreliable as datum markers.

Hole 1192B

Sample 194-1192B-1H-CC, from the first core in this hole, is assigned to Zones N22–N23 based on the presence of *G. truncatulinoides.* A core break occurs between Samples 194-1192B-1H-CC and 4H-CC. Samples 194-1192B-4H-CC through 11X-CC were assigned to Zone N17 based on the lack of *G. tumida* and the presence of *G. pseudomiocenica* and their relevant datums as discussed above. The top of Zone N16 is signified by the FO of *G. plesiotumida,* which is absent in Sample 194-1192B-12X-CC. This is corroborated by the appearance of the *Paragloborotalia mayeri-siakensis* morphological range. The LO of the latter morphospecies marks the Zone N14/N15 boundary. Between Samples 194-1192B-12X-CC and 16X-CC, the two end-member species occur intermittently. Therefore, age diagnosis is difficult because of the often barren or semibarren nature of these samples with respect to planktonic foraminifers.

For Samples 194-1192B-17X-CC to 32X-CC, a Zone N7–N8 date was attributed based on a tentatively identified *Globigerinoides sicanus-bispherica* lineage together with the descendant *Praeorbulina curva* datums. The *P. curva* LO denotes the Zone N8/N9 boundary, whereas the FA occurs near the base of Zone N8. The *G. sicanus-bispherica* zone spans the entire interval from the base of Zone N8 to the top of Zone N9. The morphological differences between *G. sicanus-bispherica* and *P. curva* are based on small variations in test sphericity and number of supplementary apertures (Kennett and Srinivasan, 1983). In addition, recrystallization of the tests made this a problematic determination.

Benthic Foraminifers

Benthic foraminifers were relatively rare in all samples examined from Hole 1192A (Samples 194-1192A-1H-CC through 29H-CC). Specimens in Sample 194-1192A-1H-CC are distinct both in preservation and assemblage. The diverse assemblage of benthic taxa, which includes several porcellaneous genera (*Pyrgo, Spiroloculina, Triloculina,* and *Quinqueloculina*) indicates a mid-outer neritic (<200 m) paleoenviron-

ment. In the rest of Hole 1192A, benthic foraminifers are relatively rare as compared to the dominant, well-preserved planktonic assemblage, although occasionally large *Cibicidoides,* nodosarids, and agglutinated benthics are conspicuous. The relatively diverse assemblages of rotaliid, buliminid, nodosarid, and agglutinated taxa are characteristic upper bathyal habitats.

Benthic foraminiferal assemblages in Hole 1192B are similar. Porcel-laneous miliolid taxa are only found in any abundance in the top of Core 194-1192B-1H and in Sample 194-1192B-1H-CC. The presence of small, flat *Amphistegina* and *Operculina,* whose modern equivalents host algal endosymbionts (e.g., Hallock, 1999), along with several porcella-neous taxa in the Core 194-1192B-1H top, indicate a deep euphotic (~50–120 m) habitat depth (middle to outer neritic). Samples 194-1192B-4H-CC through 12X-CC are relatively similar to Samples 194-1192A-2H-CC through 22X-CC, with benthic foraminifers relatively rare compared to planktonic foraminifers. Large individual *Cibicidoides* are conspicuous in some cores. Preservation distinctly declines down-hole, likely the result of reworking by bottom currents. Winnowing is inferred from observation in thin section Sample 194-1192B-1H-1, 28–32 cm, of planktonic foraminiferal tests that were infilled by micrite that was not observed outside the tests (Fig. **F5;** see also **"Lithostratig-raphy and Sedimentology,"** p. 4). Below Sample 194-1192B-13X-CC, both benthic and planktonic foraminifers are rare, probably as a result of winnowing of medium- and coarse-sand fractions, combined with poor preservation.

PALEOMAGNETISM

The natural remanent magnetization (NRM) of archive sections from Site 1192 was measured at 5-cm intervals using the pass-through cryo-genic magnetometer. Initially a 20-mT alternating-field demagnetiza-tion was used, but this was increased to 30 mT in an attempt to increase the signal to noise ratio. The Tensor tool is usually employed to orient the cores taken with the APC beginning with the third core at each hole, but the predominant zero-declination artifact in the cores of this site precluded orientation.

Discrete samples were collected from Holes 1192A and 1192B at a general sample rate of two per core. These were used to aid in the inter-pretation of the long-core record of magnetization by providing addi-tional measurements of polarity and basic magnetic characterization. Most of these samples were demagnetized at 5, 10, 15, 20, 40, 60, and 80 mT to permit principal component analysis. For rock magnetic char-acterization, anhysteretic remanent magnetization (ARM) was mea-sured in 0.2 direct current (DC) and 200-mT AC fields and isothermal remanent magnetization (IRM) in a DC field of 1 T. Samples were also measured after progressive magnetization in fields measuring up to 1.0 T to study the acquisition of the IRM.

Results

Long-Core Measurements

The intensity of magnetization in the uppermost 100 m of Holes 1192A and 1192B was between 10^{-2} and 10^{-4} A/m (Figs. **F9A, F10**). Thus, all measurements were well above the noise level of the instru-

F9. Long-core measurements, Hole 1192A, p. 35.

F10. Long-core measurements, Hole 1192B, p. 38.

ment, and the background noise from core liners and core top contamination was not significant. At depths below 100 mbsf in Holes 1192A and 1192B, the intensities fell to between 10^{-3} and 10^{-5} A/m (Figs. **F9B, F9C, F11**), so that core top contamination became potentially more important.

The NRM invariably had a strong downward overprint (Fig. **F12**). More than 90% of the NRM measurements from the top 150 m of Hole 1192A yield a positive inclination as a result of the downward overprint, which is reflected in the concentration of data points near the center of the stereographic projection (Fig. **F12A**). When the samples are demagnetized at 30 mT, the inclination concentration at the center significantly decreases (Fig. **F12B**). However, even after this demagnetization, the large variation in inclination and the nonrandom declination demonstrate that the samples are far from being cleaned of all secondary remagnetization.

Anomalous NRM intensities occur at the tops of most cores (Fig. **F13**). Some of these have associated magnetic susceptibility anomalies, suggesting that magnetic material has been introduced into the top of the core. Others do not exhibit these anomalies, indicating that remagnetization alone is involved without the addition of new magnetic material. These anomalies in remanence can degrade the magnetostratigraphy by giving false positive inclinations that may be misinterpreted as reverse polarity intervals. This is particularly problematic when the magnetization is not completely cleaned, as there will be a difference in intensity between normal and reversed intervals resulting from the effect of the persistent positive overprint.

The sequence of reversals in the uppermost 100 m of Hole 1192A recorded all of the Pliocene reversals (Table **T5;** Fig. **F9A**). However, the Brunhes/Matuyama boundary and the Jaramillo Subchron are missing, although limits could be placed on the location of the Brunhes/Matuyama boundary and on the onset of the Jaramillo. Good evidence of both the Kaena and Mammoth Subchrons was found within the Gauss. Within the Gilbert Chron, evidence for the Cochiti-Thvera sequence is also seen.

Below 100 mbsf, the intensity of magnetization falls by an order of magnitude and interpretation of the magnetostratigraphy from the reversal sequence becomes problematic. Down to 150 mbsf, an attempt has been made to interpret a magnetostratigraphy (Fig. **F9B**), but it is not possible to place the same confidence in the magnetostratigraphy compared with the uppermost 100 mbsf.

In general, there was insufficient continuous recovery from Hole 1192B to permit sequences of reversals to be identified (Fig. **F11**). However, a short normal interval in Core 194-1192B-1H is likely to represent the Jaramillo (Fig. **F10**). Below 180 mbsf where the cored section overlaps with Hole 1192A (Fig. **F11**), the same C4n C4r sequence may exist (Fig. **F9C**).

Discrete Samples

The rock magnetic properties of the sediments from Hole 1192A were investigated using discrete samples taken throughout the recovered length of core. Plots of demagnetization of ARM, IRM, and the acquisition of IRM were used to interpret the nature of the magnetic carriers. Variability in all measured parameters is greater in the upper 50 m of the section and significantly less in samples from below 100 mbsf (Fig. **F14**). However, the IRM acquisition is consistent with the dominance of

F11. Long-core measurements showing interpreted reversal sequence, Hole 1192B, p. 39.
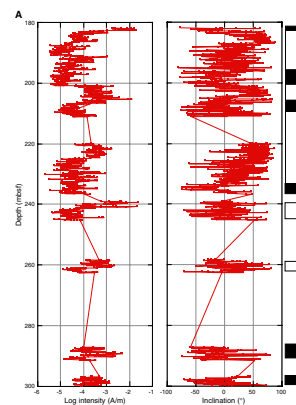
F12. Stereographic plot of directions of magnetization, p. 41.
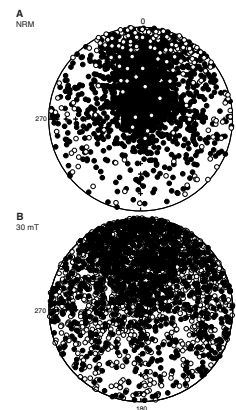
F13. Core-top anomalies, p. 42.
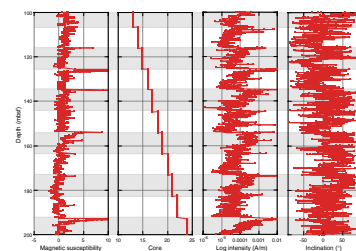
T5. Magnetostratigraphic results, p. 69.

relatively fine-grained magnetite throughout, with the intermittent addition of some harder coercivity magnetic material at depths of <100 mbsf.

Both saturation IRM and ARM show parallel trends with considerable variability in the first 50 mbsf and then show a decrease of about two orders of intensity magnitude to 120 mbsf (Fig. F15). ARM then shows very little variation to the bottom of the hole, whereas the IRM shows a minor increase from 200 to 250 mbsf.

Given that the dominant carrier is magnetite, the ratio of ARM:IRM is a measure of grain size. The variability in the top 50 mbsf includes such high values of intensity that it is unlikely to be detrital in origin but rather could be indicative of a single domain magnetosome contribution (Fig. F14). However, the low value of the crossover of IRM demagnetization and acquisition seen in Figure F13 reveals that these single domain magnetosomes are not positively interacting and so must be disaggregated. Elsewhere in the section the ARM:IRM value is typical pseudo-single domain grain size, with a slight increase in magnetic grain size toward the bottom of the hole.

The patterns of variation downcore in rock magnetic properties are consistent with those reported for magnetic susceptibility and density (see "Core Physical Properties," p. 18). They record a change from variable concentrations of magnetic material above 100 mbsf to more consistent but significantly lower concentrations below 100 mbsf.

Magnetostratigraphy and Age Depth Estimates

The magnetostratigraphy interpreted for Site 1192 is given in Table T5. It appears from the rock magnetism that at ~100 mbsf, close to the Pliocene/late Miocene boundary, a predominantly negative diamagnetic susceptibility gave way to a positive susceptibility. This is consistent with the input of siliciclastic material into a carbonate depositional environment. The recovery from Hole 1192B was not sufficient to permit interpretation of a useful magnetostratigraphy.

AGE MODEL

The age model for the 355-m-thick Miocene to Pleistocene sequence cored at Site 1192 is defined by 12 calcareous nannofossils and seven planktonic foraminifer datums (Table T6; Fig. F16) (see "Biostratigraphy and Paleoenvironments," p. 8). Magnetostratigraphic age-depth estimates are considered to be reliable in the top 80 m of the section and moderately reliable between 80 and 150 mbsf (see "Paleomagnetism," p. 11). However, the estimates are mostly offset (younger) from the biostratigraphic results by up to 1 m.y. and are not used in the construction of the shipboard age model.

The biostratigraphic data indicate a hiatus of ~1 m.y. at 29 mbsf. Although hiatuses are to be expected in the drift deposits of Megasequence D, this particular one is close to the error range of the shipboard age estimates and may be insignificant.

A major discrepancy exists between control points from Holes 1192A and 1192B, in the middle to upper Miocene sediments recovered in both holes (~180 to ~250 mbsf) (Fig. F16). This discrepancy stems from the LO of *Cyclicargolithus floridanus* in Hole 1192A (11.9 Ma; 182–202 mbsf) and the presence of the same species in Sample 194-1192A-29H-CC (11.0–13.6 Ma; 242 mbsf) (Table T6; Fig. F16). These two (old) ages

F14. Remanent magnetic characteristics, p. 43.
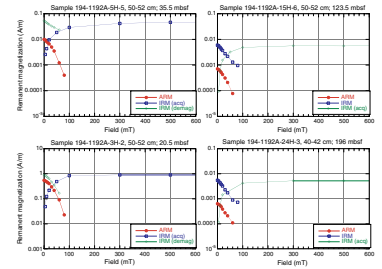
F15. Variation downcore of ARM and IRM, ARM/IRM, and ratio of IRM, p. 44.
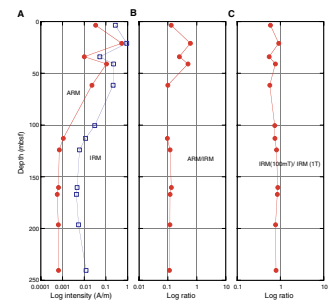
T6. Age-depth control points, p. 70.

F16. Age-depth model and sedimentation rates, p. 45.
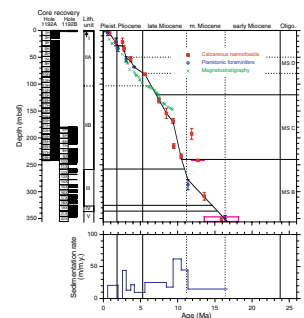
produce an age discrepancy of up to 3 m.y. below a depth of 180 mbsf when compared to Hole 1192B. The discrepancy could be the result of a coring depth error of 38–56 m, but a coring depth error of that magnitude is very unlikely. An initial comparison of magnetic susceptibility and bulk density core logging data from Holes 1192A and 1192B did not support a coring depth error of more than a few meters, but interpretation of the core logging data is not unequivocal. More likely, the discrepancy is the result of reworking of the older calcareous nannofossils *C. floridanus*. Reworking is indicated by the sparse occurrence of *C. floridanus* in Cores 194-1192A-21H through 29H, and the uninterrupted succession of *Discoaster neohamatus* and *Discoaster hamatus* in Samples 194-1192A-4H-CC to 5H-CC and 4H-6CC to 4H-8CC, respectively (see "Biostratigraphy and Paleoenvironments," p. 8). In addition, planktonic foraminifers in Samples 194-1192A-25H-CC through 29H-CC are from Zone 16, which is 8.2–11 m.y. in duration. These younger foraminifer ages in the same depth interval of Hole 1192A and the younger calcareous nannofossil ages given in Hole 1192B for the same depth interval strongly suggest that *C. flondanus* is probably reworked and an unreliable age datum. Consequently, these two age datums are ignored for the age vs. depth curve (Fig. F16).

We also ignored the reported LO of *D. hamatus* (9.5 Ma; 215 mbsf) because including this control point created an unrealistic peak in sedimentation rate (450 m/m.y.) over a very short time interval (0.1 m.y.). Shore-based analysis should resolve this problem.

For the purpose of picking age estimates for lithologic and seismic unit boundaries (Table T7), the straight-line segment defined in the interval 80–150 mbsf was extended to the bottom of the sequence (dashed line in Fig. F16). This line represents an "average model" for Holes 1192A and 1192B below 150 mbsf.

Interval sedimentation rates range from 0 (hiatus) to 44 m/m.y. The overall average rate is ~22 m/m.y.

GEOCHEMISTRY

Volatile Hydrocarbons

Concentrations of volatile hydrocarbon gases were measured from every core using the standard ODP headspace sampling technique and gas chromatographic analysis. Methane only occurred in very minor concentrations (2 ppmv); near the surface, methane content increases slightly to 11 ppmv (Table T8).

The low gas content at Site 1192 is likely a function of three characteristics of the sediment. First, the sediments contain very little organic matter as a source of natural gas. Second, pore water profiles show that appreciable SO_4^{2-} exists to the bottom of the hole; thus, sulfate reduction is likely to be limiting methanogenesis in this interval. Third, the organic matter that does exist here is immature relative to hydrocarbon expulsion and petroleum generation, so no thermogenic component to the gas fraction is expected.

Interstitial Waters

Pore water samples were taken approximately every 10 m in Hole 1192A, which reached a total depth of 240 mbsf. After having taken one core close to the mudline, Hole 1192B was washed to 179.9 mbsf

and was then cored to 345.0 mbsf. Additional pore water samples were taken at 10-m intervals in Hole 1192B. Results from both holes are discussed together.

The concentrations of dissolved constituents at Site 1192 (Table **T9;** Fig. **F17**) are relatively constant with depth compared to changes observed at many other ODP sites. Dissolved chloride decreases from a value at the sediment surface of 570 to ~562 mM at 140 mbsf and increases again to 570 mM at 340 mbsf near the bottom of Hole 1192B (Fig. **F17A**). Titrated alkalinity increases very slightly in the upper 40 m at this site, from 1.7 to 2.4 meq/L, and thereafter varies unsystematically between 1.8 and 3.2 meq/L (Fig. **F17B**).

Dissolved potassium concentrations decrease downhole from 12 mM in the shallowest samples to ~6.5 mM in the deepest samples (Fig. **F17C**). Such a decrease has been observed in many Deep Sea Drilling Project (DSDP)/ODP sites and is usually attributed to clay mineral diagenesis. The concentration of lithium in the pore waters increases from ~30 µM near the sediment surface to 150 µM at the bottom of Hole 1192B.

Magnesium concentrations decrease downhole from near seawater concentrations (55 mM) in surface sediments to ~38 mM toward the bottom of Hole 1192B (Fig. **F17E**). Calcium concentrations increase downhole from 12.1 mM at 5.9 mbsf to ~18 mM at 342 mbsf (Fig. **F17D**). It is not clear whether the decrease in Mg^{2+} is caused by carbonate precipitation or is simply a diffusion gradient between seawater and basement rocks underlying the sediments. The latter mechanism has often been used to explain similar trends in pelagic sediments underlain by oceanic crust, which acts as a sink for magnesium and a source for calcium because of low-temperature basalt alteration. Basement underneath the Marion Plateau drilled at Site 1194 consists of generally basaltic volcanics and volcaniclastic sediments. More mafic components are also present. Alternatively, dolomite precipitation via the reaction

$$Mg^{2+} + 2CaCO_3 <—> CaMg(CO_3)_2 + Ca^{2+}$$
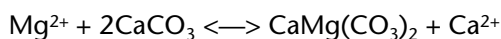
could remove magnesium and simultaneously input calcium to the pore waters. This mechanism is supported by the presence of minor amounts of fine-grained dolomite through much of the sediment column (see **"Lithostratigraphy and Sedimentology,"** p. 4). Carbonate precipitation would also explain the low alkalinity values. Even the modest amount of sulfate reduction at Site 1192 would normally be expected to be associated with increasing alkalinity in a 1:2 ratio. Dolomitization by the above reaction should produce an approximately linear trend in Ca^{2+} against Mg^{2+}, with a slope of –1. Such a trend is not seen (Fig. **F18**). Mg^{2+} is highly correlated to SO_4^{2-}, however (Fig. **F19**), which suggests dolomite formation might be proceeding through the less commonly observed reaction

$$Mg^{2+} + HCO_3^- + CaCO_3 <—> CaMg(CO_3)_2 + H^+,$$
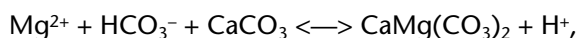
with the bicarbonate sourced from sulfate reduction. This reaction results in a 2-mM reduction in alkalinity per mole of Mg^{2+} consumed; 1 mole of SO_4^{2-} reduced to sulfide should produce 2 moles of alkalinity. It follows that the overall $Mg^{2+}:SO_4^{2-}$ ratio for dolomitization should be 1:1, approximately what is observed in the pore waters of Site 1192. Thus, Mg^{2+} is likely removed from the pore waters by dolomite forma-

tion, whereas Ca^{2+} is added by alteration of basement rocks. These two independent processes explain why there is no correlation between pore water Ca^{2+} and Mg^{2+} concentrations.
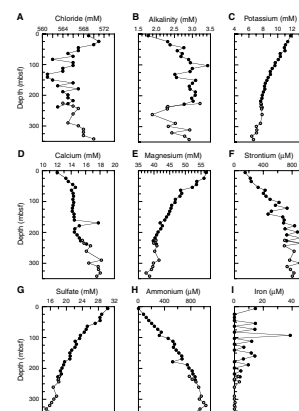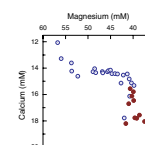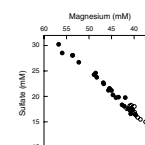
As a result of carbonate recrystallization, strontium concentrations increase steadily downhole through Site 1192 sediments (Fig. F17F). At ~250 mbsf, a value of ~800 µM is reached. The high strontium concentration and low amount of sulfate reduction result in celestite precipitation in the deeper parts of the sediment section at Site 1192.

In response to a moderate rate of bacterial sulfate reduction, dissolved sulfate (Fig. F17G) decreases from 30.4 mM in the shallowest sample at 5.9 mbsf to ~18 mM at the bottom of Hole 1192A. A further decrease to 15 mM is seen through the section drilled in Hole 1192B. The oxidation of sedimentary organic matter associated with sulfate reduction results in a steady increase in ammonium concentrations (Fig. F17H) throughout Site 1192. Values near the sediment surface are 24 µM and are ~1000 µM at the bottom of Hole 1192B. Sulfate and ammonium are highly negatively correlated ($r^2 = 0.96$).

Manganese and iron concentrations were also measured in all Site 1192 samples. Manganese was below detection limits (i.e., were within the 1-σ error of 0) in all samples. Iron values were also either very low or within a measurement error of 0 (Fig. F17I). In all likelihood, the low organic carbon concentration in the sediments results in limited reduction of iron and manganese oxides and subsequent input to the pore fluids. The small amount of iron or manganese that is released to the pore water is probably rapidly precipitated as sulfide minerals. This conclusion is supported by the presence of Fe sulfide minerals through much of the sedimentary section.

Sedimentary Geochemistry

Calcium carbonate ($CaCO_3$) content in samples from Site 1192 range from ~66 to 94 wt% (Fig. F20; Table T10). Calcium carbonate content exhibits an overall decrease from values of ~91 wt% at ~2 mbsf to ~73 wt% at ~51 mbsf. From ~51 to 99 mbsf, an increasing trend in weight percent $CaCO_3$ was measured, with values ranging from ~74 to 82 wt%. Between ~99 and 263 mbsf, calcium carbonate content is consistently high at ~80–92 wt%. Sediments from ~263 to ~343 mbsf display the entire range in $CaCO_3$ contents observed at Site 1192, including two excursions with low weight percent $CaCO_3$ values (<70 wt%) at 262.86 and 327.85 mbsf.

The total organic carbon content for all intervals at Site 1192 is <0.3 wt%. Note that weight percent total organic carbon (TOC) values determined using Rock-Eval pyrolysis and CNS analysis provide similar values (Fig. F20; Tables T10, T11). Hydrogen index (HI) values from Rock-Eval pyrolysis range from 83 to 366 mg HC/g TOC at Site 1192 (Fig. F20; Table T11). The lowest values were observed in horizons between 0–6, 55–105, 157, 239–245, and 328–329 mbsf. The highest HI value occurs in sediments at ~137.25 mbsf. Oxygen index (OI) values vary between 411 and 3785 mg CO_2/g TOC (Table T11). T_{max} values obtained from Rock-Eval pyrolysis range from 364° to 435°C (Table T11), although the most reliable T_{max} values cluster between 400° and 420°C.

The low percent TOC values obtained from Rock-Eval pyrolysis of the sediment at Site 1192 limit the reliability of some of the HI and OI values. However, duplicate and triplicate analyses were performed on many of the sediments to validate the results. The high OI values mea-

F20. Carbon, hydrogen index, and sulfur, p. 49.
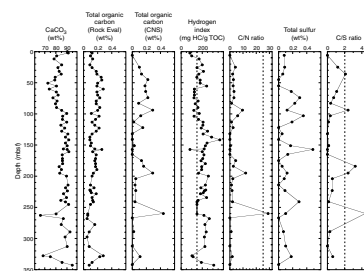
T10. Carbon, nitrogen, sulfur, and hydrogen values, p. 74.

T11. Rock-Eval pyrolysis results, p. 75.

sured are attributed to the thermal degradation of calcium carbonate during pyrolysis and are not considered in this interpretation.

Total sulfur content in Site 1192 sediments is generally low, ranging from 0 to >0.4 wt% (Fig. F20; Table T10). Intervals of relative sulfur enrichment are visible at ~64–113, 151–165, 241, and 310–330 mbsf.

The high calcium carbonate content of sediments at Site 1192 mainly reflects dominance of foraminifers in the sediments (see "Biostratigraphy and Paleoenvironments," p. 8, and "Lithostratigraphy and Sedimentology," p. 4). The downhole increase in calcium carbonate content below ~99 mbsf corresponds to an increase in color reflectance and benthic constituents preserved in the sediment. These changes are suggestive of increased input of detritus from the adjacent carbonate platforms to the sediments of Site 1192. From ~99 to 263 mbsf, calcium carbonate contents display reduced variability, corresponding to an interval of sediment dominated by planktonic foraminifers. Interestingly, two intervals within this zone exhibit calcium carbonate contents ranging from ~84 to >90 wt% and are separated by an interval of sediment containing 80 to 85 wt% $CaCO_3$. These two intervals (~100–160 and ~200–250 mbsf) correspond to units containing firmgrounds, suggesting that episodes of seafloor sediment starvation affected calcium carbonate preservation. The zone of widely ranging calcium carbonate contents from ~263 to ~343 mbsf corresponds to observations of fine-grained carbonate sediments of unknown origin mostly barren of planktonic foraminifers. This zone from ~263 to ~343 mbsf also corresponds to lithologic Units III and IV, where the content of glauconite and phosphate grains is notable and dolomite rhombs and quartz were observed.

The low organic carbon contents preserved in the sediments at Site 1192 is suggestive of a well-mixed water column and/or relatively oxic seafloor conditions during deposition. The T_{max} values obtained from Rock-Eval pyrolysis are indicative of immature organic matter; therefore, we are confident that our analyses of organic matter type (discussed below) record a primary signal. The anomalously low T_{max} values just beneath the seafloor are likely attributable to the presence of relatively "fresh" Type I organic matter, which can generate erroneously low T_{max} values.

The type of organic matter encountered provides further insight into depositional processes at Site 1192. Both C/N ratios and HI values are indicative of mostly marine to oxidized marine organic matter preservation. However, at least four intervals were observed that display HI values (<150) characteristic of terrigenous or oxidized marine organic matter with relative enrichments in total sulfur content. These horizons either correspond to decreases in carbonate content or the existence of firmgrounds (see "Lithostratigraphy and Sedimentology," p. 4), suggesting that episodes of enhanced terrigenous or oxidized marine organic matter input/preservation to the seafloor occurred during those times when carbonate deposition waned. Increased sulfur content may be indicative of iron limitation during pyrite formation in the intervening sediments, as the total organic carbon content is similar throughout the sediment column. Therefore, we might expect increased clay content (as a source of reduced iron) to be associated with these relatively elevated terrigenous organic matter and sulfur intervals.

Of further interest are four relative peaks in C/S values (>2) at Site 1192, which may record episodes of brackish pore water in the sediments. Admittedly, the use of the C/S method may be limited in high

carbonate content sediments (Berner and Raiswell, 1984). However, in each case, the C/S peaks correspond to relatively lower carbonate contents and exist ~20 m beneath the intervals of elevated terrigenous organic matter and sulfur content. Therefore, episodes of terrigenous organic matter input to the seafloor may have been accompanied by the presence of brackish pore waters in a biologically mediated diagenetic depth zonation in the underlying sediments.

Within a broader sequence stratigraphic perspective, some of the geochemically defined intervals correspond to major seismic sequence boundaries (see "Seismic Stratigraphy," p. 23). The most instructive is the recognition of the boundary between seismic sequences C and B at ~240 mbsf. This surface closely corresponds, within the range of seismic resolution and depth uncertainties, to a geochemically defined boundary between ~234 and 260 mbsf (i.e., low HI and high C/N values [terrigenous or Type III organic matter] overlain by a relatively high HI value [marine organic matter]). These observations may be explained by terrigenous organic matter deposition within a relative lowstand setting, whereas marine organic matter was deposited during subsequent marine flooding. Furthermore, the lowest carbonate content at Site 1192 was measured at ~263 mbsf, suggesting that a break in production on the carbonate platform, likely by an exposure, was followed by more terrigenous organic matter inputs and/or organic matter oxidation.

Between ~142 and 157 mbsf, the entire range in HI values at Site 1192 was observed; therefore, a similar sequence stratigraphic model for organic matter deposition/preservation may be invoked. Here, however, the seismic sequence boundary pick at ~120 mbsf does not correspond to the geochemically defined surface, suggesting that higher-frequency geochemical cycles may represent parasequence-scale deposition.

CORE PHYSICAL PROPERTIES

Evaluation of physical properties at Site 1192 included nondestructive measurements of bulk density, bulk magnetic susceptibility (MS), natural gamma radiation (NGR), and *P*-wave velocity on whole cores using the multisensor track (MST). Transverse *P*-wave velocity (x-direction) and moisture and density (MAD) were measured on split cores and plug samples. Low recovery in Cores 194-1192B-11X, 13X, 14X, and 22X precluded the use of the MST. Thermal conductivity was measured on whole cores and semilithified half core samples.

Density and Porosity

Bulk density at Site 1192 was computed from gamma ray attenuation (GRA) using unsplit cores and from mass and volume measurements on plug samples. GRA bulk density decreases from 1.70 to 1.65 g/cm³ in core from the upper 20 m of Hole 1192A (Fig. F21). Below 20 mbsf, the general bulk density trend is an overall increase down to ~345 mbsf. Small-scale variations in density occur downhole. Between 85 and 160 mbsf, the bulk density is rather uniform. Below ~180 mbsf, the variability increases markedly. Composite profiles of these independently derived bulk density estimates indicate a similar trend in the two data sets (Fig. F21). With the exception of a few outliers, the GRA bulk density values exceed the MAD values between 0 and 245 mbsf by ~0.1 g/cm³. Cores from this interval were recovered using the APC. Such a discrepancy is not uncommon (e.g., see "Core Physical Properties" in the "Site

F21. GRA bulk density, p. 50.
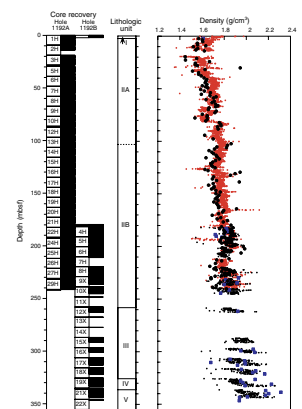
1109" and "Site 1115" chapters of the Leg 180 *Initial Reports* volume
[Taylor, Huchon, Klaus, et al., 1997]). Sites 1109 and 1115 chapters, Leg
180) and is likely a function of the core diameter variations produced
by the type of coring (e.g., Fig. F21; Cores 194-1192B-7H through 9X),
problems with the GRA calibration, excessive drying of the core prior to
sampling for MAD measurements, and/or mass loss during the sample
drying and pycnometer measurement. Nevertheless, the repeatability of
the MAD measurements suggests that the consistent difference between
GRA and MAD densities arise because of either the variability in core di-
ameter or problems with instrument calibration. Given these caveats,
the GRA bulk densities otherwise agree well with the MAD measure-
ments.

Grain density averages 2.77 g/cm³ and shows a distinct pattern of
variability as a function of depth (Fig. F22). Three distinct zones can be
recognized:

1. Zero to 100 mbsf, where data are scattered;
2. One hundred to 250 mbsf, where the density is ~2.72 g/cm³, ex-
   cept for apparent outliers with unreasonable grain densities >3.0
   g/cm³; and
3. Below 300 mbsf, where data again show high variability (note
   that there is a data gap between 250 and 300 mbsf).

Values in Zone 2 are compatible with a high carbonate content (85–90
wt%) (see "Geochemistry," p. 14), whereas the higher variability in
Zones 1 and 3 reflects the input and variability of a terrigenous clastic
component. This terrigenous component is assumed to be the result of
hemipelagic deposition across the region (see "Lithostratigraphy and
Sedimentology," p. 4). Suspect grain densities, especially those >3.0 g/
cm³, have been noted in Figure F22 (open circles). These densities are
considered suspect because they are also associated with either anoma-
lous bulk density or porosity. In turn, the bulk density and porosity out-
liers in the depth interval <100 mbsf do result in reasonable grain densi-
ties, suggesting that these values may be correct.

Porosity profiles generally reflect a combination of stress history and
sedimentologic and diagenetic effects such as variability in compress-
ibility, permeability, sorting, grain fabric, and cementation. Porosity is
calculated from the pore water content, assuming complete saturation
of the wet sediment sample (Blum, 1997) (see "Core Physical Proper-
ties," p. 21, in the "Explanatory Notes" chapter). The porosity curve
mirrors that of the bulk density curve, with minor differences caused by
changes in grain density (Fig. F22). The variability in porosity at Site
1192 shows a general decrease with depth. Superimposed on this trend
are shorter wavelength variations. No abrupt steps in porosity, a com-
mon characteristic of erosional unconformities, are observed.

Typically, seafloor porosities of abyssal plain marine oozes are high
(85%–90%). For homogeneous sediments that are not overpressured,
porosity may be approximated by an exponential function of depth
(e.g., Athy, 1930). Porosities from Site 1192 show relatively low values
at the seafloor (60%–70%) and decrease gradually to 40%–50% at a
depth of 300–350 mbsf (Fig. F22). This low surface porosity may reflect
surficial reworking, sorting, and efficient grain packing by oceano-
graphic currents. Distinct zones of relatively higher porosity are found
between 20 and 30 mbsf and between 210 and 240 mbsf. The general
behavior of Site 1192 porosity as a function of depth is broadly consis-
tent with Athy's relationship:

F22. Bulk density, grain density,
and porosity, p. 51.
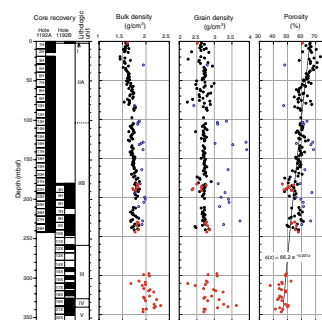
$$\phi(z) = \phi_o \, e^{-kz},$$

where $\phi(z)$ is the porosity as a function of depth z, ϕ_o is the surface porosity, and k controls the rate of decay of porosity with depth (Athy, 1930). A least-squares fit to this equation estimates a surface porosity of 66.2% and a compaction decay constant of 0.001 m^{-1} (Fig. F22) (correlation coefficient of 0.78). The inverse of the decay constant (1000 m) can be physically interpreted as the depth over which porosity is halved with respect to the surface or initial value. Porosity shows no obvious correlation with relative clay content (see "Lithostratigraphy and Sedimentology," p. 4), color reflectance, an indirect proxy for clay content, or grain size (Fig. F2).

P-Wave Velocity

P-wave velocities were measured with the MST P-wave logger (PWL) on whole cores and the PWS3 contact probe system on both split cores (within the core liner) and ~9.5-cm^3 cube samples of semilithified and lithified sediments. The cubes were used to measure velocities in the transverse (x and y) and longitudinal (z) directions. Insufficient x- and y-direction P-wave sensor (PWS) data precluded a study of velocity anisotropy. Extreme scatter and unreasonable velocities, likely a function of drilling disturbance, call into question the quality of the PWL, and thus these data were not used.

Initially, it appeared that sediment plasticity and induration prevented reliable use of the PWS1 and PWS2 probes. However, it was eventually determined that a software problem failed to set the minimum receiver voltage to recognize the seismic waveform. Once fixed, the PWS system operated within acceptable limits and was used to remeasure the velocity in Cores 194-1192-1H through 12H. These measurements show that most of the earlier velocities measured at Site 1192 have been compromised to systematically higher velocities (Fig. F23A). Originally, velocity measurements from ~40 to 345 mbsf ranged from 1940 to 2500 m/s. To salvage some of the older velocity data, a constant value of 346.5 m/s was subtracted to make the earlier velocities consistent with the newer, correctly measured velocity data (Fig. F23B). Corrected velocity values increase gradually from ~1580 to a maximum of 2097 m/s with an average of 1662 m/s.

Two features of the corrected velocity profile shown in Figure F23B are worth noting. First, an abrupt downcore increase is followed by a slower decrease in velocity over a depth of 80–105 mbsf. Below this interval, the velocities are characterized by low scatter over a depth range of 105–175 mbsf. This same depth range correlates with high carbonate content (see "Geochemistry," p. 14) and relatively constant grain density and porosity (Fig. F22). Below ~180 mbsf, the velocities show high scatter, as do bulk density and porosity.

Thermal Conductivity

Thermal conductivity measurements at Site 1192 show an overall increase with depth, ranging from ~0.8 W/(m·K) near the seafloor to ~1.35 W/(m·K) at the base of Hole 1192B (Fig. F24). Large scatter is observed between 0 and 40 mbsf, which is broadly consistent with the porosity data (Fig. F22). A direct inverse relationship should exist between porosity and thermal conductivity as a result of the power law depen-

F23. P-wave velocity, p. 52.
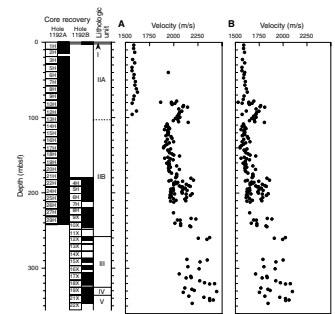
F24. Average thermal conductivity, p. 53.
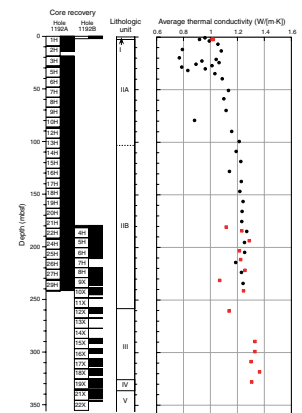
dence of bulk thermal conductivity, K_{bulk}, on the solid matrix grain thermal conductivity, K_{grain}, and the thermal conductivity of the interstitial fluid, K_w, namely (e.g., Keen and Beaumont, 1990):

$$K_{bulk} = K_w{}^\phi \cdot K_{grain}{}^{(1-\phi)}.$$

The relationship between the observed thermal conductivities, porosity, and sediment facies (i.e., degree of mixing of siliciclastic, clay, and carbonate components) can be investigated by calculating the variation in bulk thermal conductivity for the observed porosity range obtained at Site 1192 (Fig. F22).

The result (Fig. F25) is based on grain thermal conductivities summarized in Table T6, p. 56, in the "Explanatory Notes" chapter (Keen and Beaumont, 1990). Except for a small number of outliers, the majority of the measured thermal conductivities lie between the shale and sandstone power law relationship, giving confidence in the viability of the observed thermal conductivities. Given the predominance of carbonate through the various sections, the observed thermal conductivity is consistent with the mixing of siliciclastic/carbonate and clay/carbonate sediment facies.

Magnetic Susceptibility

High values of MS are a function of the existence and concentration of ferro- and ferrimagnetic minerals such as magnetite, hematite, goethite and titanomagnetite within a sediment. The source of this material may be associated with the coarse sediment fraction of, for example, proximal turbidites and/or single-domained magnetic material contained within the clay fraction. In the absence of ferro- and ferrimagnetic minerals, the MS often displays low values induced by paramagnetic and diamagnetic minerals such as clays and evaporites. NGR values are also a function of the terrigenous clay content within sediment. Clay minerals, being charged particles, tend to attract and bond with K, U, and Th atoms so that an increasing NGR count typically correlates with increasing clay/shale content. Both MS and NGR contain independent information concerning source provenance and magnetic mineral derivation. For example, a noncorrelation between NGR and MS may imply the existence of biogenically produced ferrimagnetic minerals or the mixing of distinct terrigenous sources.

As with the grain density (Fig. F21), the MS measured at Site 1192 can be divided into three zones with distinct patterns (Fig. F26):

1. Zero to 100 mbsf, where the susceptibility data are scattered and characterized by high-frequency variations;
2. One hundred to 250 mbsf, where the data are nearly constant; and
3. Below 250 mbsf, where the susceptibility again shows relatively high variability.

In Zone 1, the magnetic susceptibility is characterized by high-frequency variability that ranges in amplitude from 0 to 25×10^{-6} SI units, which is in contrast with the subdued signal of Zone 2 where susceptibility values, apart from a few outliers, consistently range from 0 to 2×10^{-6} SI units. Zone 3 shows increased values ranging from 0 to 15×10^{-6} SI. It is inferred that Zones 1 and 3 represent times of enhanced terrigenous in-

F25. Crossplot of porosity and thermal conductivity, p. 54.
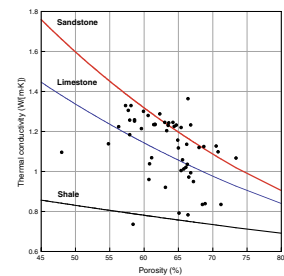
F26. Comparison of physical properties, p. 55.
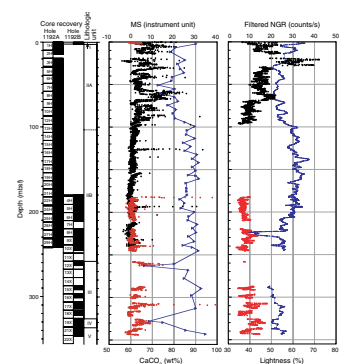
put and hemipelagic deposition in the basin. Coeval with the change in MS, there is an abrupt but relatively small decrease in the carbonate content of the section and a corresponding decrease in reflectance, again a proxy for clay content in a clay-carbonate two-component system (Fig. F26). If the MS values in Zone 2 were solely due to the dilution effects of carbonates and clays, then the ~10% decrease in carbonate in Zone 1 would result in a minimal change in susceptibility values, inconsistent with the observed tenfold increase. It is concluded that the MS is not the result of changing the mixing ratio between clays and carbonates but, rather, of an increase in continental clastic flux.

Natural Gamma Ray

The NGR count was recorded on the MST for core from Holes 1192A and 1192B. However, a series of problems related to possible electrical "cross-talk" within the data acquisition circuitry produced significant amplitude and high-frequency noise. The form of this noise was a recursive NGR count whose periodicity was linked to section length and whose count amplitude rapidly increased toward the end of the section (Fig. F27A). This problem persisted for all of the NGR measurements for Hole 1192A. Only after shutting down the acquisition system and rebooting the controlling computers prior to MST measurements of Hole 1192B core did the problem disappear. Neither the exact reason for the source of the problem nor its solution is known. Remeasuring Cores 194-1192A-1H through 12H confirmed that the NGR count was now acceptable (Fig. F27B). However, in comparing the original and remeasured NGR, it is clear that the high-frequency and high-amplitude spikes are superimposed on the same "baseline" signal observed in the remeasured sections (Fig. F27B). It is concluded that the NGR count can be used, with care, for geological interpretation.

For Site 1192, the interpretational use of NGR data is limited because of poor core recovery from 100 to 180 mbsf and from 260 to 290 mbsf (Fig. F26). However, even with the limited NGR data, it is clear that the variations with depth are compatible with the sediment facies interpretations based on the MS, carbonate concentration and sediment reflectance (Fig. F26). In particular, the NGR count associated with the carbonate-dominated section between 180 and 245 mbsf is very low, ranging from 0 to 10 cps. In contrast, the NGR count ranges from 10 to 40 cps between 0 and 90 mbsf and correlates with the magnetic susceptibility and grain density of Zone 1, considered to be the result of increased terrigenous sediment flux (Figs. F22, F26).

Hole-to-Hole Correlation

GRA density was used to estimate the depth offset between Holes 1192A and 1192B (Fig. F28). This estimate is based on matching characteristic features in the data sets. For example, Figure F28 shows a small but general decrease and subsequent increase in GRA density between 204.5 and 205.1 mbsf in Cores 194-1192A-24H to 25H. The interpreted counterpart density variation exists within Cores 194-1192B-5H to 6H at 203.2–203.7 mbsf, suggesting an ~1.27 m offset between these two cores. This offset will not apply to other cores or even other intervals in these cores. However, it represents the typical margin of uncertainty in depth measurements with the drill string.

F27. NGR data, p. 56.
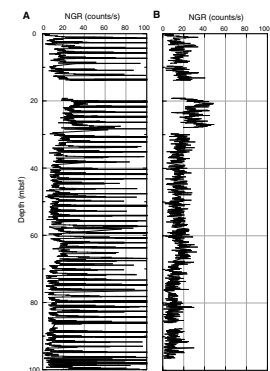
F28. Depth offset between Holes 1192A and 1192B, p. 57.
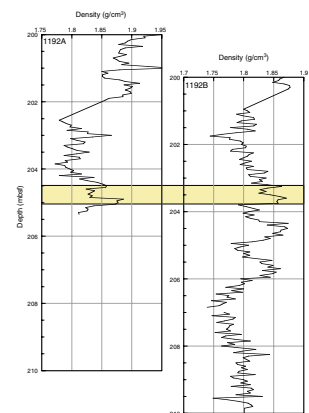
SEISMIC STRATIGRAPHY

Site 1192 penetrated 355.5 m of sediment through seismic Megasequences D, C, and part of B (Fig. F29). The site is located on multichannel seismic line MAR20 at shotpoint 4126, a location that lies midway between the NMP and the Southern Marion Platform (SMP) on top of an ~50-m-deep incision in the basement surface (Figs. F7, p. 67, in the "Leg 194 Summary" chapter; F29).

Time-Depth Conversion

Because the primary objective of Site 1192 was an engineering test for the HYACE tools, no downhole logging operations were performed. Consequently, no velocity log or check shot information is available to tie the seismic record with maximum accuracy to the cores. The time-to-depth conversion is calculated by integrating shipboard velocity measurements performed with the PWS tool (see "Core Physical Properties," p. 18; the reliability of the PWS velocity data is discussed within that section). The resulting traveltime-to-depth conversion for seismic reflections and sequence boundaries is shown in Figure F30. A synthetic seismogram was calculated with the GRA bulk density and the PWS velocities. It is superimposed on line MAR20 and displayed at the left on Figure F30. A normal polarity zero-phase wavelet of 80 ms in length was statistically extracted from the seismic data of line MAR20. No time-control points were used for calculation of these synthetic seismograms.

Megasequence D

Seismic Facies and Geometries

The seismic facies of Megasequence D is characterized by laterally continuous reflections that dip gently toward the southeast. Reflection amplitudes are generally low, with one prominent intramegasequence high-amplitude reflection at 650 ms two-way traveltime (TWT). The southeast dip of the reflections seen on line MAR20 (Fig. F7, p. 67, in the "Leg 194 Summary" chapter) results in an eastward thickening of Megasequence D. This thickening forms a drift wedge toward the pre-existing topographic high of the SMP. Low-angle lapout and toplap reflections within the wedge indicate that modern sedimentation at Site 1192 is condensed or that the seafloor is an unconformity surface. In addition, several smaller-scale unconformities within Megasequence D indicate the occurrence of hiatuses within the drift package. The seismic Megasequence C/D boundary is defined along line MAR20 toward the southeast by a downlap onto underlying seismic Megasequence C at the base of the SMP escarpment and toward the northwest by an onlap onto the NMP (Fig. F7, p. 67, in the "Leg 194 Summary" chapter).

Correlation with Cores

Seismic Megasequence D incorporates lithologic Unit I and part of Unit II, ranging in age from late Miocene to Pleistocene. The absence of Holocene sediments at this site confirms the assumption that modern sedimentation is strongly reduced or absent and that the actual seafloor represents an unconformity. The high-amplitude intrasequence reflection at ~650 ms TWT, marking a seismic sequence boundary within
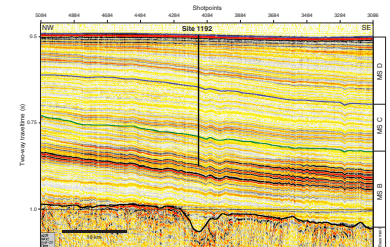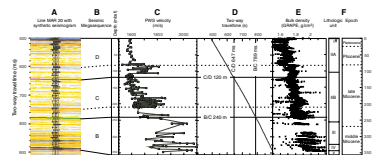
Megasequence D, coincides with a downcore increase in bulk density at 81 mbsf (upper dashed line in Fig. F30). The interpretation of Megasequence D to be a drift deposit is based on seismic geometry and is supported by the increased siliciclastic fraction in lithologic Subunit IIA (2.5–103 mbsf). In addition, the dominant wackestone to packstone lithology of this interval also contrasts with the underlying dominant mudstone of Subunit IIB (see "Lithostratigraphy and Sedimentology," p. 4). Megasequence C/D boundary, positioned at ~120 mbsf, is characterized southeast of Site 1192 by a change in shedding direction, because the dip of the reflections changes at the base of the SMP upcore from northwest to southeast (Fig. F8, p. 68, in the "Leg 194 Summary" chapter). This change indicates a halt to the export of platform-derived material from the SMP to the northwest. Such a change in sedimentation pattern could be caused by an exposure and/or drowning of the SMP around or just prior to the Miocene/Pliocene boundary, which would reduce the carbonate input into the current-controlled depositional system. In the area of Site 1192, this sequence boundary is conformable, and no large stratigraphic hiatus was observed in the drill cores. The applied time-depth correlation places the seismic Megasequence C/D boundary at 120 mbsf (Fig. F30), which coincides with an age of ~7.2 Ma (see "Age Model," p. 13).

Megasequence C

Seismic Facies and Geometries

At this site, the overall seismic facies character does not change across seismic Megasequence C/D boundary. The amplitudes of the laterally continuous reflections remain low, and only one couplet of reflections displays a high amplitude at 750 ms TWT (Fig. F29). Regionally, Megasequence C wedges out toward the northwest by forming an onlap onto underlying Megasequence B/C boundary, as can be seen on line MAR20 (Fig. F7, p. 67, in the "Leg 194 Summary" chapter). Toward the southeast, the facies of Megasequence C changes into a more irregular high-amplitude unit dipping toward the northwest. This indicates potential sediment shedding from the SMP and accumulation of platform-derived sediments in an apron at the base of the escarpment. At Site 1192, seismic Megasequence C/D boundary is calculated to occur at 240 mbsf.

Correlation with Cores

Megasequence C correlates roughly with lithologic Unit II (late Miocene). The generally low amplitude seismic facies reflects a homogenous lithology over most of Megasequence C. This conclusion is supported by very monotonous mudstone lithology between 100 and 200 mbsf and by almost constant bulk density values (Fig. F30). The only high-amplitude couplet of reflections right below 750 ms TWT coincides with increases in gamma ray attenuation density at 200 and 230 mbsf (lower dashed line inn Fig. F30). Megasequence B/C boundary at 240 mbsf correlates approximately with the boundary between lithologic Units II and III (259 mbsf). This interval is characterized in the geochemical signature of the sediments by the lowest measured carbonate content of this site (65 wt%), by a negative excursion in the Hydrogen Index, and by a very high C/N ratio (see "Geochemistry," p. 14). All these sedimentological and geochemical "anomalies" point toward

a relative increase of noncarbonate input into the depositional system during a period that can be seismically correlated with the exposure of the NMP. Using the established age model, this sequence boundary can be dated at ~10.5 Ma (see "Age Model," p. 13).

Megasequence B

Seismic Facies and Geometries

The top of Megasequence B is characterized by a more or less conformable succession of low-amplitude reflections that increase in amplitude between 800 and 850 ms TWT. Hole 1192B was abandoned within these stronger reflections that dip to the southeast and terminate about 30 km updip toward the northwest in the more chaotic, partly horizontally stratified seismic facies of the NMP.

Correlation with Cores

Cores at Site 1192 penetrated the upper part of Megasequence B, which incorporates lithologic Units III, IV, and V, all of middle Miocene age. The top of lithologic Unit III at 259 mbsf is characterized by abundant glauconitic grains and coincides fairly well with seismic Megasequence B/C boundary at 240 mbsf, using the proposed time-depth correlation. In addition to the geochemical signature of B/C described above, the boundary also marks the top of an ~50-m-thick interval that is rich in coarse glauconitic and phosphatic grains. Lithologic and petrophysical changes within lowermost Units IV and V correlate with high-amplitude reflections at the base of the hole.

REFERENCES

Athy, L.F., 1930. Density, porosity, and compaction of sedimentary rocks. *AAPG Bull.,* 14:1–24.

Berner, R.A., and Raiswell, R., 1984. C/S method for distinguishing freshwater from marine sedimentary rocks. *Geology,* 12:365–368.

Blum, P., 1997. Physical properties handbook: a guide to the shipboard measurement of physical properties of deep-sea cores. *ODP Tech. Note,* 26 [Online]. Available from World Wide Web: <http://www-odp.tamu.edu/publications/tnotes/tn26/INDEX.HTM>. [Cited 2001-01-10]

Hallock, P., 1999. Symbiont-bearing foraminifera. *In* Sen Gupta, B.K. (Ed.), *Modern Foraminifera:* Amsterdam (Kluwer), 123–149.

Keen, C., and Beaumont, C., 1990. Geodynamics of rifted continental margins. *In* Keen, M.J., and Williams, G.L. (Eds.), *Geology of the Continental Margin of Eastern Canada.* Geol. Soc. Am., 1:391–472.

Kennett, J.P., and Srinivasan, M.S., 1983. *Neogene Planktonic Foraminifera: A Phylogenetic Atlas:* Stroudsburg, PA (Hutchinson Ross).

Taylor, B., Huchon, P., Klaus, A., et al., 1999. *Proc. ODP, Init. Repts.,* 180 [CD-ROM]. Available from: Ocean Drilling Program, Texas A&M University, College Station, TX 77845-9547, U.S.A.

Figure F1. Bathymetry map showing locations of Leg 194 sites.
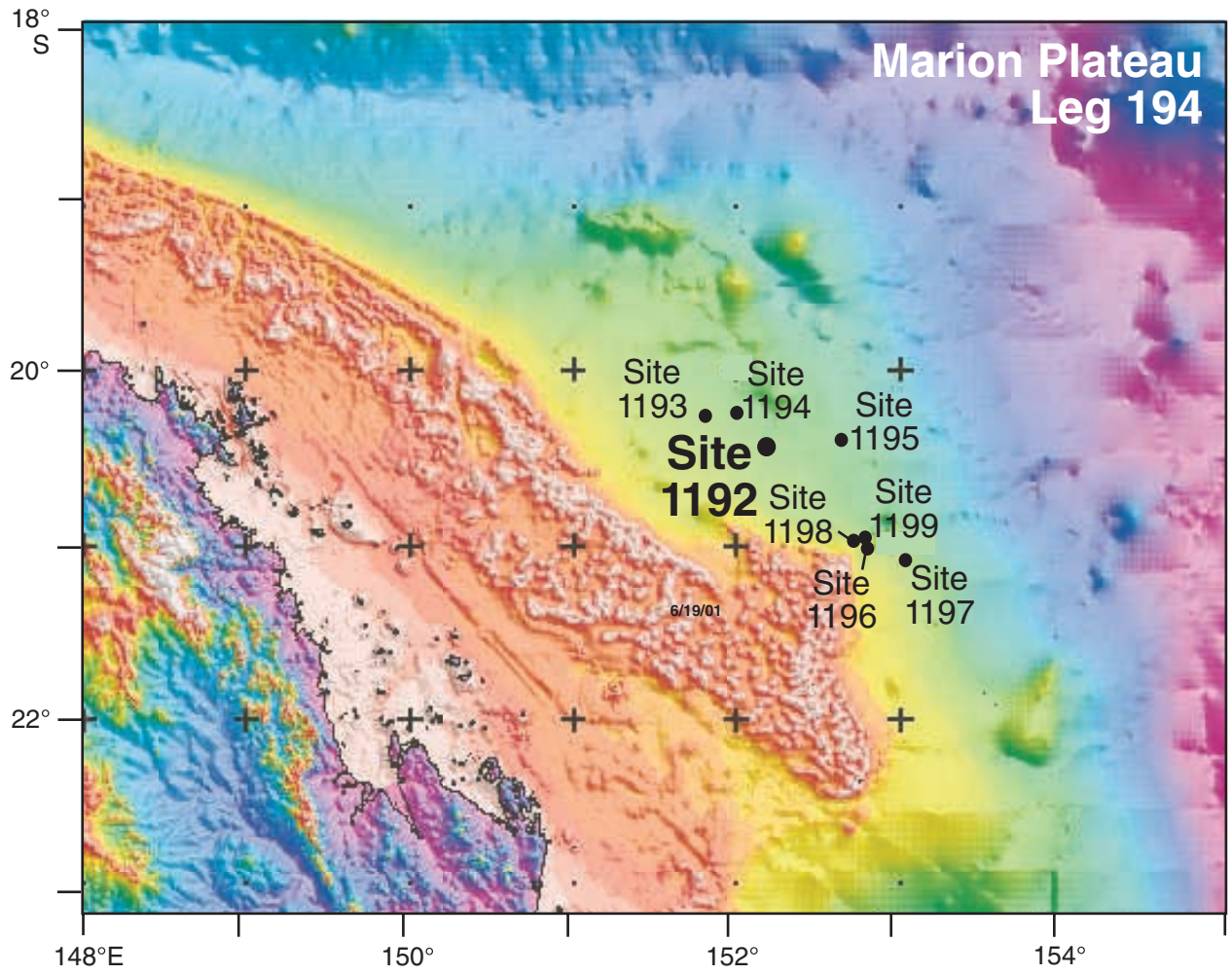
Figure F2. Lithologic summary for Site 1192. **A.** Recovery for Holes 1192A and 1192B. Black = recovered, white = gap. **B.** Lithologic unit boundaries. **C.** Graphic representation of the major sedimentary rocks encountered. **D.** Lightness (%) measured at 5-cm intervals and smoothed (thick blue line = Hole 1192A, thin red line = Hole 1192B). **E.** Sedimentary texture. **F.** Degree of lithification. **G.** Sedimentary environment. **H.** Age model derived from biostratigraphy (see **"Biostratigraphy and Paleoenvironments,"** p. 8).
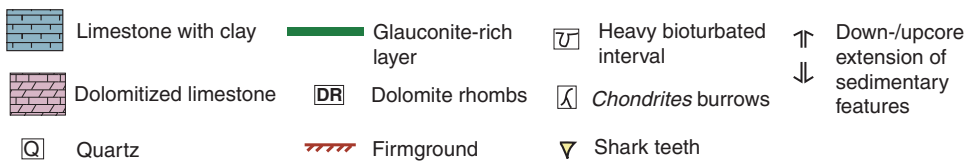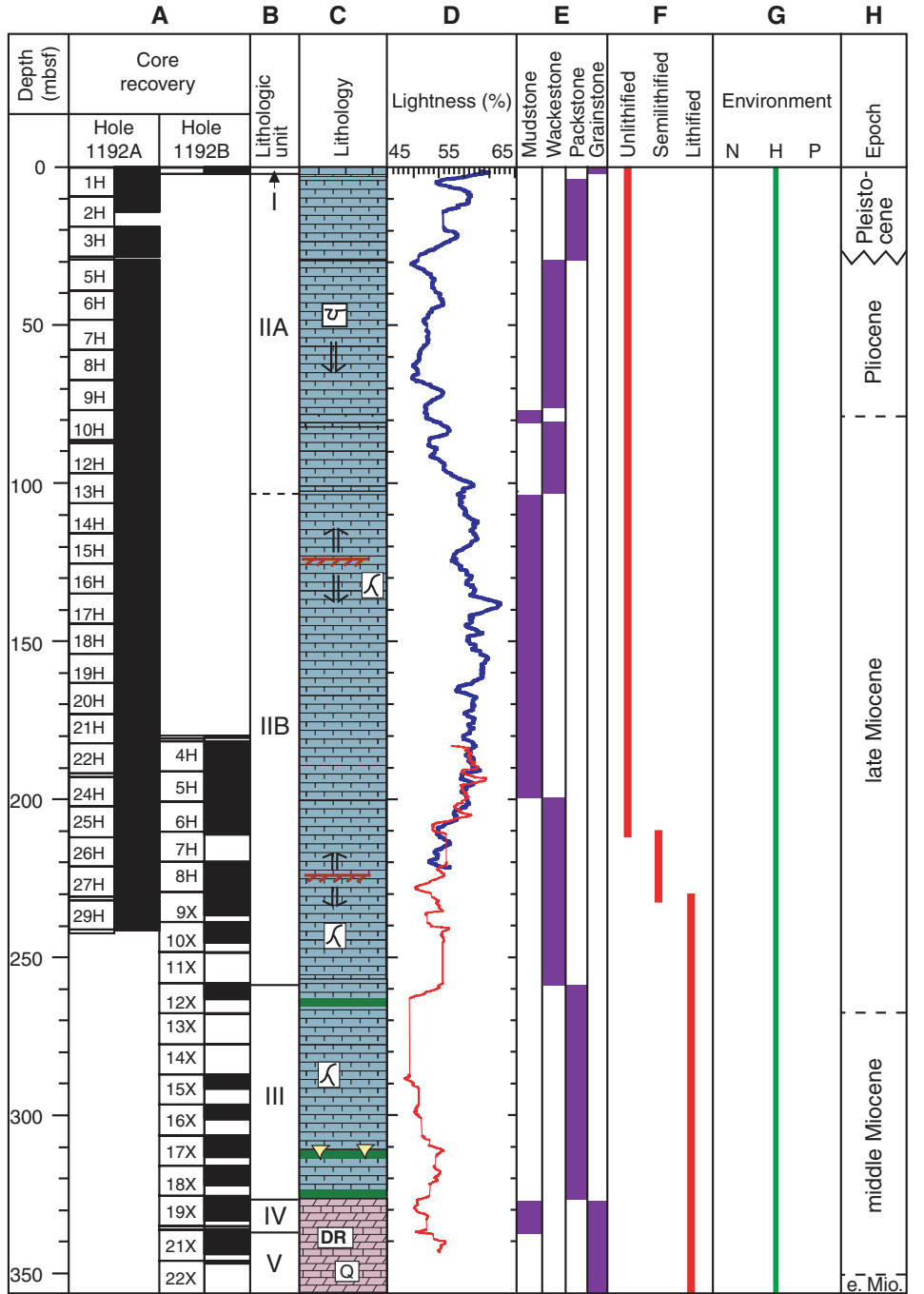
Figure F3. A. Close-up photograph of Sample 194-1192A-13H-5, 15–35 cm, showing a *Teichichnus* ichno-fossil crosscutting a *Chondrites* ichnofossil. **B.** Close-up photograph of Sample 194-1192A-15H-6, 40–65 cm, showing a firmground at 48 cm. Below the firmground is a bioturbated mudstone revealing *Chondrites* ichnofossils. The firmground, perhaps having an eroded surface, is immediately covered by a packstone.

Figure F4. Color reflectance data and calcium carbonate content data plotted against depth, indicating a relationship between these two properties.
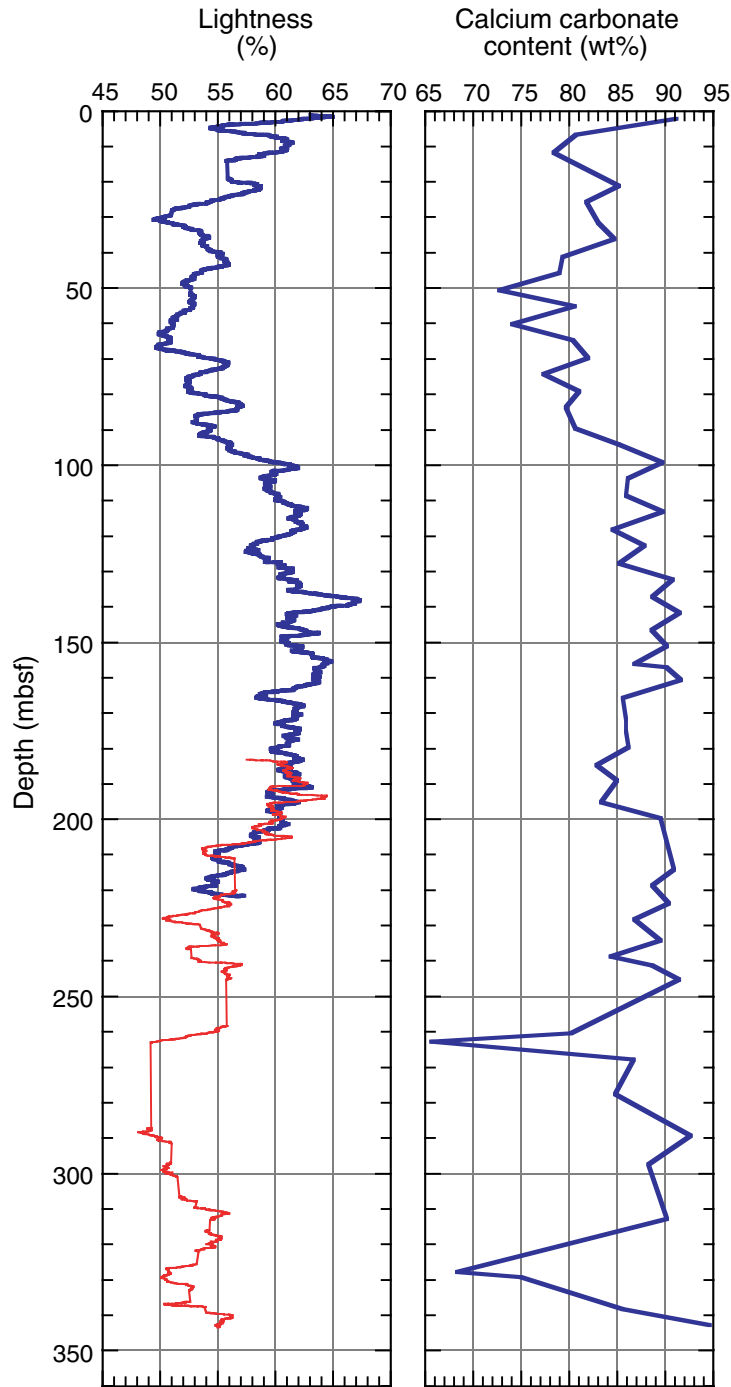
Figure F5. Photomicrograph of Unit I microfacies from Sample 194-1192B-1H-1, 58 cm, illustrating a skeletal packstone with planktonic and benthic foraminifers. Note the difference in lithology between in-fillings of intragranular pores (dense micrite) and those of intergranular pores (peloidal, silt-sized micrite) indicative of grain reworking.
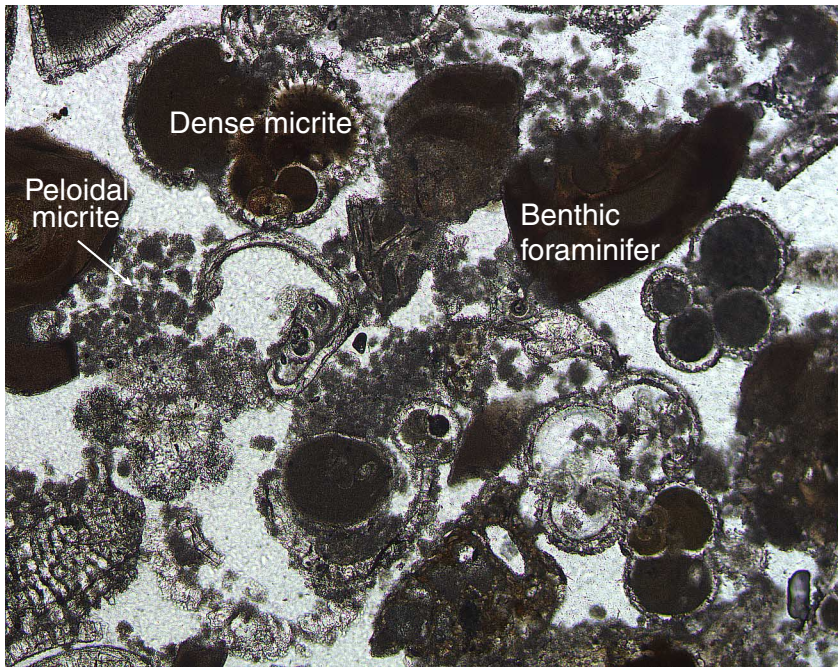
200 µm

Figure F6. A. Subunit IIA microfacies from Sample 194-1192B-9X-1, 140–142 cm, under cross-polarized light. This photomicrograph illustrates a skeletal wackestone with planktonic foraminifers. **B.** Subunit IIA microfacies from Sample 194-1192B-9X-1, 140–142 cm, under cross-polarized light. This photomicrograph illustrates a skeletal wackestone with planktonic foraminifers. Broken specimen shows evidence of early compaction.
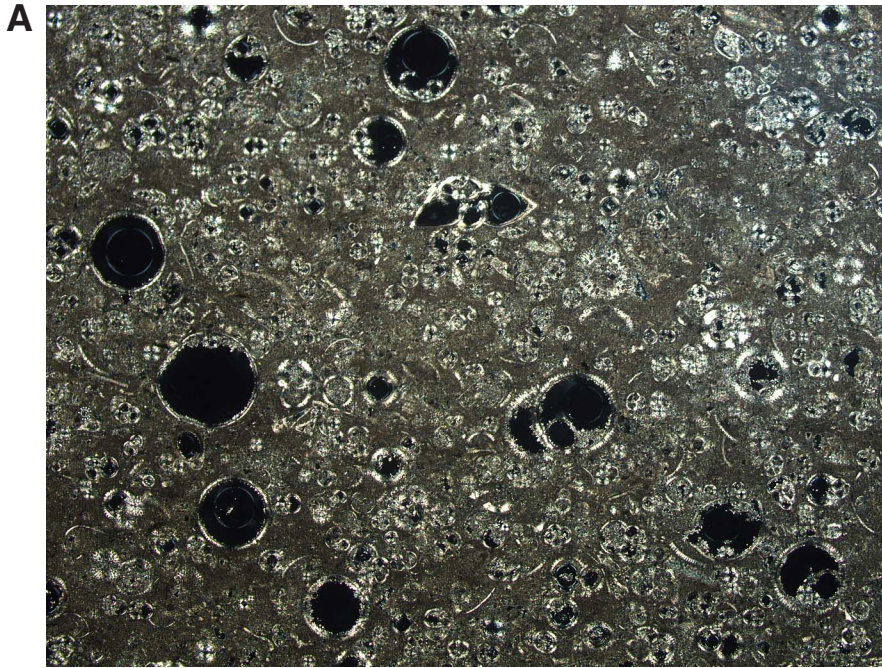
1 mm
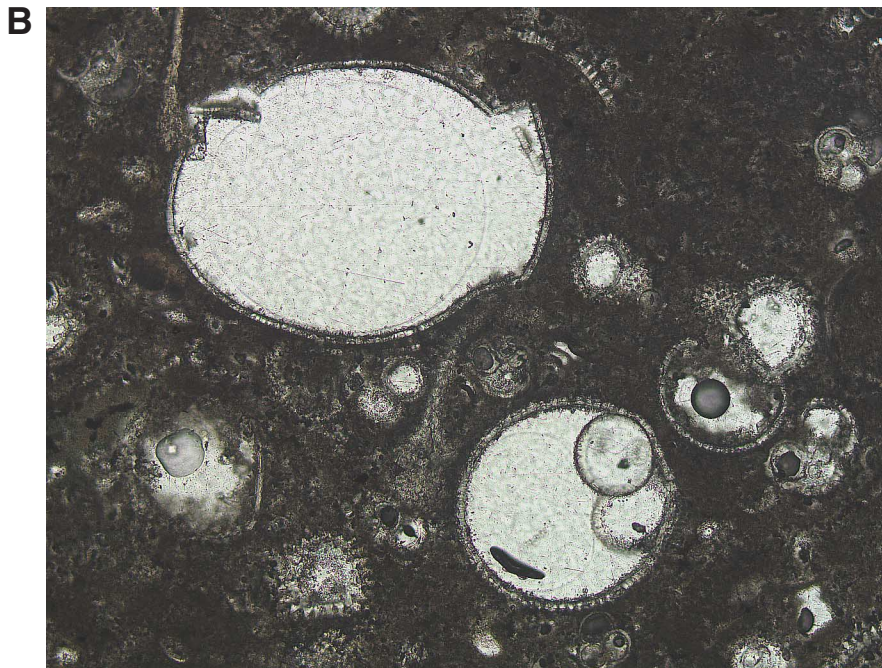
200 µm

Figure F7. A. Unit III microfacies from Sample 194-1192B-12X-3, 25–27 cm, under cross-polarized light. This photomicrograph illustrates a skeletal wackestone with planktonic foraminifers (pf) and quartz (qz). Quartz grains are ~300 µm in diameter and are irregularly distributed. **B.** Unit III microfacies from Sample 194-1192B-12X-3, 25–27 cm, under cross-polarized light. This photomicrograph illustrates skeletal wackestone with planktonic foraminifers, thin-shelled fragments, quartz, glauconite, and pyrite. **C.** Unit III microfacies from Sample 194-1192B-12X-3, 25–27 cm, under plane-polarized light. This photomicrograph illustrates a skeletal wackestone with planktonic and benthic foraminifers. Benthic foraminifers are pervasively glauconitized, whereas planktonic foraminifers are not. The former could represent reworked grains from older sediment or could originate from a coeval but shallower depositional setting.
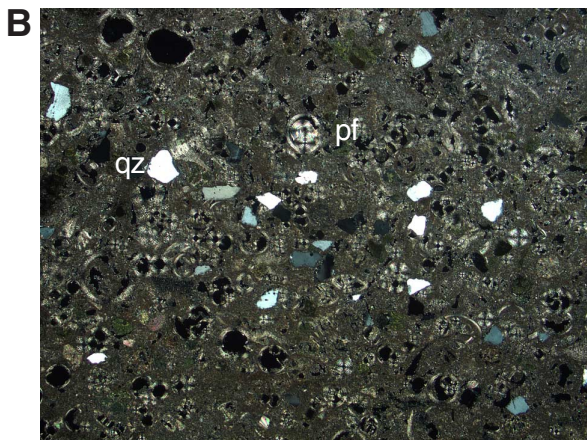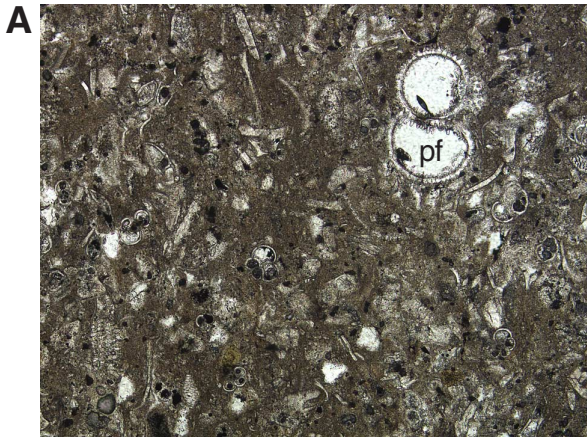
Figure F8. A. Unit IV microfacies from Sample **194-1192B-19X-5, 124–126 cm,** under plane-polarized light. This photomicrograph illustrates a skeletal packstone containing both platform-derived and pelagic skeletal fragments and quartz (qz). Wispy laminations can also be seen. **B.** Unit IV microfacies from Sample 194-1192B-19X-5, 124–126 cm, under plane-polarized light. This photomicrograph illustrates a skeletal packstone. Greater magnification more effectively reveals the pelagic and neritic components (planktonic foraminifers [pf] and bryozoan fragments).
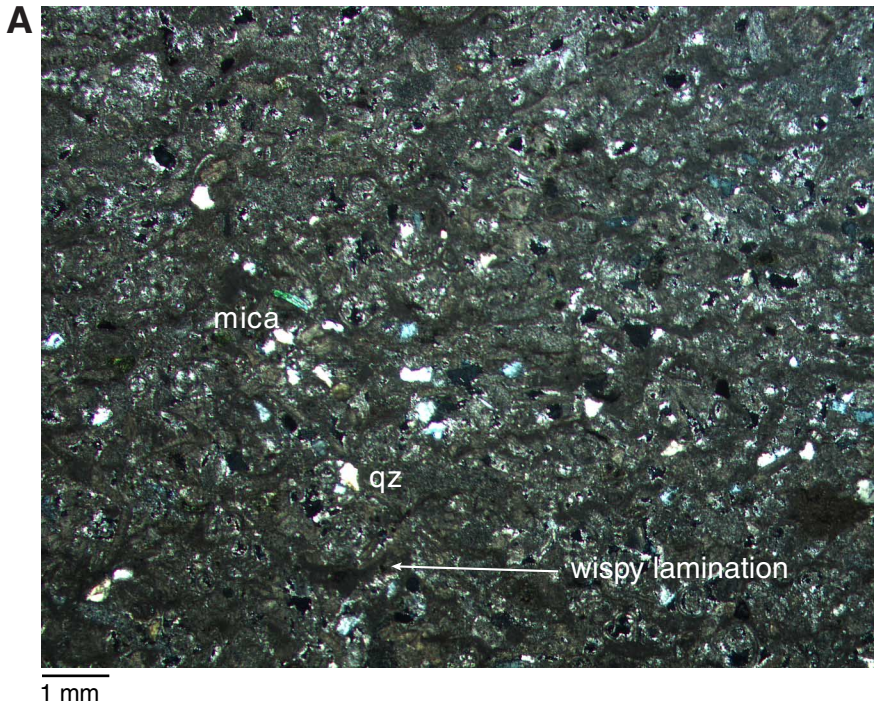
Figure F9. Long-core measurements for Hole 1192A showing intensity, inclination, and interpreted magnetostratigraphy. **A.** Measurements for 0–100 mbsf. (Continued on next two pages.)
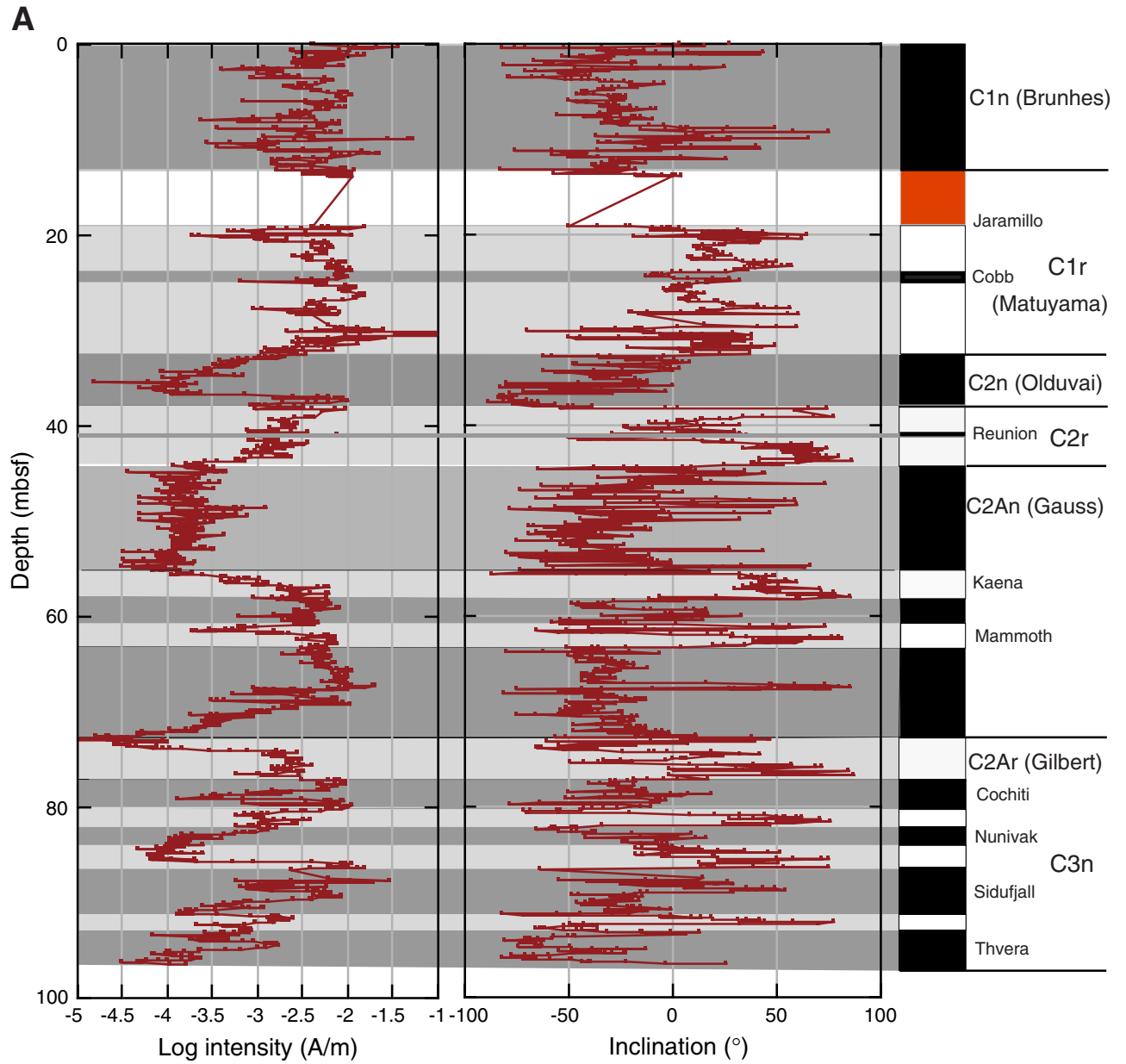
Figure F9 (continued). B. Measurements for 100–150 mbsf.
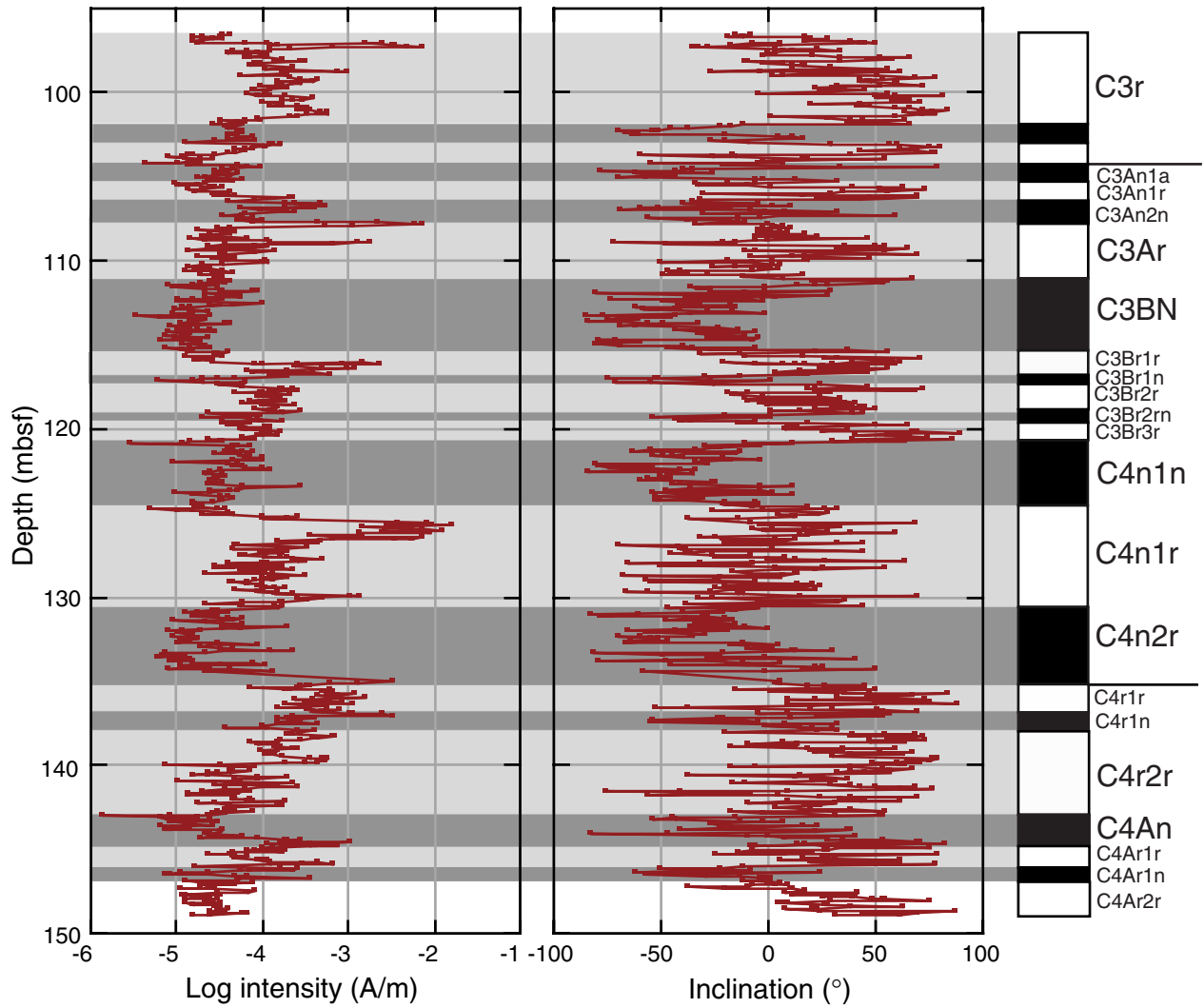
Figure F9 (continued). C. Measurements for 150–270 mbsf.
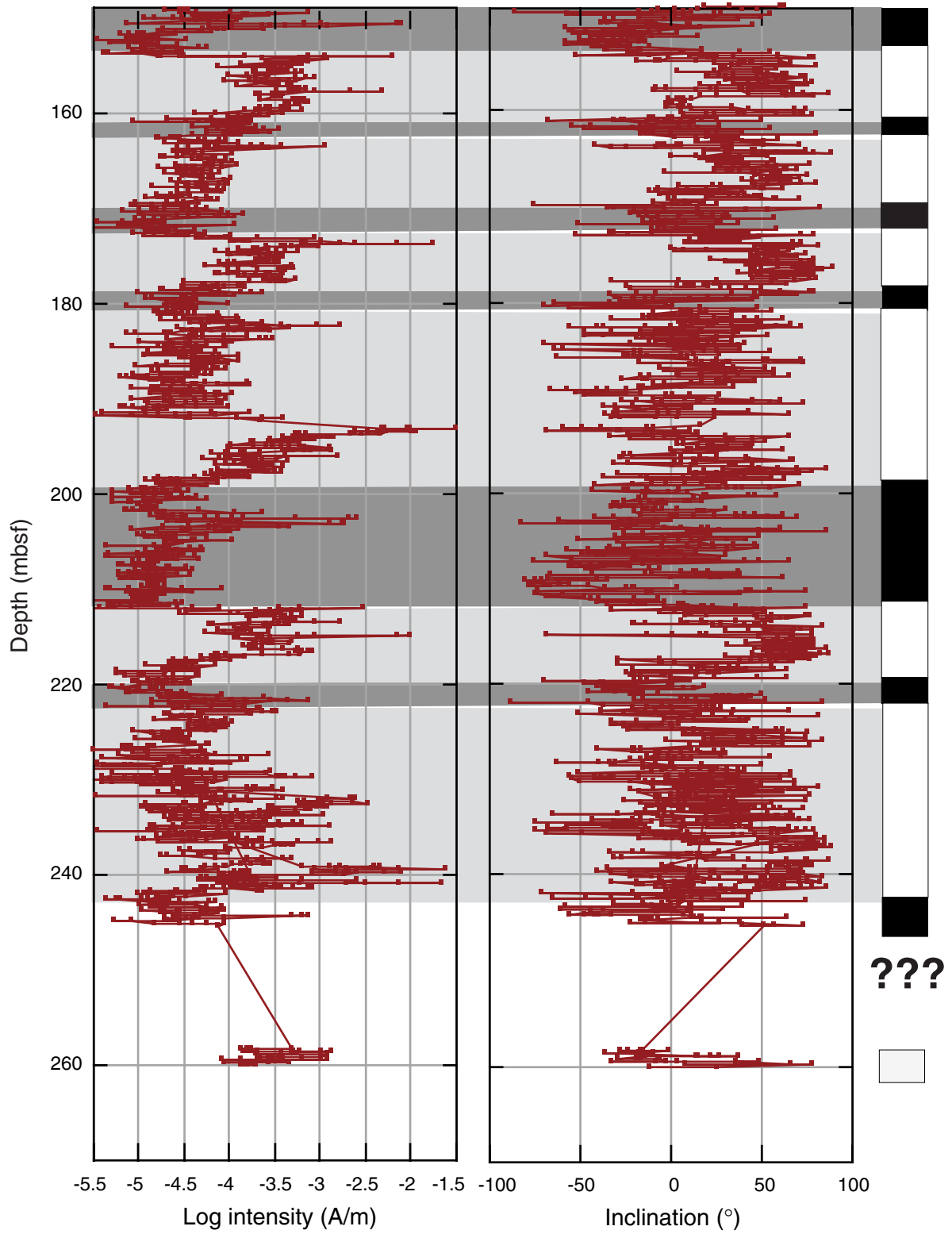
Figure F10. Long-core measurements for Hole 1192B, 0–2.5 mbsf, showing intensity, inclination, and interpreted magnetostratigraphy. Shading = normal polarity interval.
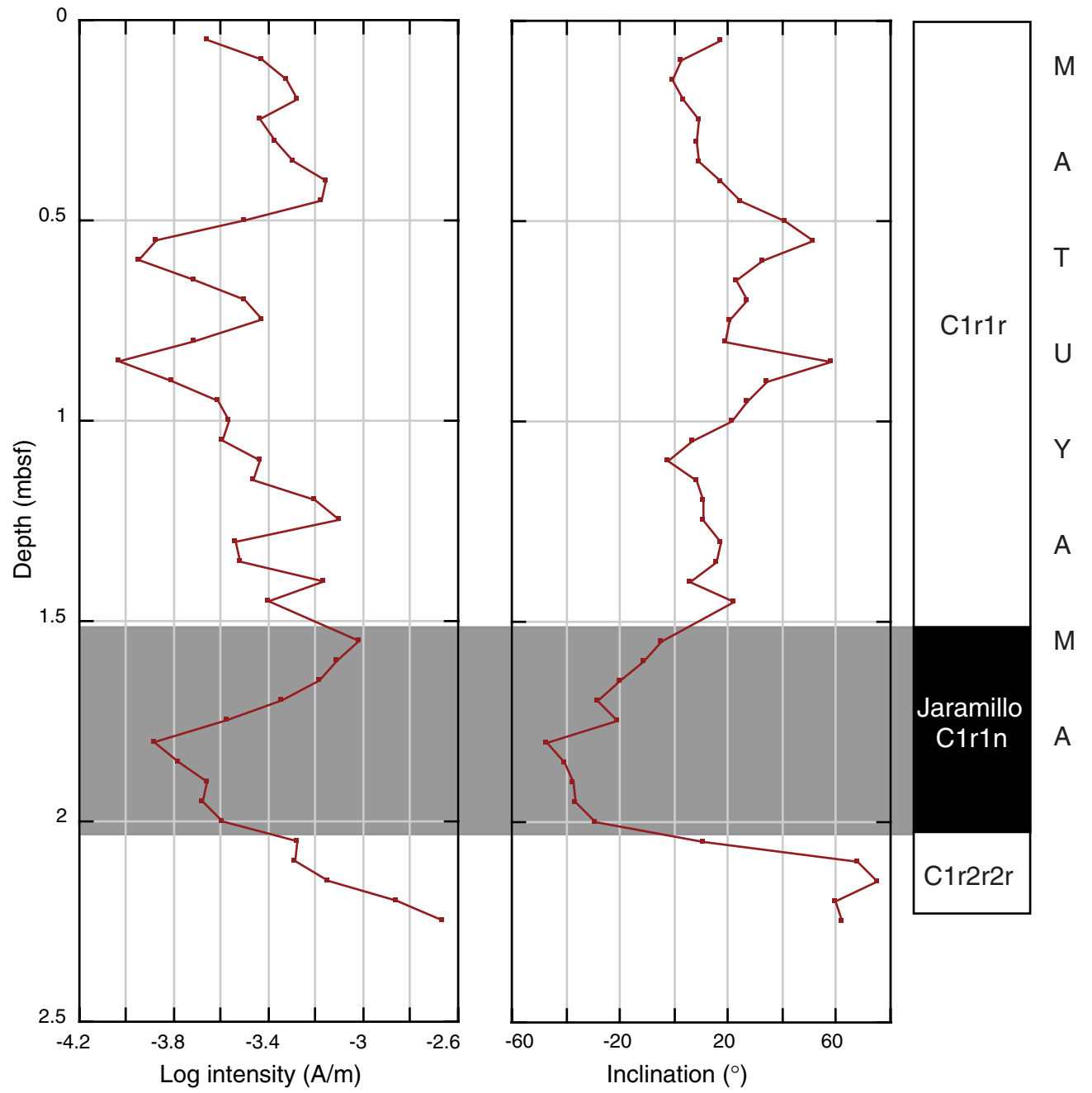
Figure F11. Long-core measurements for Hole 1192B showing intensity, inclination, and interpreted reversal sequence. **A.** Measurements for 180–300 mbsf. (Continued on next page.)
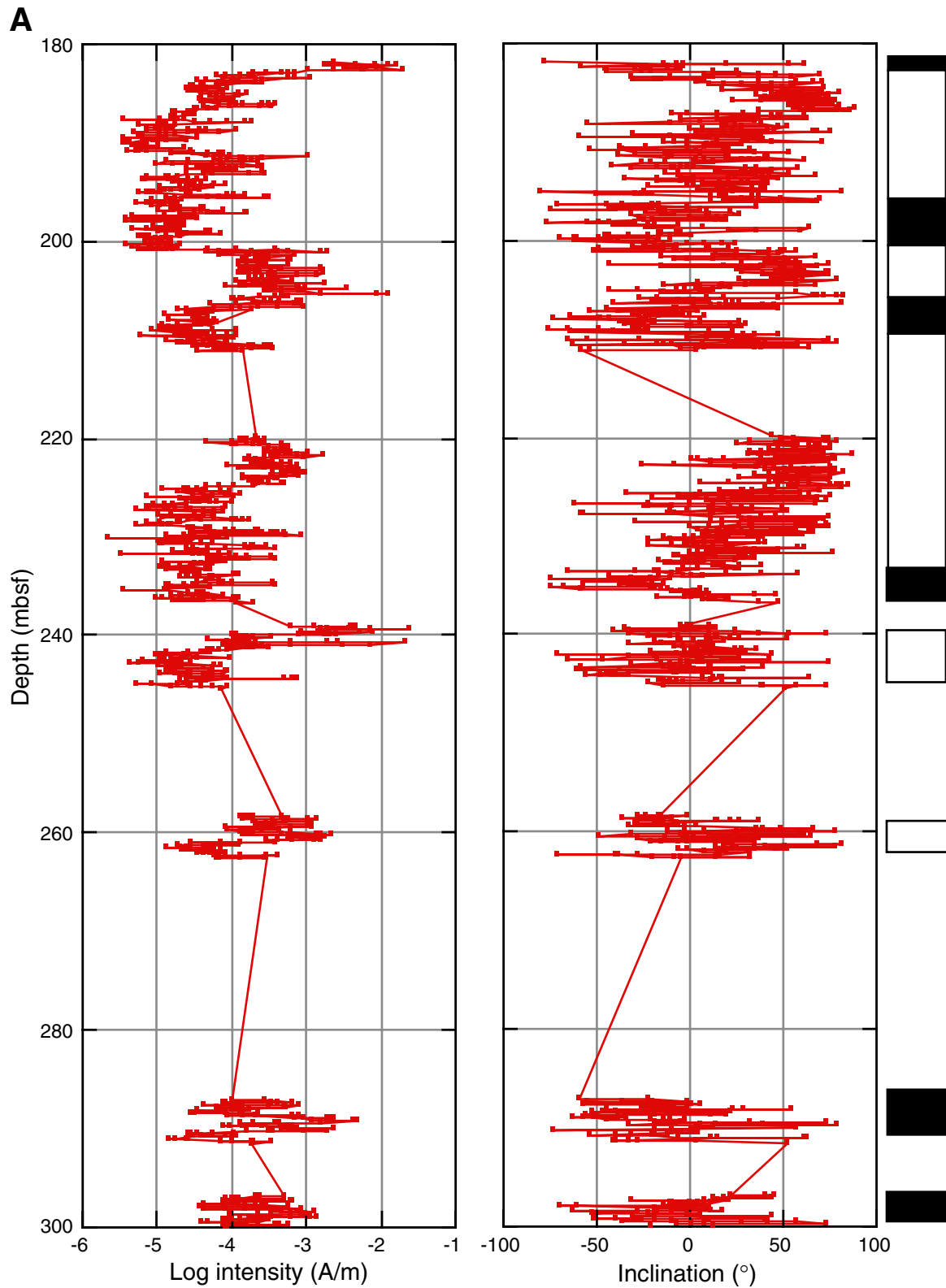
Figure F11 (continued). B. Measurements for 300–350 mbsf.
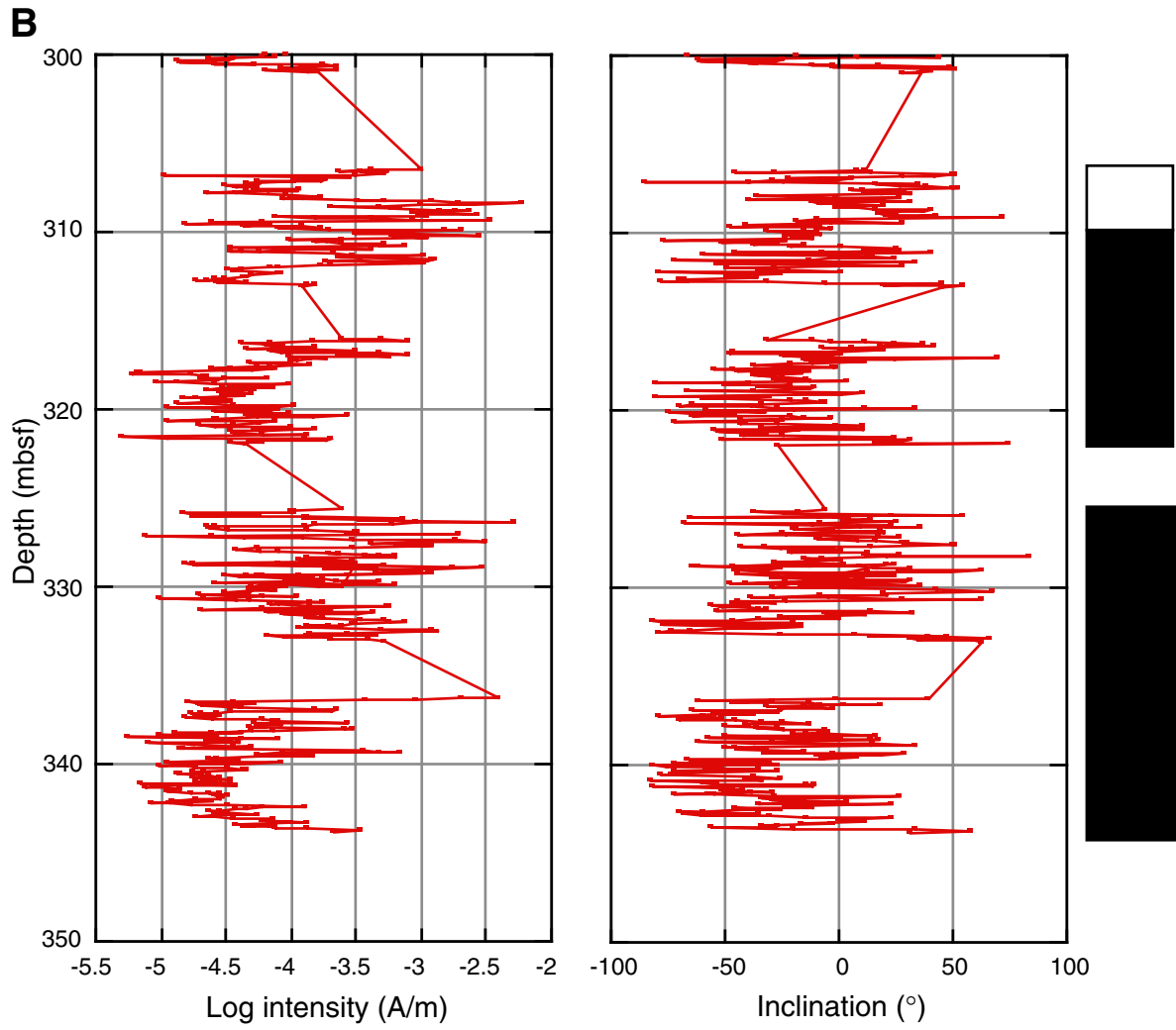
Figure F12. Stereographic plot of directions of magnetization in ODP coordinates (i.e., +z = down, +x = in the direction of the double line on the working half of core liners). **A.** Natural remanent magnetization (NRM). **B.** After 30-mT demagnetization.
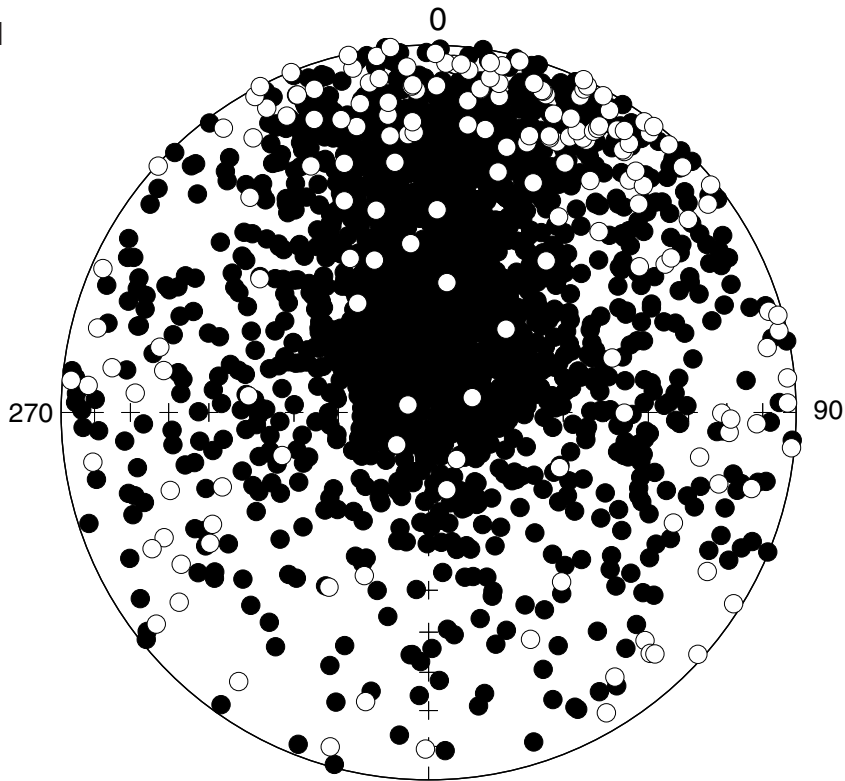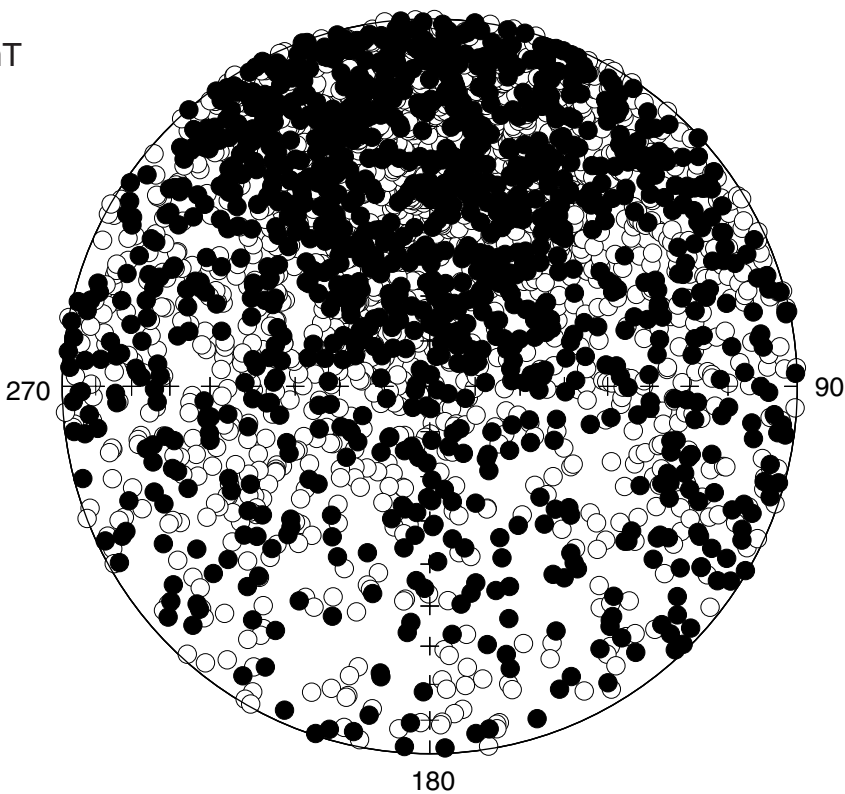
Figure F13. Core-top anomalies in the paleomagnetic data of Hole 1192A: plots of magnetic susceptibility, core depths, intensity, and inclination from 100 to 200 mbsf. Note the increases in susceptibility and remanence associated with core tops.
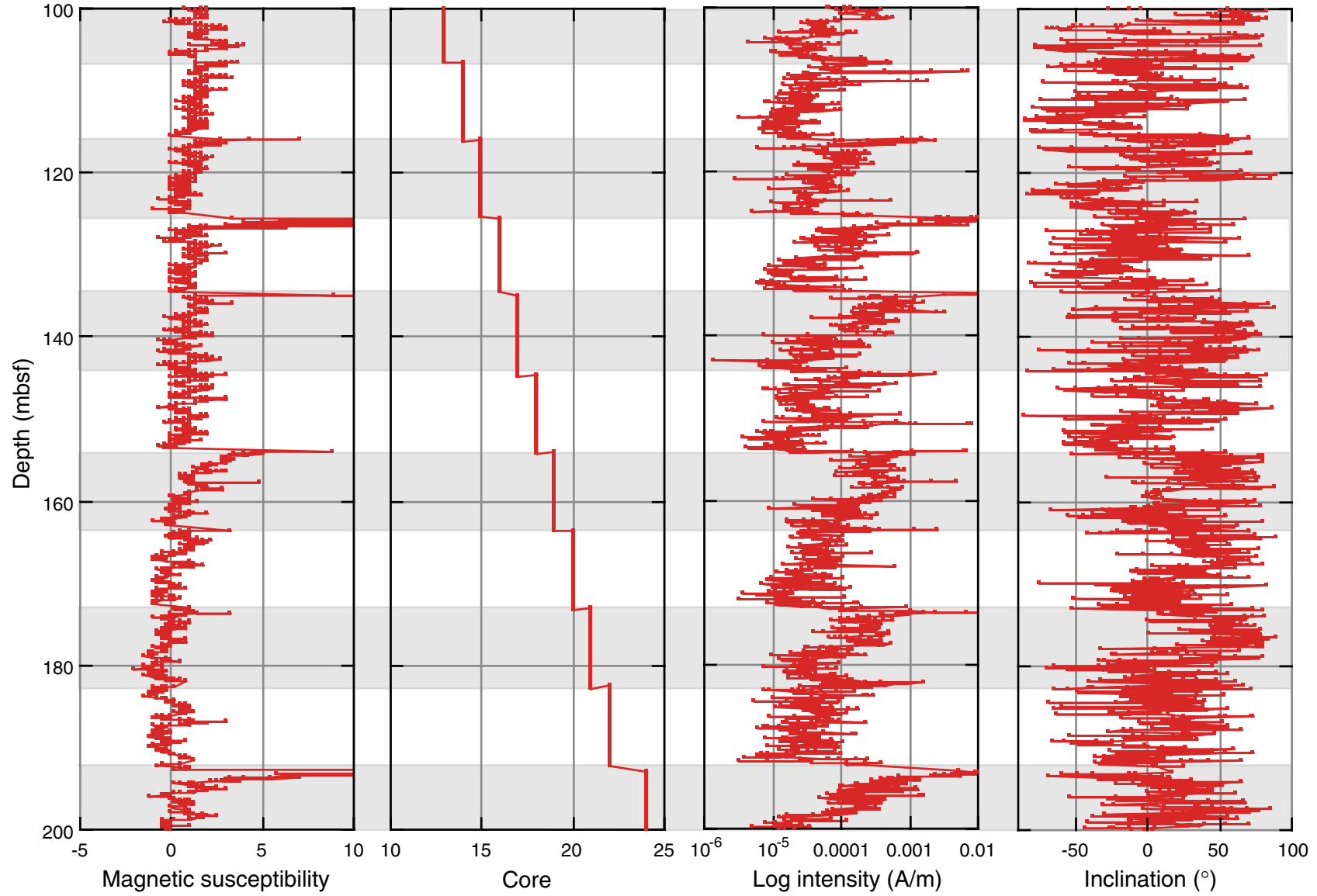
Figure F14. Remanent magnetic characteristics of Samples 194-1192A-3H-2, 50–52 cm; 5H-5, 50–52 cm; 15H-6, 50–52 cm; and 24H-3, 40–42 cm. Note the differences between the upper two samples, which are only separated by one intervening core, and the similarity between the lower samples, which are from intervals almost 100 m apart. ARM = anhysteretic remanent magnetization, IRM = isothermal remanent magnetization, acq = acquisition, demag = demagnetization.
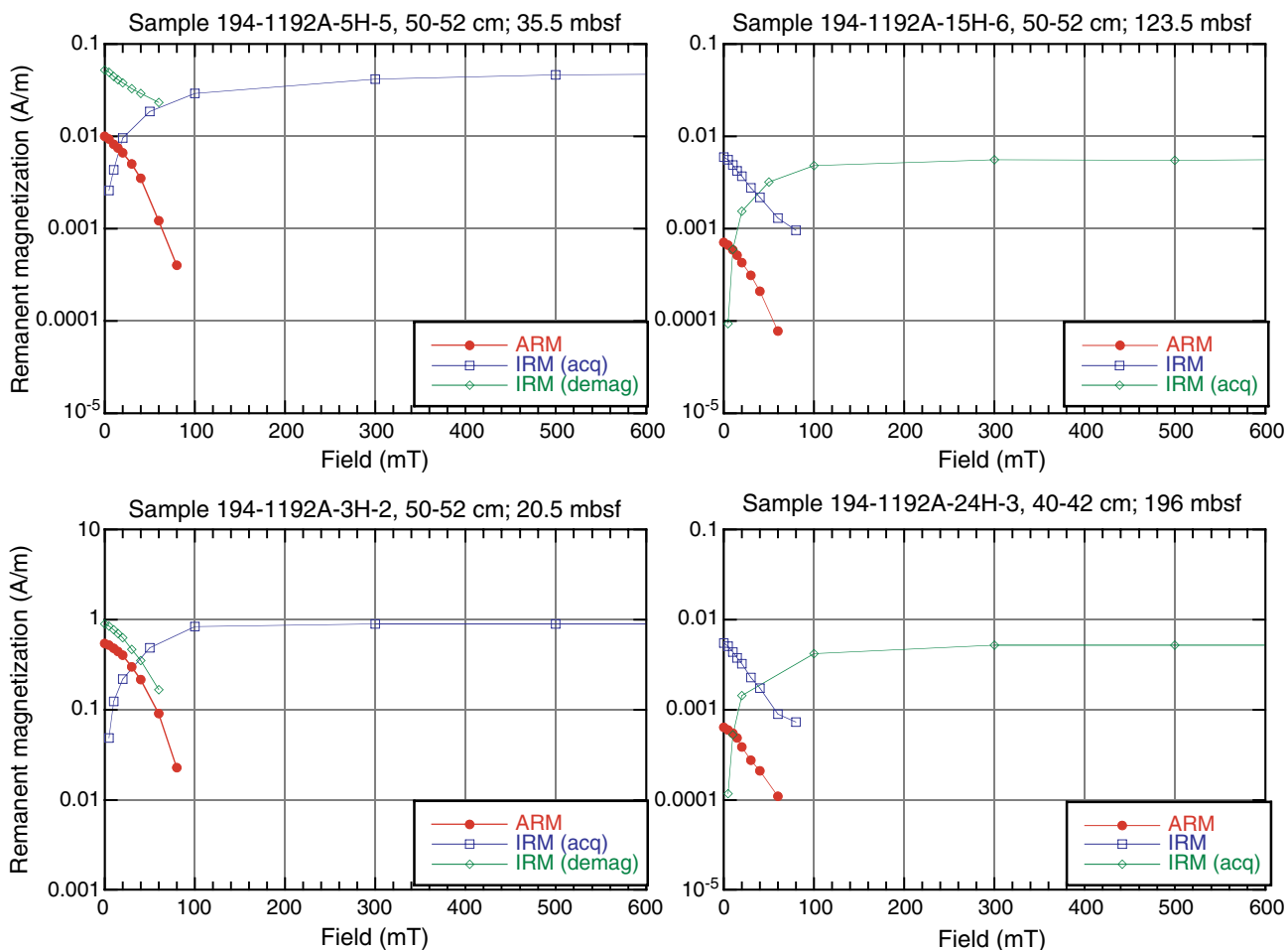
Figure F15. Variation downcore in Hole 1192A of (**A**) anhysteretic remanent magnetization (ARM) and isothermal remanent magnetization (IRM), (**B**) ARM/IRM, and (**C**) ratio of IRM acquired at 100 mT to IRM acquired at 1 T.
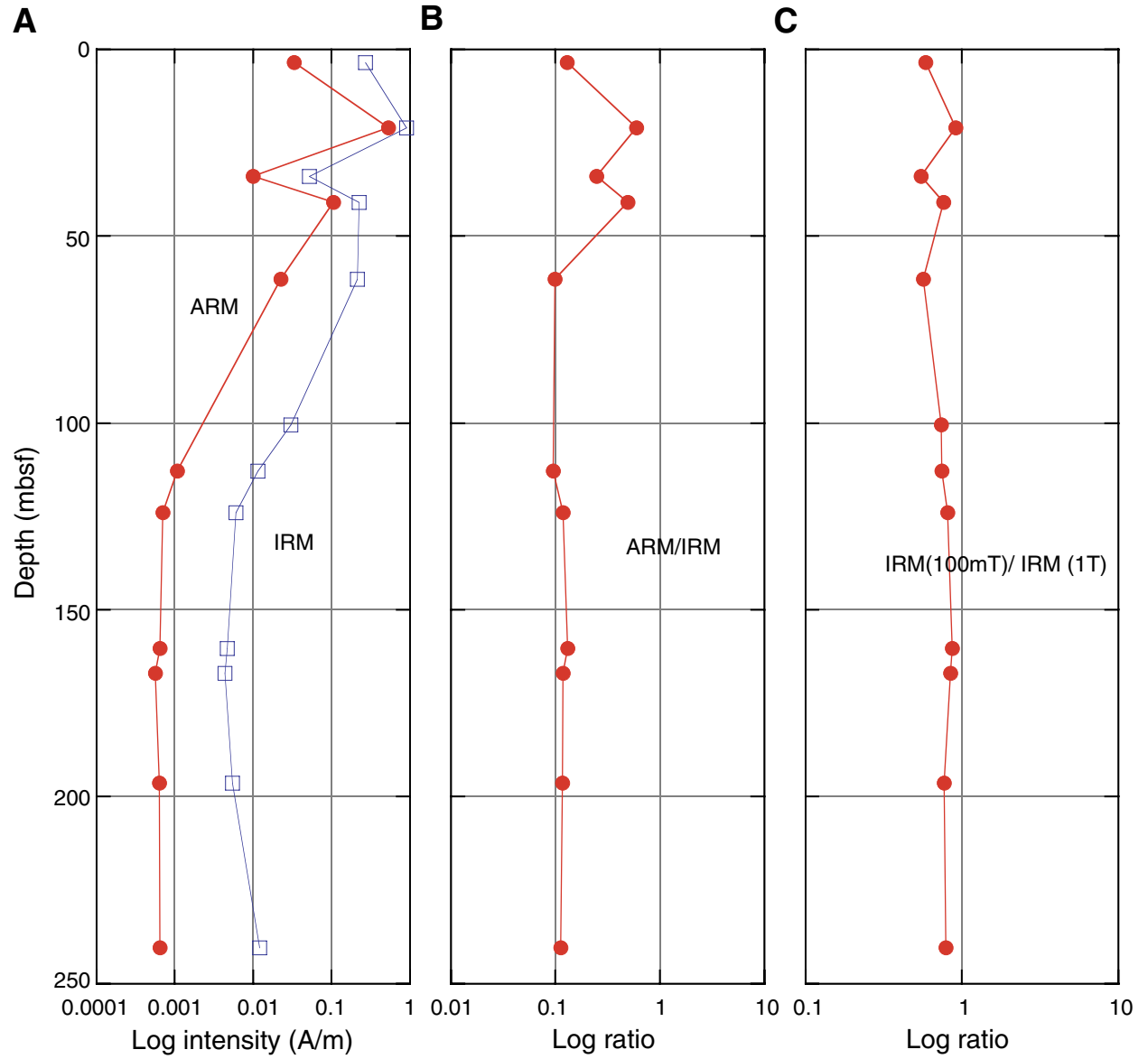
Figure F16. Age-depth model and sedimentation rates at Site 1192. Horizontal lines spanning from the left figure margin to the age-depth curve are lithologic unit (solid) and subunit (dashed) boundaries. Horizontal lines spanning from the right margin of the figure to the age-depth curve are seismic megasequence boundaries (solid) and major reflectors within megasequences (dashed). Vertical lines are epoch boundaries as labeled at the top of the diagram. MS = Megasequence.
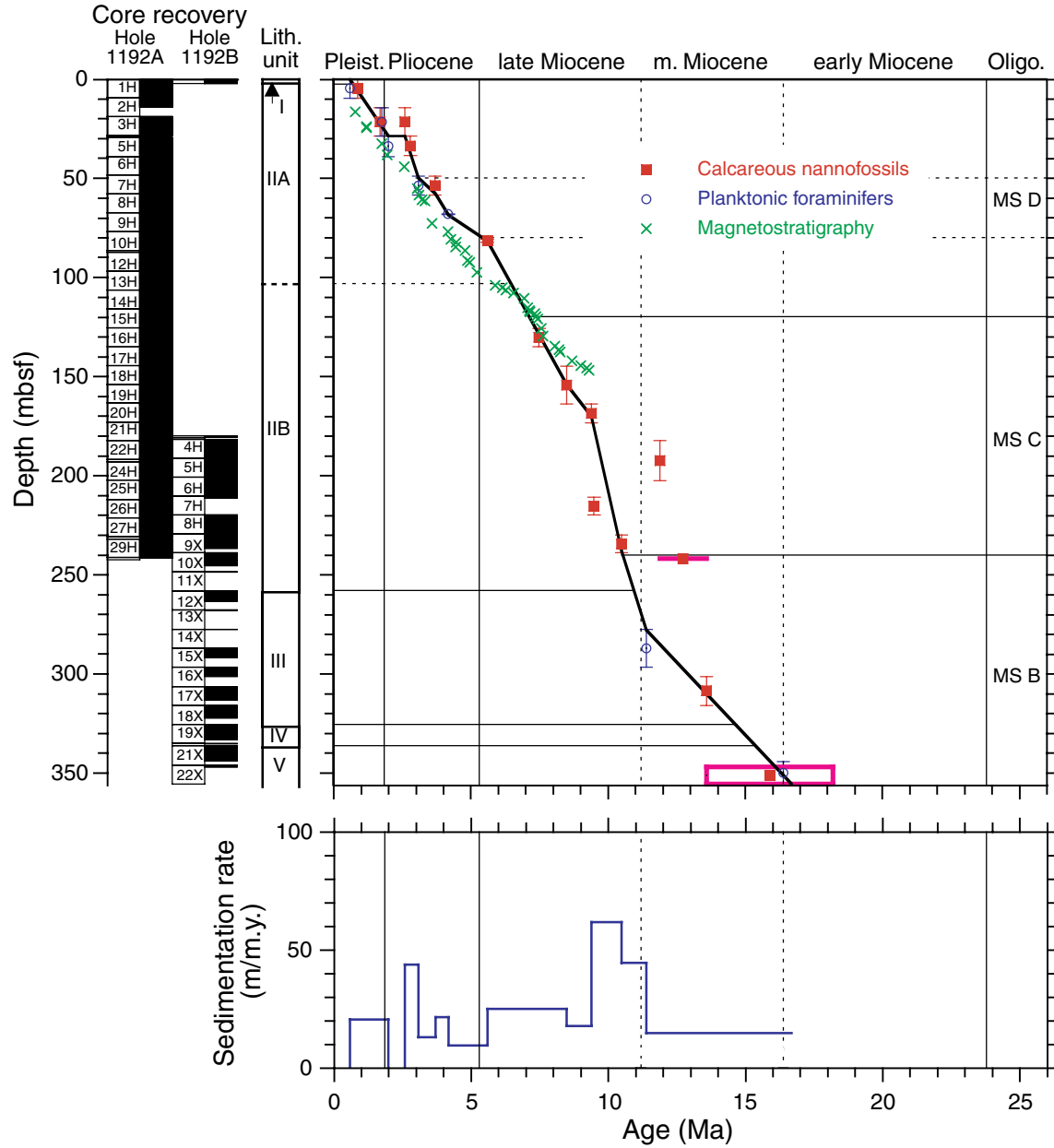
Figure F17. Concentrations of dissolved constituents vs. depth. **A.** Chloride. **B.** Alkalinity. **C.** Potassium. **D.** Calcium. **E.** Magnesium. **F.** Strontium. **G.** Sulfate. **H.** Ammonium. **I.** Iron. Solid circles = Hole 1192A, open circles = Hole 1192B.
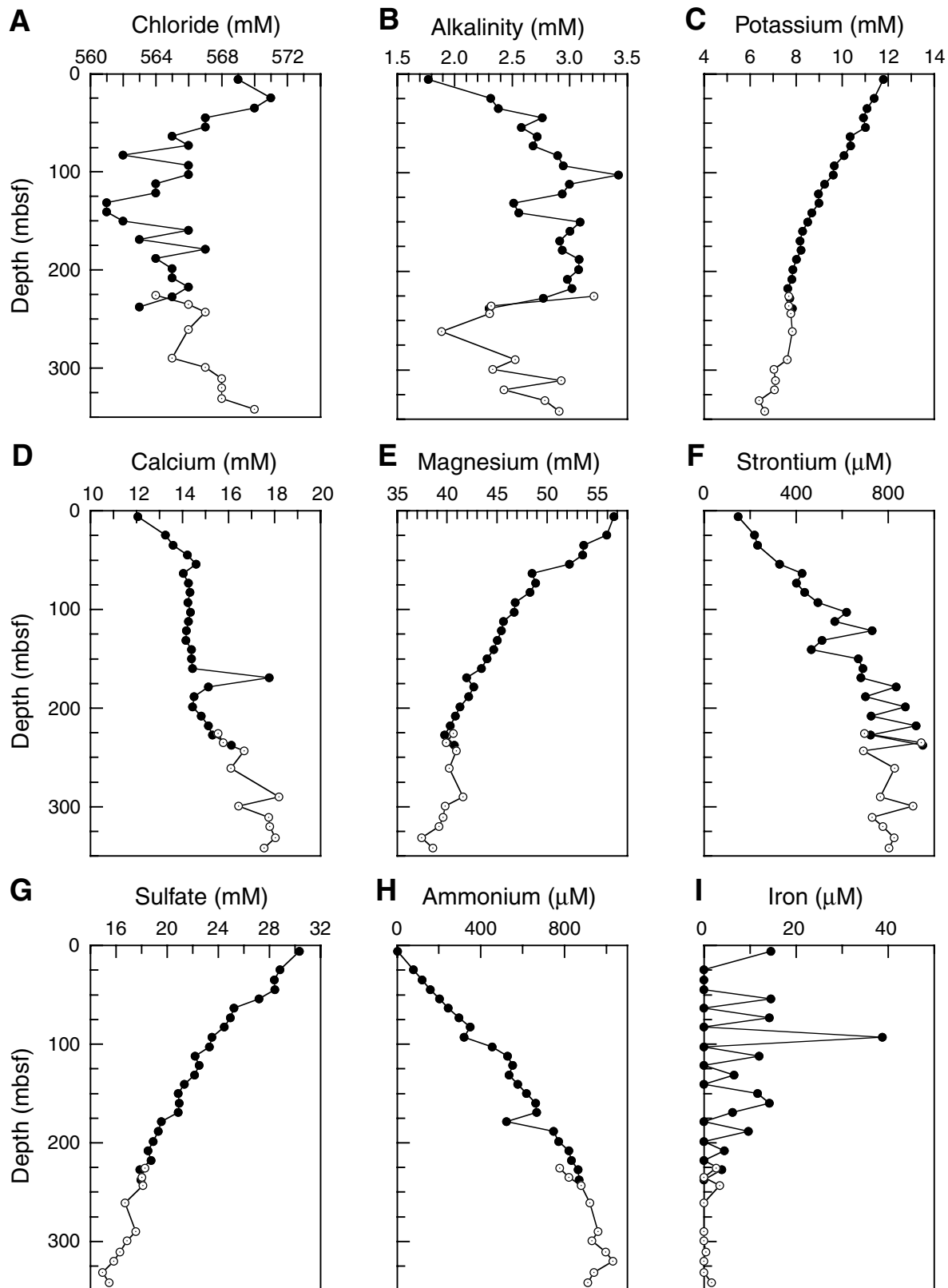
Figure F18. Dissolved magnesium vs. calcium at Site 1192. Solid circles = Hole 1192A, open circles = Hole 1192B.
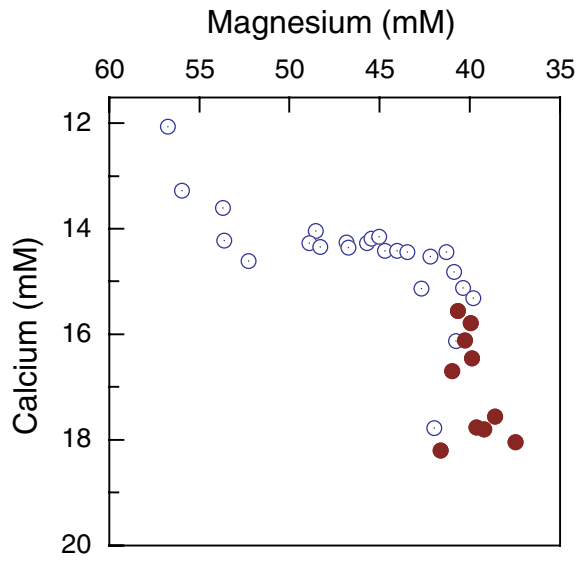
Figure F19. Dissolved magnesium vs. sulfate at Site 1192, illustrating the covariation of the two parameters (r^2 = 0.98). Solid circles = Hole 1192A, open circles = Hole 1192B.
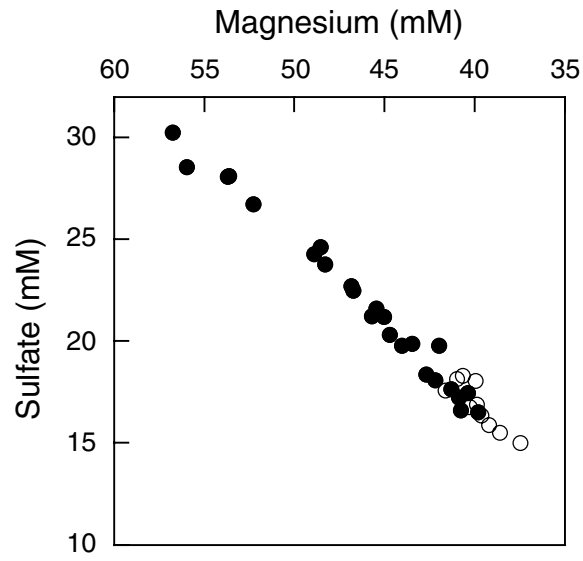
Figure F20. Calcium carbonate, total organic carbon, C/N ratios, hydrogen index values, total sulfur, and C/S ratios at Site 1192. The dashed line at HI = 150 marks the approximate boundary between terrigenous (<150) and marine organic matter, and the dashed line at C/N = 25 approximates the terrigenous organic matter field (~25–35).
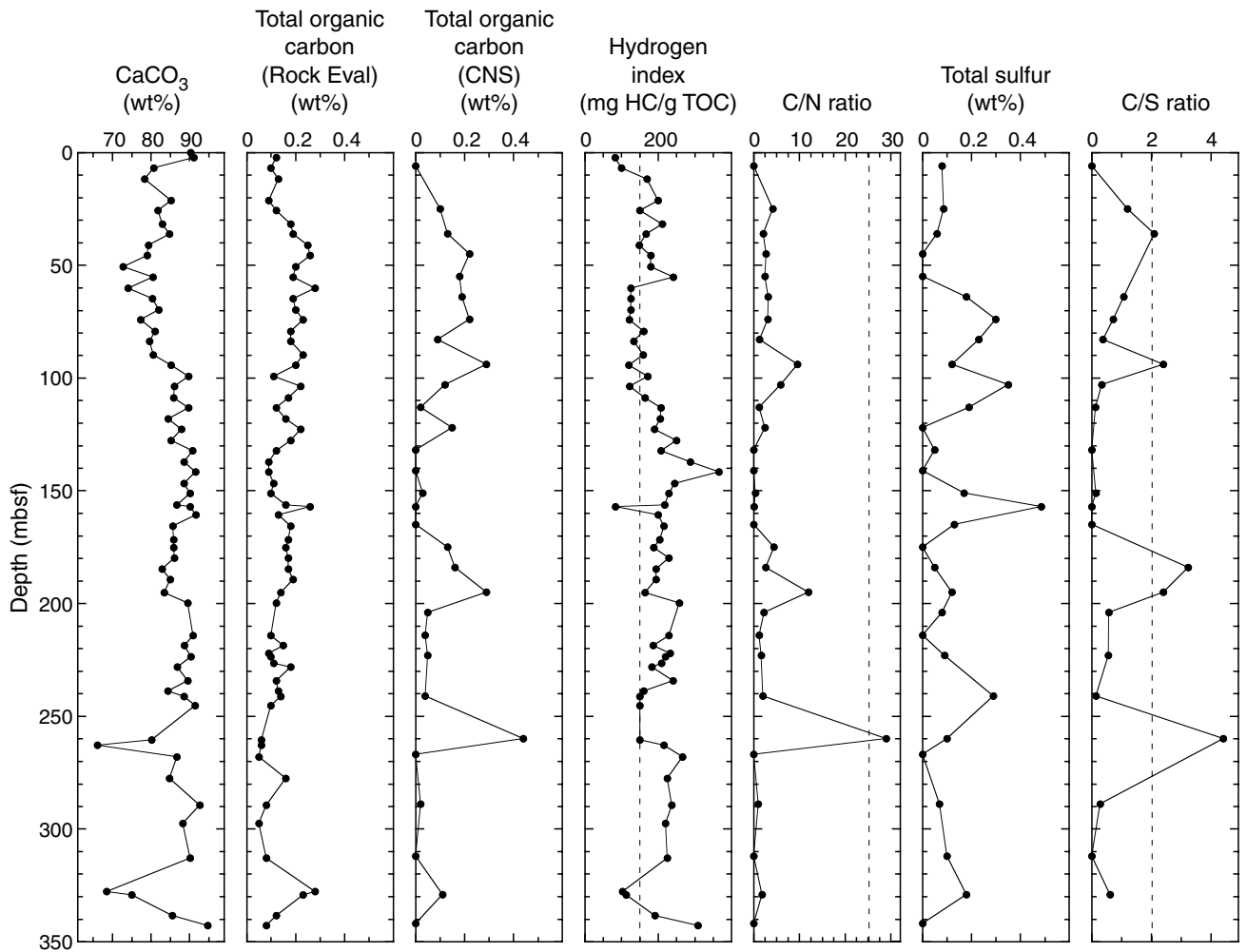
Figure F21. GRA bulk density for Holes 1192A (red dots) and 1192B (black lines) and MAD bulk density for Holes 1192A (black dots) and 1192B (blue squares) plotted as a function of depth.
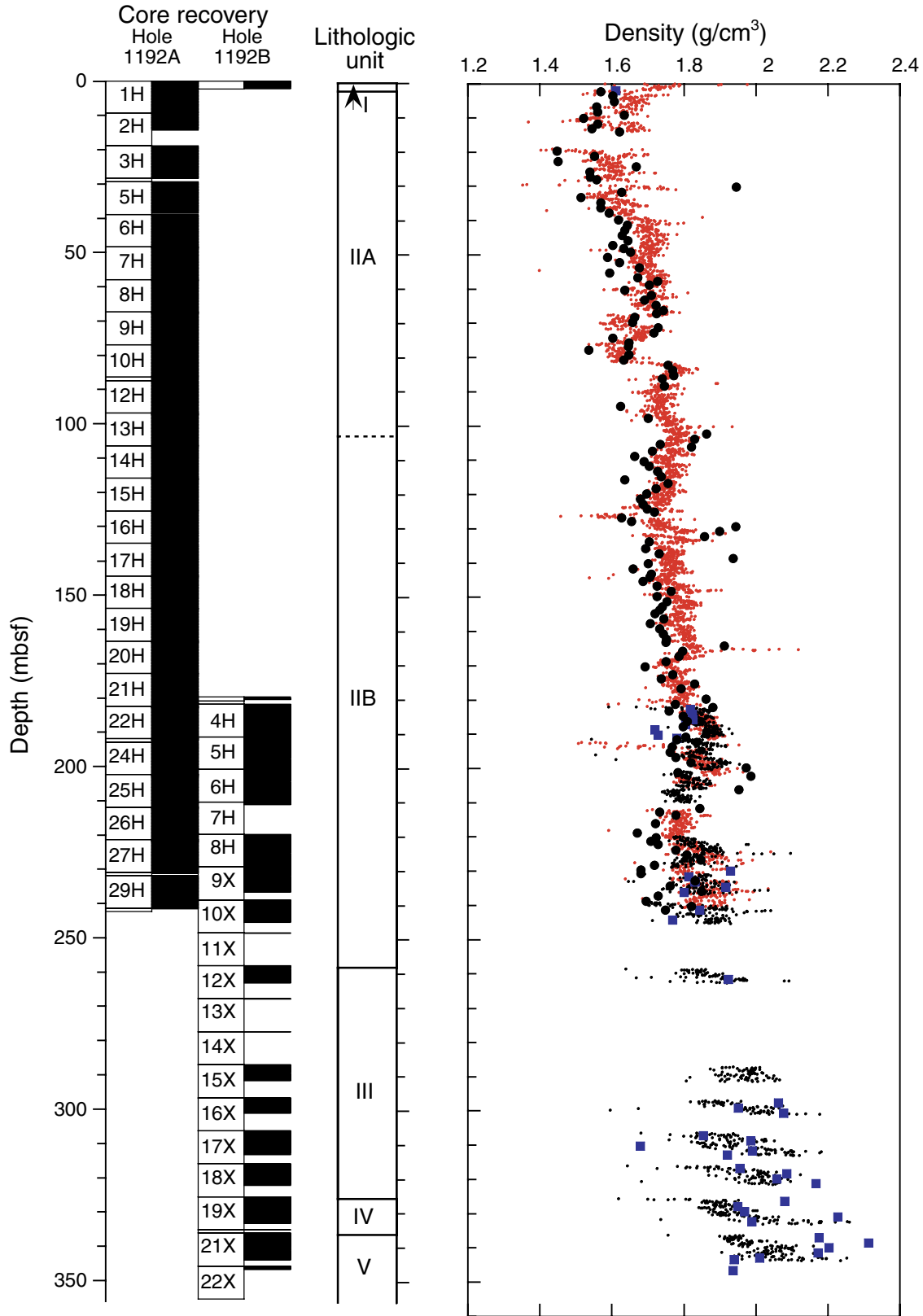
Figure F22. Bulk density, grain density, and porosity as a function of depth at Site 1192. Exponential least-squares regression of porosity using the combined Holes 1192A and 1192B data set is shown superposed on the porosity. Black circles = Hole 1192A data, gray circles = Hole 1192B data, open circles = data suspected of possible analytical error.

$$\phi(z) = 66.2\ e^{-0.001z}$$
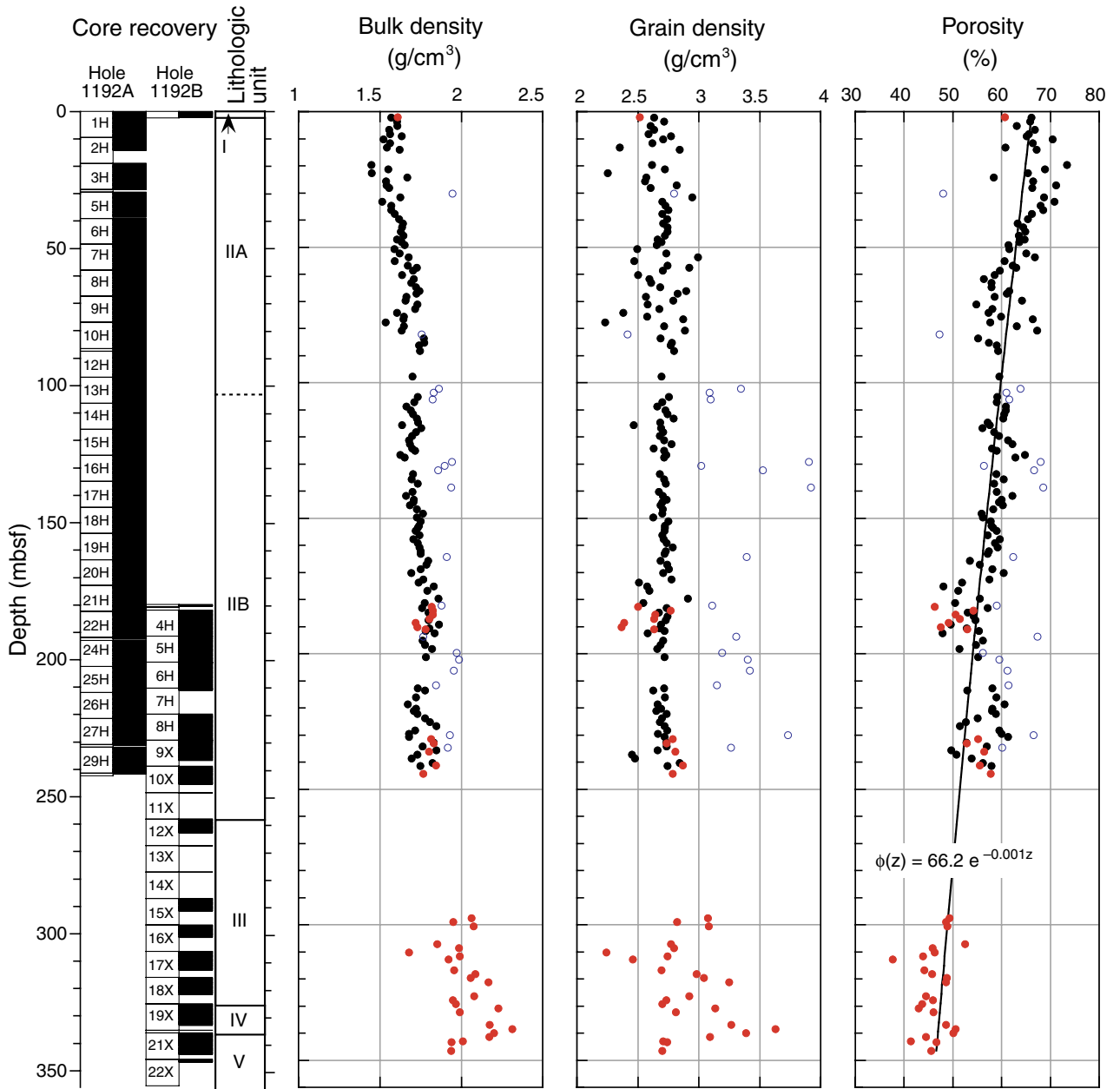
Figure F23. *P*-wave velocity (cross-core velocity; x-direction) as a function of depth at Site 1192 using the PWS3 contact probe system. **A.** Originally determined velocities for the 80–245 mbsf interval and remeasured velocities for the interval 0–80 mbsf. The velocity data that varies ~1580 m/s (0–80 mbsf) is considered reliable. **B.** Adjusted velocity data. A constant value of 346.5 m/s was subtracted from the higher values to match the lower ones.
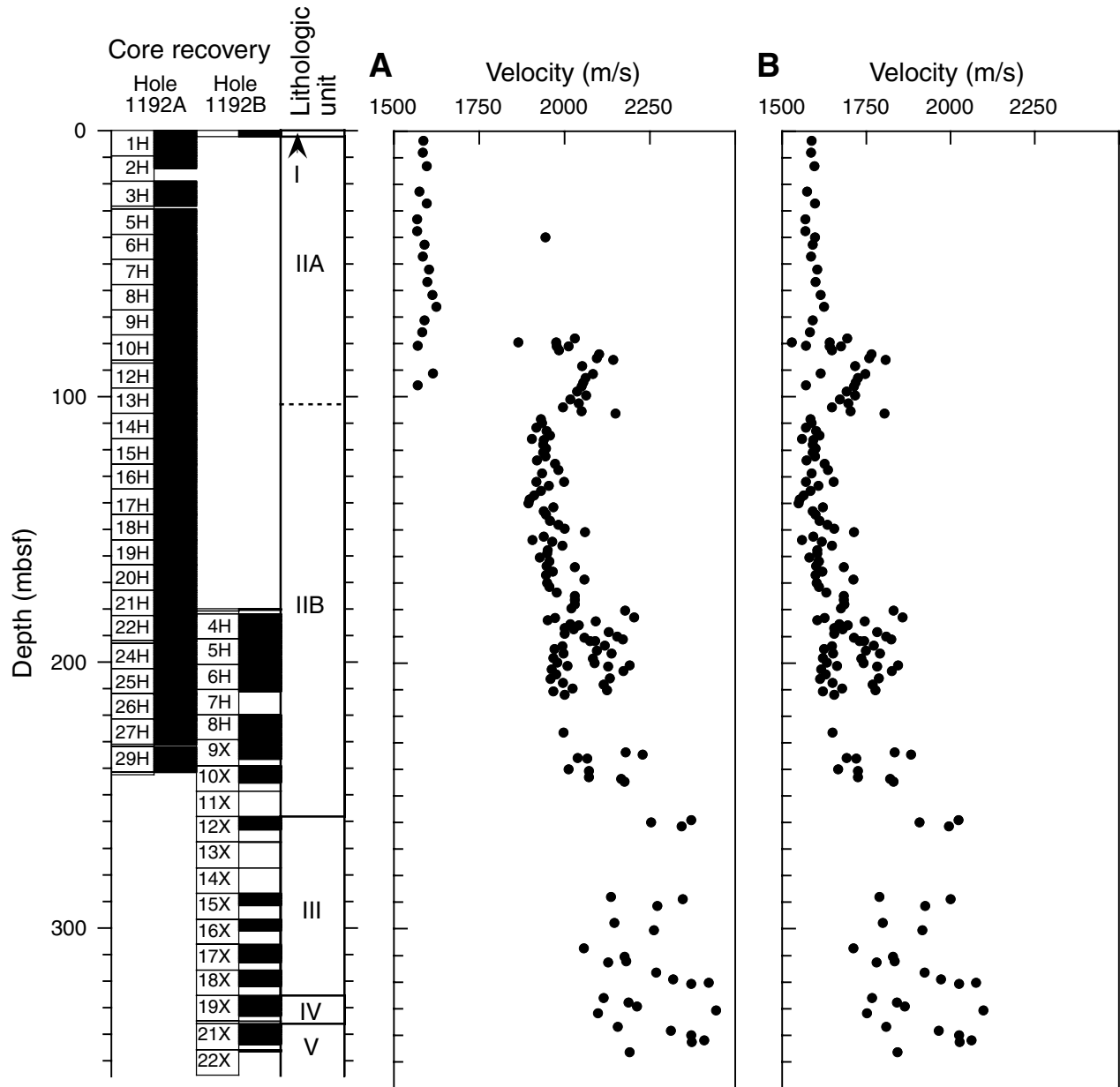
Figure F24. Average thermal conductivity at Site 1192 as a function of depth. Solid circles = Hole 1192A data, solid squares = Hole 1192B data.
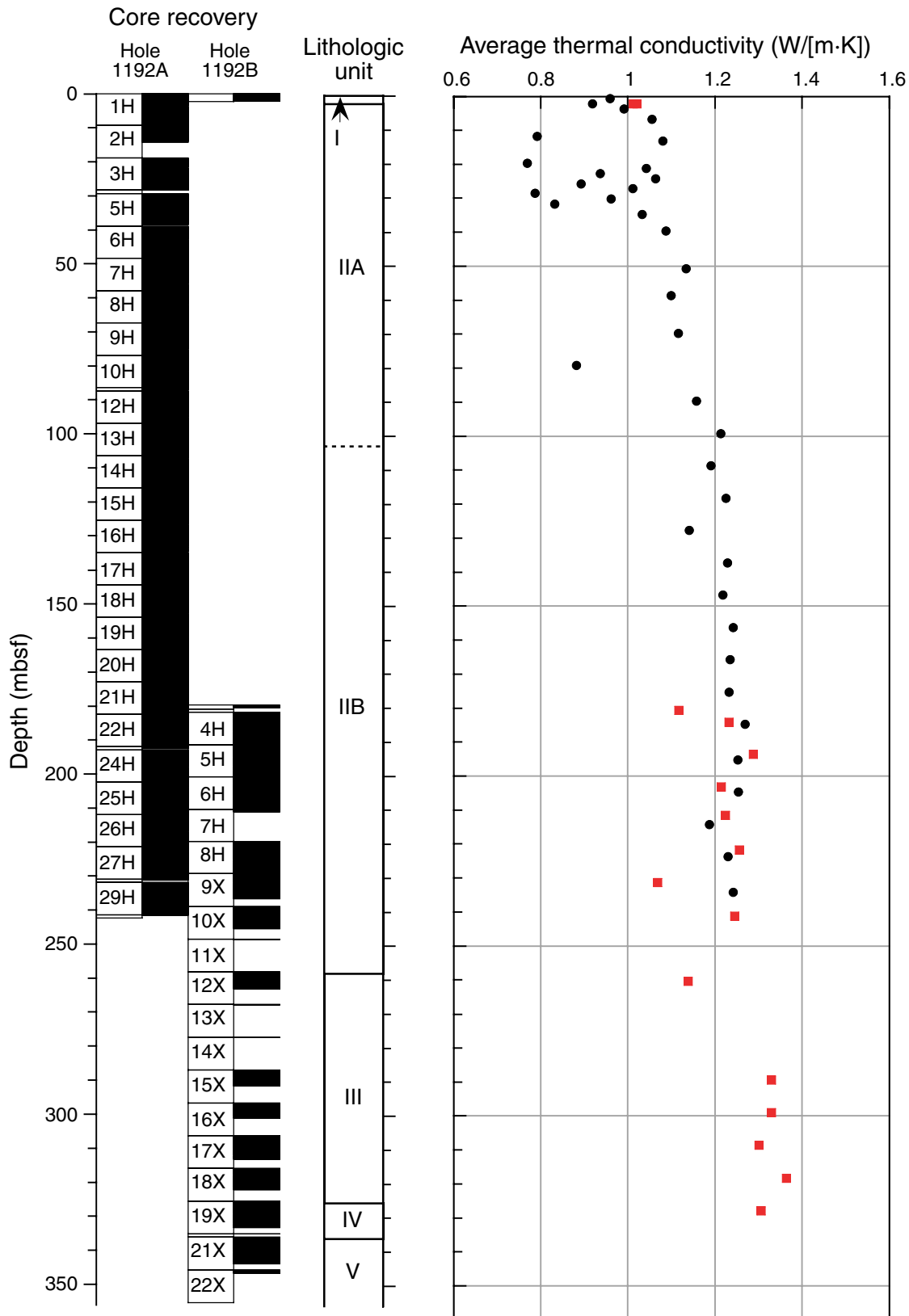
Figure F25. Crossplot of Site 1192 porosity and thermal conductivity. Superimposed are the power law curves, constructed from the observed range in porosity, for ideal end-member sedimentary facies: sandstones (red/upper curve), limestones (blue/center curve), and shales (black/lower curve). The observed thermal conductivities lie between the shale and sandstone curves, suggesting that much of the sediment at Site 1192 represents primarily mixed clay/sandstone sediment facies.
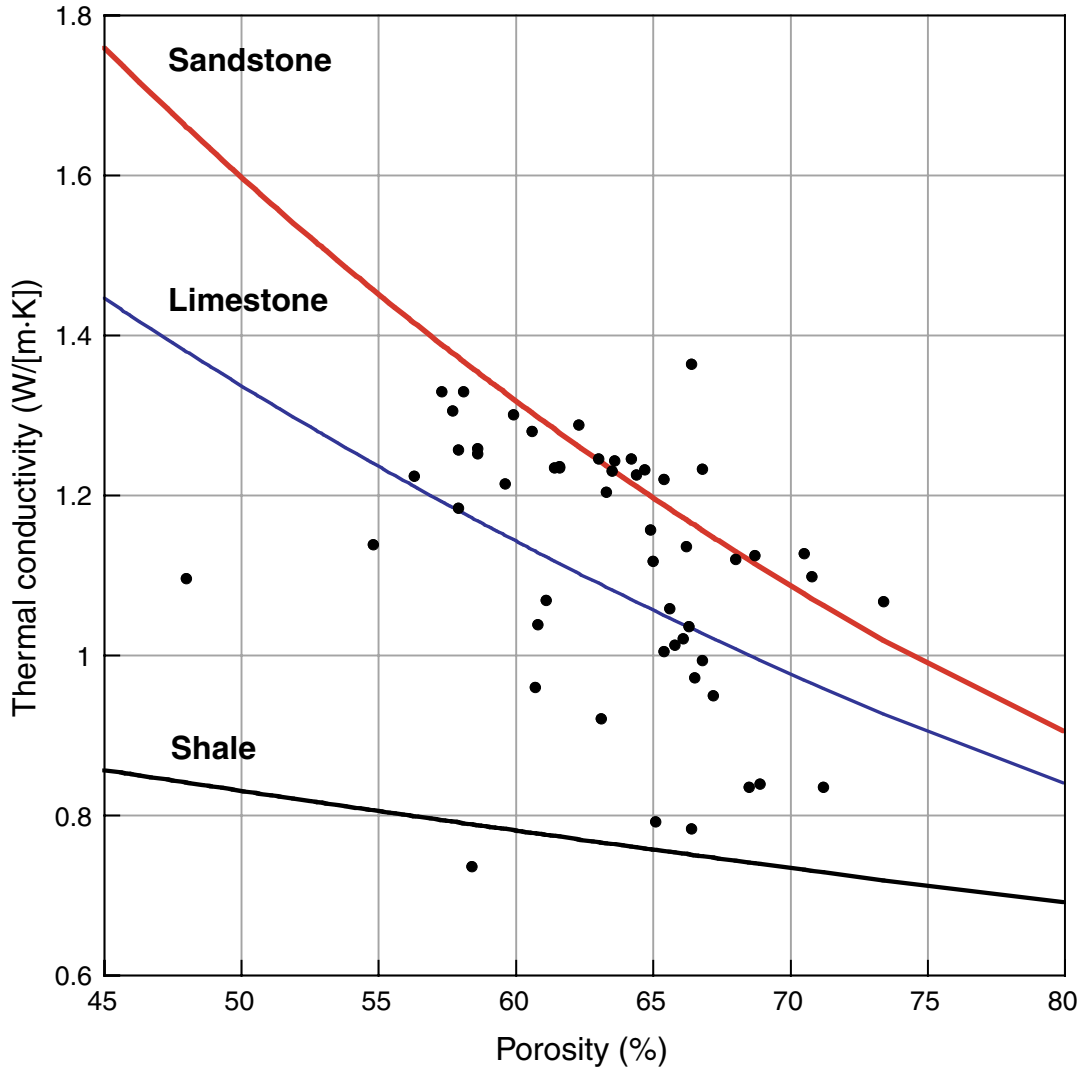
Figure F26. Comparison of physical properties for Site 1192. Solid circles = magnetic susceptibility (MS) for Hole 1192A, open circles = MS for Hole 1192B, triangles = carbonate content, black line = natural gamma radiation (NGR) for Hole 1192A, gray line = NGR for Hole 1192B, and thin black line = sediment reflectance (lightness).
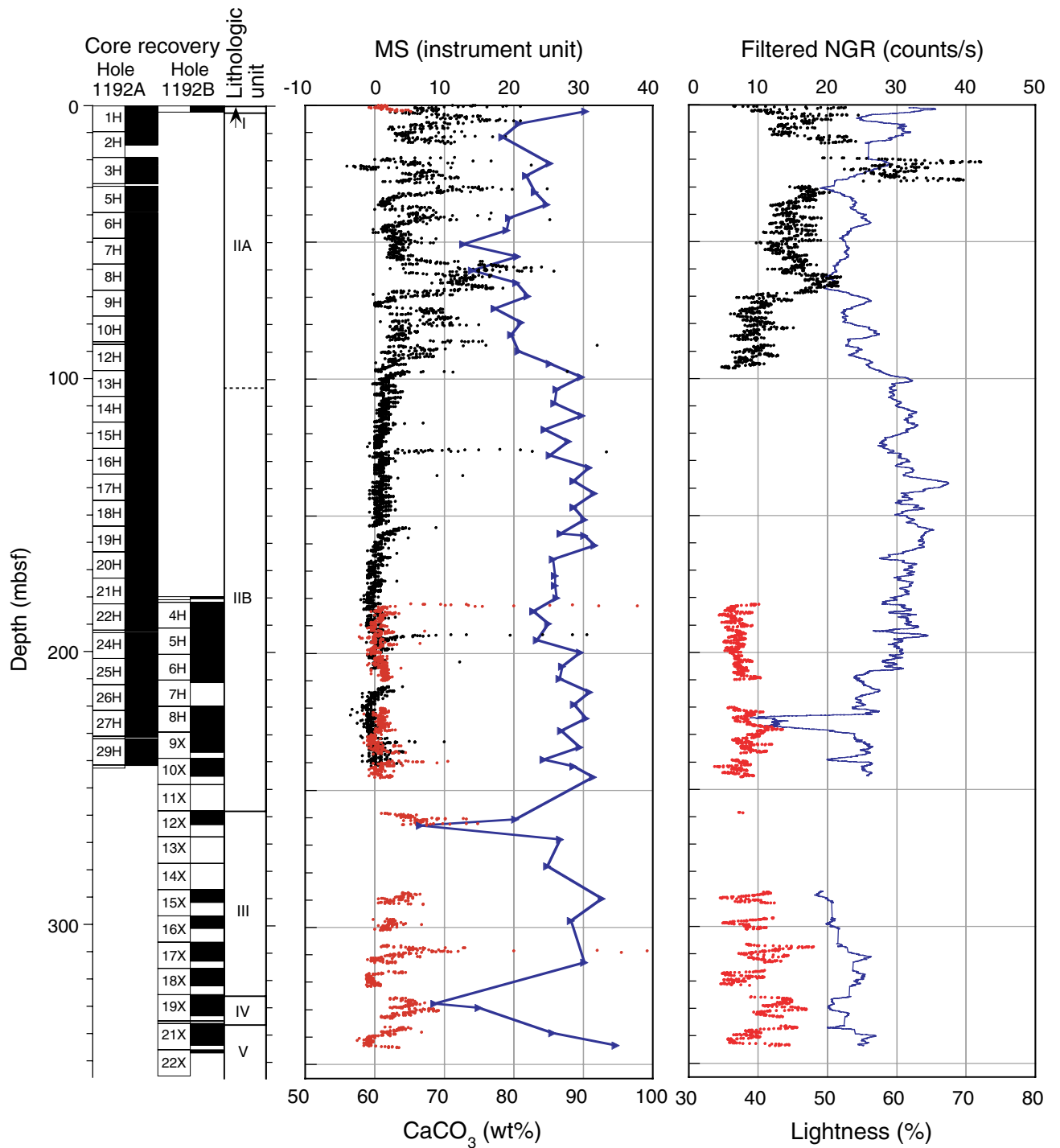
Figure F27. A. Part of the natural gamma radiation (NGR) data for Hole 1192A over the depth interval of 0–100 mbsf. The high-frequency noise had a periodicity defined by section length and a count amplitude that increased rapidly toward the end of the section. The exact cause of the problem and its solution remain puzzling. **B.** Remeasured NGR data for Hole 1192A over the depth interval of 0–100 mbsf. Comparison between the original and remeasured NGR data indicates that real geological information may exist as the lower-frequency component of the signal.
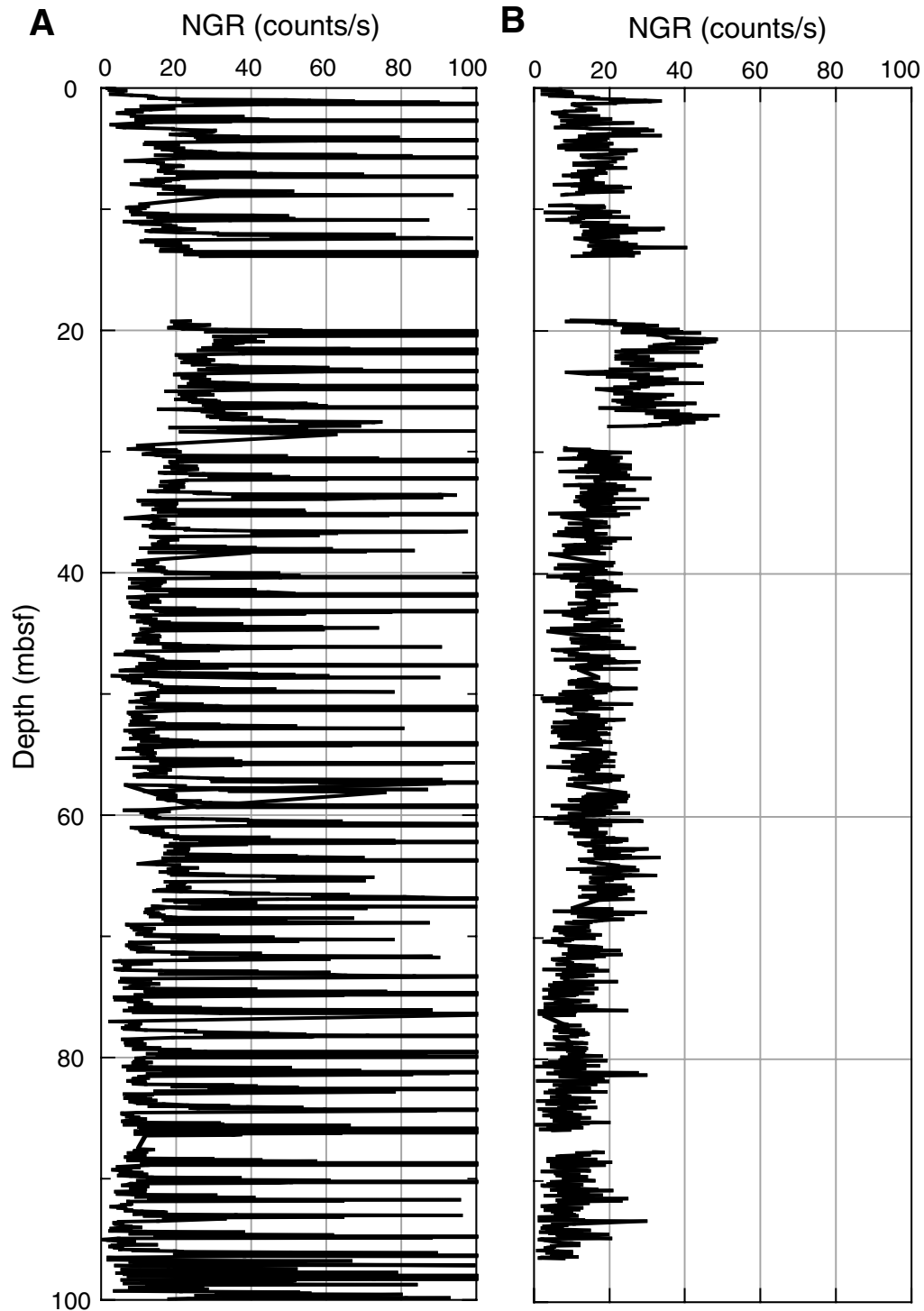
Figure F28. Depth offset between Holes 1192A and 1192B estimated from GRA bulk density data for the interval of 200–210 mbsf.
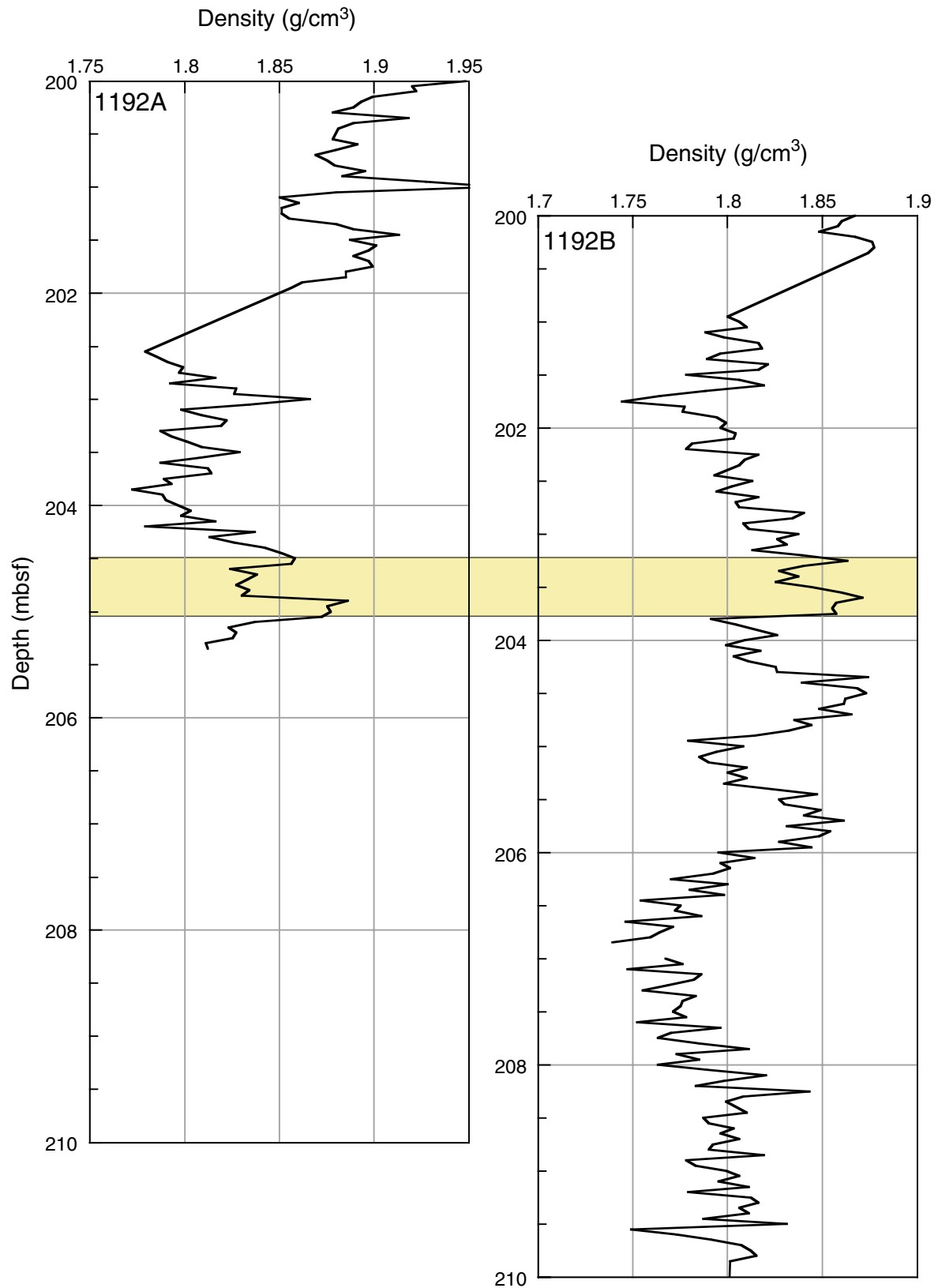
Figure F29. Multichannel line MAR20 with location and penetration depth of Site 1192 located at shotpoint 4126. The seismic megasequences (MS) and basement are marked and traced along the section.
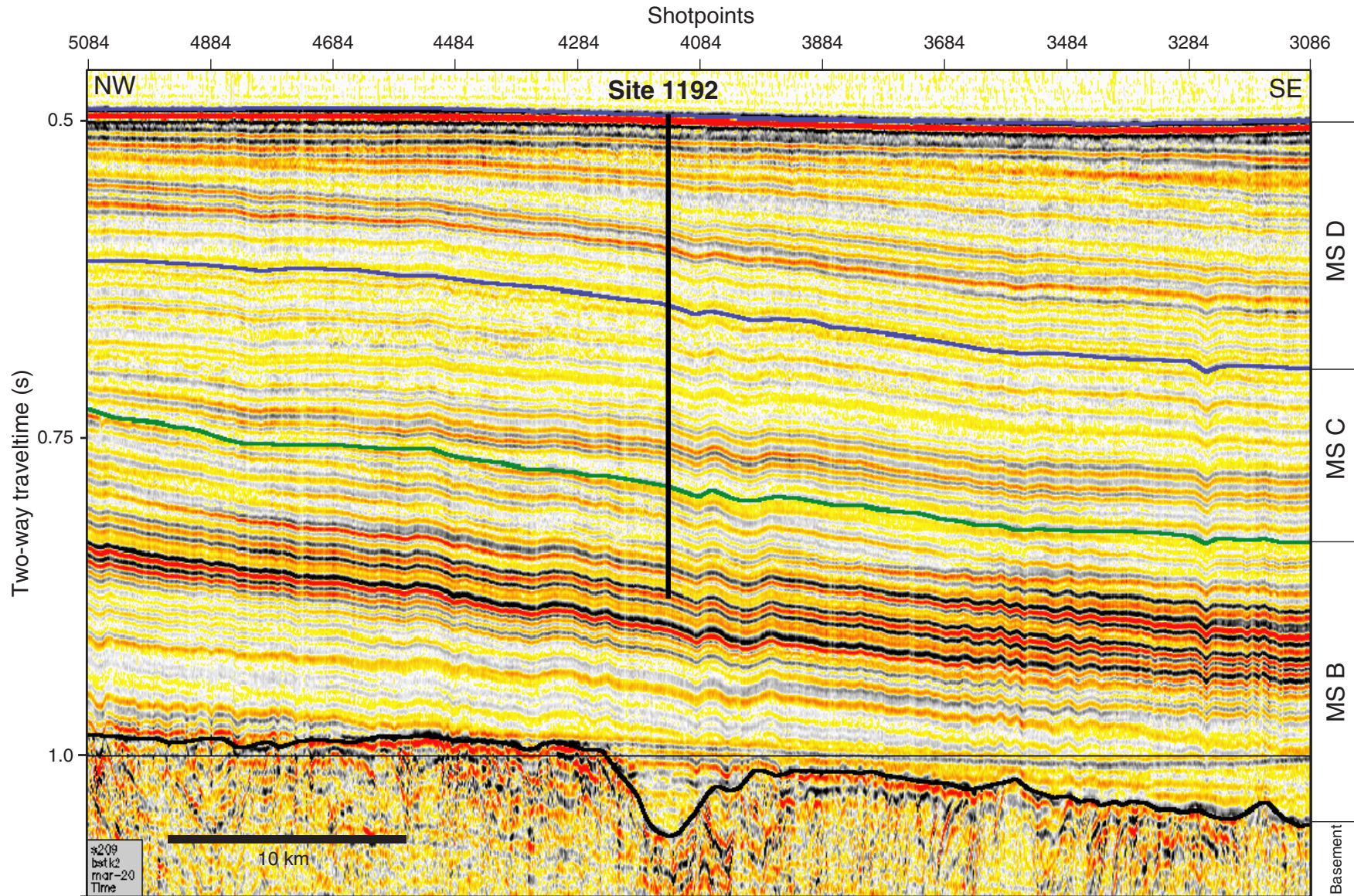
Figure F30. A. Synthetic seismogram plotted on line MAR20. **B.** Seismic megasequence definition. **C.** *P*-wave velocity data. **D.** Two-way traveltime-to-depth conversion. **E.** Bulk density. **F.** Lithologic units and ages. The traveltime-vs.-depth plot links seismic reflection events to depth in the cores, as shown for positions of Megasequence C/D and B/C boundaries. Dashed lines indicate high-amplitude reflections on line MAR20 (see Fig. F29, p. 58), which coincide with prominent shifts in downcore density and velocity measurements.
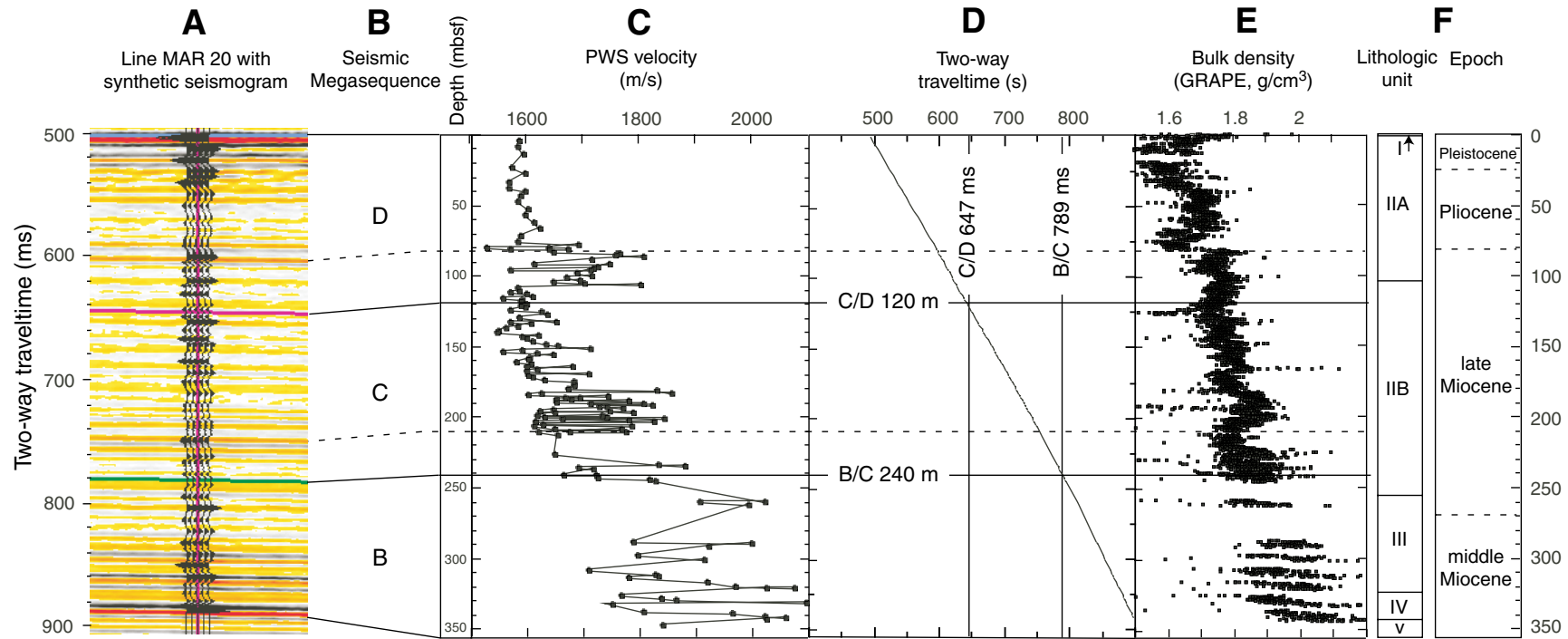
Table T1. Coring summary, Site 1192.

Core	Date (Jan 2001)	Time (local)	Depth (mbsf) Top	Depth (mbsf) Bottom	Length (m) Cored	Length (m) Recovered	Recovery (%)	Comment
194-1192A-								
1H	10	0225	0.0	9.5	9.5	9.60	101.1	
2H	10	0315	9.5	19.0	9.5	4.97	52.3	Started tensor at 0310 hr
3H	10	0350	19.0	28.5	9.5	9.66	101.7	
4M	10	0515	28.5	29.5	1.0	0.19	19.0	HF-VS run #1
5H	10	0600	29.5	39.0	9.5	9.22	97.1	
6H	10	0655	39.0	48.5	9.5	10.03	105.6	
7H	10	0715	48.5	58.0	9.5	9.90	104.2	
8H	10	0745	58.0	67.5	9.5	10.05	105.8	
9H	10	0820	67.5	77.0	9.5	9.52	100.2	
10H	10	0850	77.0	86.5	9.5	9.70	102.1	Camera out at 0850 hr
11M	10	1030	86.5	87.5	1.0	0.91	91.0	HF-VS run #2-AHC on
12H	10	1110	87.5	97.0	9.5	9.98	105.1	Camera in at 1050 hr
13H	10	1140	97.0	106.5	9.5	9.81	103.3	
14H	10	1220	106.5	116.0	9.5	9.98	105.1	
15H	10	1300	116.0	125.5	9.5	9.72	102.3	
16H	10	1325	125.5	135.0	9.5	9.32	98.1	
17H	10	1430	135.0	144.5	9.5	9.94	104.6	
18H	10	1505	144.5	154.0	9.5	9.99	105.2	
19H	10	1530	154.0	163.5	9.5	10.00	105.3	
20H	10	1550	163.5	173.0	9.5	9.96	104.8	
21H	10	1615	173.0	182.5	9.5	10.14	106.7	
22H	10	1655	182.5	192.0	9.5	10.06	105.9	
23M	10	1755	192.0	193.0	1.0	0.77	77.0	HF-VS run #3
24H	10	1825	193.0	202.5	9.5	10.08	106.1	Tensor at 1800 hr
25H	10	1900	202.5	212.0	9.5	10.05	105.8	
26H	10	1930	212.0	221.5	9.5	10.07	106.0	
27H	10	2000	221.5	231.0	9.5	9.98	105.1	
28M	10	2135	231.0	232.0	1.0	0.00	0.0	H-PCS run #1
29H	10	2355	232.0	241.5	9.5	9.86	103.8	Camera out at 2355 hr
30M	11	0450	241.5	242.5	1.0	0.00	0.0	H-PCS run #2
				Cored total:	242.5	243.46	100.4	
				Drilled total:	0.0			
				Total:	242.5			
194-1192B-								
1H	11	1155	0.0	2.4	2.4	2.44	101.7	Mudline adding up
20	11	1545	2.4	179.9	0.0	0.00	NA	Wash core
2M	11	1645	179.9	180.9	1.0	0.84	84.0	HF-VS run #4
3M	11	1745	180.9	181.9	1.0	0.00	0.0	H-PCS run #3
4H	11	1945	181.9	191.4	9.5	9.74	102.5	
5H	11	2020	191.4	200.9	9.5	10.04	105.7	
6H	11	2045	200.9	210.4	9.5	10.09	106.2	
7H	11	2110	210.4	219.9	9.5	1.09	11.5	
8H	11	2150	219.9	229.4	9.5	10.16	106.9	
9X	11	2300	229.4	239.0	9.6	7.58	79.0	
10X	11	2345	239.0	248.6	9.6	6.77	70.5	
11X	12	0025	248.6	258.2	9.6	0.23	2.4	
12X	12	0055	258.2	267.8	9.6	5.28	55.0	
13X	12	0130	267.8	277.5	9.7	0.35	3.6	
14X	12	0210	277.5	287.1	9.6	0.21	2.2	
15X	12	0250	287.1	296.8	9.7	4.81	49.6	
16X	12	0320	296.8	306.4	9.6	4.64	48.3	AHC on
17X	12	0600	306.4	316.0	9.6	7.01	73.0	AHC on
18X	12	0635	316.0	325.6	9.6	6.45	67.2	AHC on
19X	12	0910	325.6	335.2	9.6	7.92	82.5	AHC on, 2 fish runs
20M	12	1025	335.2	336.2	1.0	0.27	27.0	AHC on
21X	12	1135	336.2	345.9	9.7	8.09	83.4	AHC on
22X	12	1650	345.9	355.5	9.6	1.10	11.5	
				Cored total:	178.0	105.10	59.1	
				Drilled total:	177.5			
				Total:	355.5			

Notes: HYACE = Hydrate Autoclave Coring Equipment, AHC = active heave compensator, HF-VS = HYACE/Fugro Vibracore Sampler, H-PCS = HYACE Rotary Pressure Core Sampler. NA = not applicable.

Table T2. Expanded coring summary, Site 1192. (See table notes. Continued on next five pages.)

Core	Date (Jan 2001)	Time (local)	Core depth (mbsf) Top	Bottom	Length (m) Cored	Recovered	Recovery (%)	Section	Length (m) Liner	Curated	Section depth (mbsf) Top	Bottom	Catwalk samples	Comment
194-1192A-														
1H	10	0225	0.0	9.5	9.5	9.60	101.1							
								1	1.50	1.50	0.00	1.50		
								2	1.50	1.50	1.50	3.00		
								3	1.50	1.50	3.00	4.50		
								4	1.50	1.50	4.50	6.00	IW	
								5	1.50	1.50	6.00	7.50	HS	
								6	1.50	1.50	7.50	9.00		
								7	0.36	0.36	9.00	9.36		
								CC (w/7)	0.24	0.24	9.36	9.60	PAL	
								Totals:	9.60	9.60				
2H	10	0315	9.5	19.0	9.5	4.97	52.3							
								1	1.50	1.50	9.50	11.00		
								2	1.50	1.50	11.00	12.50		
								3	1.50	1.50	12.50	14.00		
								4	0.28	0.28	14.00	14.28		
								CC (w/4)	0.19	0.19	14.28	14.47	PAL	
								Totals:	4.97	4.97				
3H	10	0350	19.0	28.5	9.5	9.66	101.7							
								1	1.50	1.50	19.00	20.50		
								2	1.50	1.50	20.50	22.00		
								3	1.50	1.50	22.00	23.50		
								4	1.50	1.50	23.50	25.00	IW	
								5	1.50	1.50	25.00	26.50	HS	
								6	1.50	1.50	26.50	28.00		
								7	0.49	0.49	28.00	28.49		
								CC (w/7)	0.17	0.17	28.49	28.66	PAL	
								Totals:	9.66	9.66				
4M	10	0515	28.5	29.5	1.0	0.19	19.0							
								1	0.19	0.19	28.50	28.69		
								Totals:	0.19	0.19				
5H	10	0600	29.5	39.0	9.5	9.22	97.1							
								1	1.50	1.50	29.50	31.00		
								2	1.50	1.50	31.00	32.50		
								3	1.50	1.50	32.50	34.00		
								4	1.50	1.50	34.00	35.50	IW	
								5	1.50	1.50	35.50	37.00	HS	
								6	1.48	1.48	37.00	38.48		
								CC (w/CC)	0.24	0.24	38.48	38.72	PAL	
								Totals:	9.22	9.22				
6H	10	0655	39.0	48.5	9.5	10.03	105.6							
								1	1.50	1.50	39.00	40.50		
								2	1.50	1.50	40.50	42.00		
								3	1.50	1.50	42.00	43.50		
								4	1.50	1.50	43.50	45.00	IW	
								5	1.50	1.50	45.00	46.50	HS	
								6	1.50	1.50	46.50	48.00		
								7	0.79	0.79	48.00	48.79		
								CC (w/7)	0.24	0.24	48.79	49.03	PAL	
								Totals:	10.03	10.03				
7H	10	0715	48.5	58.0	9.5	9.90	104.2							
								1	1.50	1.50	48.50	50.00		
								2	1.50	1.50	50.00	51.50		
								3	1.50	1.50	51.50	53.00		
								4	1.50	1.50	53.00	54.50	IW	
								5	1.50	1.50	54.50	56.00	HS	
								6	1.50	1.50	56.00	57.50		
								7	0.70	0.70	57.50	58.20		
								CC (w/7)	0.20	0.20	58.20	58.40		
								Totals:	9.90	9.90				
8H	10	0745	58.0	67.5	9.5	10.05	105.8							
								1	1.50	1.50	58.00	59.50		
								2	1.50	1.50	59.50	61.00		
								3	1.50	1.50	61.00	62.50		
								4	1.50	1.50	62.50	64.00	IW	
								5	1.50	1.50	64.00	65.50	HS	
								6	1.50	1.50	65.50	67.00		
								7	0.87	0.87	67.00	67.87		

Table T2 (continued).

Core	Date (Jan 2001)	Time (local)	Core depth (mbsf) Top	Bottom	Length (m) Cored	Recovered	Recovery (%)	Section	Length (m) Liner	Curated	Section depth (mbsf) Top	Bottom	Catwalk samples	Comment
								CC (w/7)	0.18	0.18	67.87	68.05	PAL	
								Totals:	10.05	10.05				
9H	10	0820	67.5	77.0	9.5	9.52	100.2							
								1	1.50	1.50	67.50	69.00		
								2	1.50	1.50	69.00	70.50		
								3	1.50	1.50	70.50	72.00		
								4	1.50	1.50	72.00	73.50	IW	
								5	1.50	1.50	73.50	75.00	HS	
								6	1.50	1.50	75.00	76.50		
								7	0.34	0.34	76.50	76.84		
								CC (w/7)	0.18	0.18	76.84	77.02	PAL	
								Totals:	9.52	9.52				
10H	10	0850	77.0	86.5	9.5	9.70	102.1							
								1	1.50	1.50	77.00	78.50		
								2	1.50	1.50	78.50	80.00		
								3	1.50	1.50	80.00	81.50		
								4	1.50	1.50	81.50	83.00	IW	
								5	1.50	1.50	83.00	84.50	HS	
								6	1.50	1.50	84.50	86.00		
								7	0.58	0.58	86.00	86.58		
								CC (w/7)	0.12	0.12	86.58	86.70	PAL	
								Totals:	9.70	9.70				
11M	10	1030	86.5	87.5	1.0	0.91	91.0							
								1	0.91	0.91	86.50	87.41		
								Totals:	0.91	0.91				
12H	10	1110	87.5	97.0	9.5	9.98	105.1							
								1	1.50	1.50	87.50	89.00		
								2	1.50	1.50	89.00	90.50		
								3	1.50	1.50	90.50	92.00		
								4	1.50	1.50	92.00	93.50	IW, IW	
								5	1.50	1.50	93.50	95.00	HS, HS	
								6	1.50	1.50	95.00	96.50		
								7	0.78	0.78	96.50	97.30		
								CC (w/7)	0.20	0.20	97.28	97.48	PAL	
								Totals:	9.98	9.98				
13H	10	1140	97.0	106.5	9.5	9.81	103.3							
								1	1.50	1.50	97.00	98.50		
								2	1.50	1.50	98.50	100.00		
								3	1.50	1.50	100.00	101.50		
								4	1.50	1.50	101.50	103.00	IW	
								5	1.50	1.50	103.00	104.50	HS	
								6	1.50	1.50	104.50	106.00		
								7	0.53	0.53	106.00	106.53		
								CC (w/7)	0.28	0.28	106.53	106.81	PAL	
								Totals:	9.81	9.81				
14H	10	1220	106.5	116.0	9.5	9.98	105.1							
								1	1.50	1.50	106.50	108.00		
								2	1.50	1.50	108.00	109.50		
								3	1.50	1.50	109.50	111.00		
								4	1.50	1.50	111.00	112.50	IW	
								5	1.50	1.50	112.50	114.00	HS	
								6	1.50	1.50	114.00	115.50		
								7	0.78	0.78	115.50	116.28		
								CC (w/7)	0.20	0.20	116.28	116.48	PAL	
								Totals:	9.98	9.98				
15H	10	1300	116.0	125.5	9.5	9.72	102.3							
								1	1.50	1.50	116.00	117.50		
								2	1.50	1.50	117.50	119.00		
								3	1.50	1.50	119.00	120.50		
								4	1.50	1.50	120.50	122.00	IW	
								5	1.50	1.50	122.00	123.50	HS	
								6	1.50	1.50	123.50	125.00		
								7	0.44	0.44	125.00	125.44		
								CC (w/7)	0.28	0.28	125.44	125.72	PAL	
								Totals:	9.72	9.72				
16H	10	1325	125.5	135.0	9.5	9.32	98.1							
								1	1.50	1.50	125.50	127.00		
								2	1.50	1.50	127.00	128.50		

Table T2 (continued).

Core	Date (Jan 2001)	Time (local)	Core depth (mbsf) Top	Bottom	Length (m) Cored	Recovered	Recovery (%)	Section	Length (m) Liner	Curated	Section depth (mbsf) Top	Bottom	Catwalk samples	Comment
								3	1.50	1.50	128.50	130.00		
								4	1.50	1.50	130.00	131.50	IW	
								5	1.50	1.50	131.50	133.00	HS	
								6	1.52	1.52	133.00	134.52		
								CC (w/CC)	0.30	0.30	134.52	134.82	PAL	
								Totals:	9.32	9.32				
17H	10	1430	135.0	144.5	9.5	9.94	104.6							
								1	1.50	1.50	135.00	136.50		
								2	1.50	1.50	136.50	138.00		
								3	1.50	1.50	138.00	139.50		
								4	1.50	1.50	139.50	141.00	IW	
								5	1.50	1.50	141.00	142.50	HS	
								6	1.50	1.50	142.50	144.00		
								7	0.89	0.89	144.00	144.89		
								CC (w/7)	0.05	0.05	144.89	144.94	PAL	All to PAL
								Totals:	9.94	9.94				
18H	10	1505	144.5	154.0	9.5	9.99	105.2							
								1	1.50	1.50	144.50	146.00		
								2	1.50	1.50	146.00	147.50		
								3	1.50	1.50	147.50	149.00		
								4	1.50	1.50	149.00	150.50	IW	
								5	1.50	1.50	150.50	152.00	HS	
								6	1.50	1.50	152.00	153.50		
								7	0.70	0.70	153.50	154.20		
								CC (w/7)	0.29	0.29	154.20	154.49	PAL	
								Totals:	9.99	9.99				
19H	10	1530	154.0	163.5	9.5	10.00	105.3							
								1	1.50	1.50	154.00	155.50		
								2	1.50	1.50	155.50	157.00		
								3	1.50	1.50	157.00	158.50		
								4	1.50	1.50	158.50	160.00	IW	
								5	1.50	1.50	160.00	161.50	HS	
								6	1.50	1.50	161.50	163.00		
								7	0.73	0.73	163.00	163.73		
								CC (w/7)	0.27	0.27	163.73	164.00	PAL	
								Totals:	10.00	10.00				
20H	10	1550	163.5	173.0	9.5	9.96	104.8							
								1	1.50	1.50	163.50	165.00		
								2	1.50	1.50	165.00	166.50		
								3	1.50	1.50	166.50	168.00		
								4	1.50	1.50	168.00	169.50	IW	
								5	1.50	1.50	169.50	171.00	HS	
								6	1.50	1.50	171.00	172.50		
								7	0.69	0.69	172.50	173.19		
								CC (w/CC)	0.27	0.27	173.19	173.46	PAL	
								Totals:	9.96	9.96				
21H	10	1615	173.0	182.5	9.5	10.14	106.7							
								1	1.50	1.50	173.00	174.50		
								2	1.50	1.50	174.50	176.00		
								3	1.50	1.50	176.00	177.50		
								4	1.50	1.50	177.50	179.00	IW	
								5	1.50	1.50	179.00	180.50	HS	
								6	1.50	1.50	180.50	182.00		
								7	0.83	0.83	182.00	182.83		
								CC (w/7)	0.31	0.31	182.83	183.14	PAL	
								Totals:	10.14	10.14				
22H	10	1655	182.5	192.0	9.5	10.06	105.9							
								1	1.50	1.50	182.50	184.00		
								2	1.50	1.50	184.00	185.50		
								3	1.50	1.50	185.50	187.00		
								4	1.50	1.50	187.00	188.50	IW	
								5	1.50	1.50	188.50	190.00	HS	
								6	1.50	1.50	190.00	191.50		
								7	0.75	0.75	191.50	192.25		
								CC (w/7)	0.31	0.31	192.25	192.56	PAL	
								Totals:	10.06	10.06				
23M	10	1755	192.0	193.0	1.0	0.77	77.0							
								1	0.77	0.77	192.00	192.77		
								Totals:	0.77	0.77				

Table T2 (continued).

Core	Date (Jan 2001)	Time (local)	Core depth (mbsf) Top	Bottom	Length (m) Cored	Recovered	Recovery (%)	Section	Length (m) Liner	Curated	Section depth (mbsf) Top	Bottom	Catwalk samples	Comment
24H	10	1825	193.0	202.5	9.5	10.08	106.1							
								1	1.50	1.50	193.00	194.50		
								2	1.50	1.50	194.50	196.00		
								3	1.50	1.50	196.00	197.50		
								4	1.50	1.50	197.50	199.00	IW	
								5	1.50	1.50	199.00	200.50	HS	
								6	1.50	1.50	200.50	202.00		
								7	0.78	0.78	202.00	202.78		
								CC (w/7)	0.30	0.30	202.78	203.08	PAL	
								Totals:	10.08	10.08				
25H	10	1900	202.5	212.0	9.5	10.05	105.8							
								1	1.50	1.50	202.50	204.00		
								2	1.50	1.50	204.00	205.50		
								3	1.50	1.50	205.50	207.00		
								4	1.50	1.50	207.00	208.50	IW	
								5	1.50	1.50	208.50	210.00	HS	
								6	1.50	1.50	210.00	211.50		
								7	0.76	0.76	211.50	212.26		
								CC (w/7)	0.29	0.29	212.26	212.55	PAL	
								Totals:	10.05	10.05				
26H	10	1930	212.0	221.5	9.5	10.07	106.0							
								1	1.50	1.50	212.00	213.50		
								2	1.50	1.50	213.50	215.00		
								3	1.50	1.50	215.00	216.50		
								4	1.50	1.50	216.50	218.00	IW	
								5	1.50	1.50	218.00	219.50	HS	
								6	1.50	1.50	219.50	221.00		
								7	0.82	0.82	221.00	221.82		
								CC (w/7)	0.25	0.25	221.82	222.07	PAL	
								Totals:	10.07	10.07				
27H	10	2000	221.5	231.0	9.5	9.98	105.1							
								1	1.50	1.50	221.50	223.00		
								2	1.50	1.50	223.00	224.50		
								3	1.50	1.50	224.50	226.00		
								4	1.50	1.50	226.00	227.50	IW	
								5	1.50	1.50	227.50	229.00	HS	
								6	1.50	1.50	229.00	230.50		
								7	0.83	0.83	230.50	231.33		
								CC (w/7)	0.15	0.15	231.33	231.48	PAL	
								Totals:	9.98	9.98				
28M	10	2135	231.0	232.0	1.0	0.00	0.0							
29H	10	2355	232.0	241.5	9.5	9.86	103.8							
								1	1.50	1.50	232.00	233.50		
								2	1.50	1.50	233.50	235.00		
								3	1.50	1.50	235.00	236.50		
								4	1.50	1.50	236.50	238.00	IW	
								5	1.50	1.50	238.00	239.50	HS	
								6	1.50	1.50	239.50	241.00		
								7	0.71	0.71	241.00	241.71		
								CC (w/7)	0.15	0.15	241.71	241.86	PAL	
								Totals:	9.86	9.86				
30M	11	0450	241.5	242.5	1.0	0.00	0.0							
					Totals:	242.5	243.46	100.4							
194-1192B-														
1H	11	1155	0.0	2.4	2.4	2.44	101.7							
								1	1.50	1.50	0.00	1.50		
								2	0.81	0.81	1.50	2.31		
								CC (w/2)	0.13	0.13	2.31	2.44	PAL	
								Totals:	2.44	2.44				
20	11	1545	2.4	179.9	0.0	0.00	NA							
2M	11	1645	179.9	180.9	1.0	0.84	84.0							
								1	0.84	0.84	179.90	180.74		
								Totals:	0.84	0.84				

Table T2 (continued).

Core	Date (Jan 2001)	Time (local)	Core depth (mbsf) Top	Bottom	Length (m) Cored	Recovered	Recovery (%)	Section	Length (m) Liner	Curated	Section depth (mbsf) Top	Bottom	Catwalk samples	Comment
3M	11	1745	180.9	181.9	1.0	0.00	0.0							
4H	11	1945	181.9	191.4	9.5	9.74	102.5							
								1	1.50	1.50	181.90	183.40		
								2	1.50	1.50	183.40	184.90		
								3	1.50	1.50	184.90	186.40		
								4	1.50	1.50	186.40	187.90		
								5	1.50	1.50	187.90	189.40	HS	
								6	1.50	1.50	189.40	190.90		
								7	0.45	0.45	190.90	191.35		
								CC (w/7)	0.29	0.29	191.35	191.64	PAL	
								Totals:	9.74	9.74				
5H	11	2020	191.4	200.9	9.5	10.04	105.7							
								1	1.50	1.50	191.40	192.90		
								2	1.50	1.50	192.90	194.40		
								3	1.50	1.50	194.40	195.90		
								4	1.50	1.50	195.90	197.40		
								5	1.50	1.50	197.40	198.90	HS	
								6	1.50	1.50	198.90	200.40		
								7	0.80	0.80	200.40	201.20		
								CC (w/7)	0.24	0.24	201.20	201.44	PAL	
								Totals:	10.04	10.04				
6H	11	2045	200.9	210.4	9.5	10.09	106.2							
								1	1.50	1.50	200.90	202.40		
								2	1.50	1.50	202.40	203.90		
								3	1.50	1.50	203.90	205.40		
								4	1.50	1.50	205.40	206.90		
								5	1.50	1.50	206.90	208.40	HS	
								6	1.50	1.50	208.40	209.90		
								7	0.82	0.82	209.90	210.72		
								CC (w/7)	0.27	0.27	210.72	210.99	PAL	
								Totals:	10.09	10.09				
7H	11	2110	210.4	219.9	9.5	1.09	11.5							
								1	0.80	0.80	210.40	211.20		
								CC (w/1)	0.29	0.29	211.20	211.49	PAL	
								Totals:	1.09	1.09				
8H	11	2150	219.9	229.4	9.5	10.16	106.9							
								1	1.50	1.50	219.90	221.40		
								2	1.50	1.50	221.40	222.90		
								3	1.50	1.50	222.90	224.40		
								4	1.50	1.50	224.40	225.90	IW	
								5	1.50	1.50	225.90	227.40	HS	
								6	1.50	1.50	227.40	228.90		
								7	0.89	0.89	228.90	229.79		
								CC (w/7)	0.27	0.27	229.79	230.06	PAL	
								Totals:	10.16	10.16				
9X	11	2300	229.4	239.0	9.6	7.58	79.0							
								1	1.50	1.50	229.40	230.90		
								2	1.50	1.50	230.90	232.40		
								3	1.50	1.50	232.40	233.90		
								4	1.50	1.50	233.90	235.40	IW	
								5	1.33	1.33	235.40	236.73	HS	
								CC (w/CC)	0.25	0.25	236.73	236.98	PAL	
								Totals:	7.58	7.58				
10X	11	2345	239.0	248.6	9.6	6.77	70.5							
								1	1.50	1.50	239.00	240.50		
								2	1.50	1.50	240.50	242.00		
								3	1.50	1.50	242.00	243.50	IW	
								4	1.00	1.00	243.50	244.50	HS	
								5	0.88	0.88	244.50	245.38		
								CC (w/5)	0.39	0.39	245.38	245.77	PAL	
								Totals:	6.77	6.77				
11X	12	0025	248.6	258.2	9.6	0.23	2.4							
								CC (w/CC)	0.23	0.23	248.60	248.83	PAL	
								Totals:	0.23	0.23				
12X	12	0055	258.2	267.8	9.6	5.28	55.0							
								1	1.50	1.50	258.20	259.70		
								2	1.50	1.50	259.70	261.20	IW	

Table T2 (continued).

Core	Date (Jan 2001)	Time (local)	Core depth (mbsf) Top	Bottom	Length (m) Cored	Recovered	Recovery (%)	Section	Length (m) Liner	Curated	Section depth (mbsf) Top	Bottom	Catwalk samples	Comment
								3	1.50	1.50	261.20	262.70	HS	
								4	0.41	0.41	262.70	263.11		
								CC (w/4)	0.37	0.37	263.11	263.48	PAL	
								Totals:	5.28	5.28				
13X	12	0130	267.8	277.5	9.7	0.35	3.6							
								CC (w/CC)	0.35	0.35	267.80	268.15	PAL	
								Totals:	0.35	0.35				
14X	12	0210	277.5	287.1	9.6	0.21	2.2							
								CC (w/CC)	0.21	0.21	277.50	277.71	PAL	
								Totals:	0.21	0.21				
15X	12	0250	287.1	296.8	9.7	4.81	49.6							
								1	1.50	1.50	287.10	288.60		
								2	1.50	1.50	288.60	290.10	IW	
								3	1.43	1.43	290.10	291.53	HS	
								CC (w/CC)	0.38	0.38	291.53	291.91	PAL	
								Totals:	4.81	4.81				
16X	12	0320	296.8	306.4	9.6	4.64	48.3							
								1	1.50	1.50	296.80	298.30		
								2	1.50	1.50	298.30	299.80	IW	
								3	1.28	1.28	299.80	301.08	HS	
								CC (w/CC)	0.36	0.36	301.08	301.44	PAL	
								Totals:	4.64	4.64				
17X	12	0600	306.4	316.0	9.6	7.01	73.0							
								1	1.50	1.50	306.40	307.90		
								2	1.50	1.50	307.90	309.40		
								3	1.50	1.50	309.40	310.90	IW	
								4	1.50	1.50	310.90	312.40	HS	
								5	0.74	0.74	312.40	313.14		
								CC (w/5)	0.27	0.27	313.14	313.41	PAL	
								Totals:	7.01	7.01				
18X	12	0635	316.0	325.6	9.6	6.45	67.2							
								1	1.50	1.50	316.00	317.50		
								2	1.50	1.50	317.50	319.00		
								3	1.50	1.50	319.00	320.50	IW	
								4	1.00	1.00	320.50	321.50	HS	
								5	0.52	0.52	321.50	322.02		
								CC (w/5)	0.43	0.43	322.02	322.45	PAL	
								Totals:	6.45	6.45				
19X	12	0910	325.6	335.2	9.6	7.92	82.5							
								1	1.50	1.50	325.60	327.10		
								2	1.50	1.50	327.10	328.60		
								3	1.50	1.50	328.60	330.10		
								4	1.50	1.50	330.10	331.60	IW	
								5	1.52	1.52	331.60	333.12	HS	
								CC (w/CC)	0.40	0.40	333.12	333.52	PAL	
								Totals:	7.92	7.92				
20M	12	1025	335.2	336.2	1.0	0.27	27.0							
								1	0.27	0.27	335.20	335.47	PAL	
								Totals:	0.27	0.27				
21X	12	1135	336.2	345.9	9.7	8.09	83.4							
								1	1.50	1.50	336.20	337.70		
								2	1.50	1.50	337.70	339.20		
								3	1.50	1.50	339.20	340.70		
								4	1.50	1.50	340.70	342.20	IW	
								5	1.00	1.00	342.20	343.20	HS	
								6	0.66	0.66	343.20	343.86		
								CC (w/6)	0.43	0.43	343.86	344.29	PAL	
								Totals:	8.09	8.09				
22X	12	1650	345.9	355.5	9.6	1.10	11.5							
								1	0.81	0.81	345.90	346.71		
								CC (w/1)	0.29	0.29	346.71	347.00	PAL	
								Totals:	1.10	1.10				
								Totals:	178.0	105.11	59.10				

Notes: CC = core catcher (number in parentheses indicates which section the core catcher is stored with). Catwalk samples: IW = interstitial water, HS = headspace, PAL = paleontology sample. NA = not applicable.

Table T3. Lithologic units and subunits, Site 1192.

Unit/ Subunit	Hole 1192A Core, section, interval (cm) Top	Base	Depth (mbsf) Top	Base	Hole 1192B Core, section, interval (cm) Top	Base	Depth (mbsf) Top	Base	Description
I	1H-1, 0	1H-2, 90	0.0	2.4					Skeletal grainstone with planktonic foraminifers. Brown.
II	1H-2, 90	29H-CC, 20	2.4	291.9	1H-1, 0	12X-1, 10	0.0	258.2	Mudstone to skeletal packstone, with clay, planktonic foraminifers. Light greenish gray.
IIA	1H-2, 90	13H-5, 10	2.4	103.1					Skeletal packstone/wackestone with clay, planktonic foraminifers. Light olive-gray to light gray.
IIB	13H-5, 10	29H-CC, 20	103.1	291.9	1H-1, 0	12X-1, 10	0.0	258.2	Mudstone, with clay and meter-scale units of skeletal wackestone and packstone. Light greenish gray.
III					12X-1, 10	19X-1, 0	258.2	325.6	Skeletal packstone/grainstone, with clay, planktonic foraminifers rare. Dark greenish gray. First appearance of coarse glauconite, quartz, and shallow benthic foraminifers.
IV					19X-1, 0	21X-1, 0	325.6	336.2	Skeletal packstone/grainstone with clay, planktonic foraminifers. Light greenish gray.
V					21X-1, 0	22X-2, 30	336.2	347.0	Silt-sized grainstone, with clay, planktonic foraminifers, dolomite, rare angular quartz. Greenish to yellow.

Table T4. Biostratigraphic datums, Site 1192.

Datum	Core, section, interval (cm)	Depth (mbsf)		Mean depth (mbsf)	Age (Ma)
		First absence or presence	Last presence or absence		
194-1192A-					
LO *Globorotalia tosaensis*	1H-1, 0, to 1H-CC	0.00	9.55	4.78	0.60
LO *Reticulofenestra asanoi*	1H-1, 0, to 1H-CC	0.00	9.55	4.78	0.88
LO *Calcidiscus macintyrei*	2H-CC to 3H-CC	14.42	28.61	21.52	1.70
LO *Globigerinoides fistulosus*	2H-CC to 3H-CC	14.42	28.61	21.52	1.77
FO *Globorotalia truncatulinoides*	3H-CC to 5H-CC	28.61	38.67	33.64	2.00
LO *Discoaster surculus*	2H-CC to 3H-CC	14.42	28.61	21.52	2.60
LO *Discoaster tamalis*	3H-CC to 5H-CC	28.61	38.67	33.64	2.80
LO *Dentoglobigerina altispira*	6H-CC to 7H-CC	48.98	58.38	53.68	3.09
LO *Reticulofenestra pseudoumbilica*	6H-CC to 7H-CC	48.98	58.38	53.68	3.70
LO *Globigerina nepenthes*	8H-CC to 9H-1, 80–82	68.03	68.30	68.17	4.18
LO *Discoaster quinqueramus*	10H-3, 80–82, to 10H-4, 80–82	80.80	82.30	81.55	5.60
FO *Discoaster surculus*	15H-CC to 16H-CC	125.70	134.80	130.25	7.50
FO *Discoaster quinqueramus*	17H-CC to 19H-CC	144.80	163.98	154.39	8.50
LO *Discoaster neohamatus*	19H-CC to 20H-CC	163.98	173.44	168.71	9.40
LO *Cyclicargolithus floridanus*	21H-CC to 24H-CC	182.25	241.81	212.03	11.90
194-1192B-					
LO *Discoaster hamatus*	6H-CC to 7H-CC	210.94	211.44	211.19	9.50
FO *Discoaster hamatus*	8H-CC to 9H-CC	230.01	236.93	233.47	10.50
FO *Neogloboquadrina mayeri*	14X-CC to 15X-CC	277.68	291.88	284.78	11.40
LO *Sphenolithus heteromorphus*	16X-CC to 17X-CC	301.41	313.38	307.40	13.60
FO *Praeorbuliua sicana*	21X-CC to 22X-CC	344.27	346.98	345.63	16.40
FO *Sphenolithus heteromorphus*	Below 22X-CC	>347.00			18.20

Note: FO = first occurrence, LO = last occurrence.

Table T5. Magnetic polarity transitions, Hole 1192A.

Chron	Top observation Core, section interval (cm)	Top observation Depth (mbsf)	Bottom observation Core, section interval (cm)	Bottom observation Depth (mbsf)	Average Depth (mbsf)	Average Error	Average Age (Ma)
	194-1192A-		194-1192A-				
C1n (T)	1H-1, 0	0.00	1H-1, 0	0.00			0.0
C1n (O)	2H-3, 145	13.95	3H-1, 5	19.10	16.53	2.58	0.78
C1r2r1n (T)	3H-4, 54	24.04	3H-4, 54	24.04	24.04	0.00	1.201
C1r2r1n (O)	3H-4, 104	24.54	3H-4, 104	24.54	24.54	0.00	1.211
C2n (T)	5H-3, 15	32.65	5H-3, 15	32.65	32.65	0.00	1.770
C2n (O)	5H-6, 116	38.16	5H-6, 128	38.28	38.22	0.06	1.950
C2An.1n (T)	6H-4, 50	44.00	6H-4, 110	44.60	44.30	0.30	2.581
C2An.1n (O)	7H-5, 20	54.70	7H-5, 110	55.60	55.15	0.45	3.040
C2An.2n (T)	8H-1, 20	58.20	8H-1, 60	58.60	58.40	0.20	3.110
C2An.2n (O)	8H-2, 140	60.90	8H-3, 10	61.10	61.00	0.10	3.220
C2An.3n (T)	8H-3, 34	61.34	8H-3, 60	61.60	61.47	0.13	3.330
C2An.3n (O)	9H-4, 50	72.50	9H-4, 80	72.80	72.65	0.15	3.580
C3n.1n (T)	9H-7, 30	76.80	10H-1, 50	77.20	77.00	0.20	4.180
C3n.1n (O)	10H-3, 70	80.70	10H-3, 90	80.90	80.80	0.10	4.290
C3n.2n (T)	10H-4, 50	82.00	10H-4, 100	82.62	82.31	0.31	4.480
C3n.2n (O)	10H-5, 120	84.20	10H-6, 80	85.30	84.75	0.55	4.462
C3n.3n (T)	10H-7, 40	86.40	10H-7, 50	86.50	86.45	0.05	4.800
C3n.3n (O)	12H-3, 80	91.30	12H-3, 140	91.90	91.60	0.30	4.890
C3n.4n (T)	12H-4, 34	92.34	12H-4, 65	92.65	92.45	0.11	4.980
C3n.4n (O)	12H-6, 132	96.32	13H-2, 20	98.70	97.51	1.19	5.230
C3An1n (T)	13H-5, 71	103.71	13H-5, 149	104.49	104.10	0.39	5.890
C3An1n (O)	13H-6, 64	105.14	13H-6, 109	105.59	105.37	0.22	6.137
C3An2n (T)	13H-7, 40	106.40	13H-7, 40	106.40	106.40	0.00	6.269
C3An2n (O)	14H-1, 134	107.84	14H-1, 134	107.84	107.84	0.00	6.560
C3Bn (T)	14H-3, 46	109.96	14H-3, 144	110.94	110.45	0.49	6.935
C3Bn (O)	14H-6, 129	115.29	14H-7, 19	115.69	115.49	0.20	7.091
C3Br1n (T)	15H-1, 86	116.86	15H-1, 86	116.86	116.86	0.00	7.135
C3Br1n (O)	15H-1, 140	117.40	15H-1, 140	117.40	117.40	0.00	7.170
C3Br2rn (T)	15H-2, 39	117.89	15H-3, 11	119.11	118.50	0.61	7.341
C3Br2rn (O)	15H-3, 70	119.70	15H-3, 70	119.70	119.70	0.00	7.375
C4n1n (T)	15H-3, 92	119.92	15H-4, 42	120.92	120.42	0.00	7.432
C4n1n (O)	15H-6, 91	125.41	16H-1, 72	126.22	125.82	0.41	7.562
C4n2n (T)	16H-3, 19	128.69	16H-4, 58	130.58	129.64	0.95	7.650
C4n2n (O)	16H-6, 110	134.10	17H-1, 43	135.43	134.77	0.67	8.070
C4r1n (T)	17H-1, 146	136.46	17H-1, 146	136.46	136.46	0.00	8.225
C4r1n (O)	17H-2, 103	137.53	17H-3, 2	138.02	137.78	0.25	8.257
C4rAn (T)	17H-5, 53	141.53	17H-6, 66	143.16	142.35	0.81	8.699
C4rAn (O)	17H-7, 20	144.20	17H-7, 73	144.73	144.47	0.27	9.025
C4Ar1n (T)	18H-1, 81	145.31	18H-1, 147	145.97	145.64	0.33	9.230
C4Ar1n (O)	18H-2, 62	146.62	18H-2, 134	147.34	146.98	0.36	9.308

Note: (T) = termination, (O) = onset.

Table T6. Age-depth control points, Site 1192.

Source	Datum	Age (Ma)	Top: FO presence or LO absence Core, section interval (cm)	Depth (mbsf)	Bottom: LO presence or FO absence Core, section interval (cm)	Depth (mbsf)	Average depth (mbsf)	Uncertainty (m) Upsection	Downsection
			194-1192A-		194-1192A-				
PF	LO *Globorotalia tosaensis*	0.60	1H-1, 0	0.00	1H-CC	9.55	4.78	4.78	4.78
CN	LO *Reticulofenestra asanoi*	0.88	1H-1, 0	0.00	1H-CC	9.55	4.78	4.78	4.78
CN	LO *Calcidiscus macintyrei*	1.7	2H-CC	14.42	3H-CC	28.61	21.52	7.10	7.10
PF	LO *Globigerinoides fistulosus*	1.77	2H-CC	14.42	3H-CC	28.61	21.52	7.10	7.10
PF	FO *Globorotalia truncatulinoides*	2.00	3H-CC	28.61	5H-BCI	39.00	33.81	5.20	5.20
CN	LO *Discoaster surculus*	2.6	2H-CC	14.42	3H-CC	28.61	21.52	7.10	7.10
CN	LO *Discoaster tamalis*	2.8	3H-CC	28.61	5H-BCI	39.00	33.81	5.20	5.20
PF	LO *Dentoglobigerina altispira*	3.09	6H-CC	48.98	7H-CC	58.38	53.68	4.70	4.70
CN	LO *Reticulofenestra pseudoumbilica*	3.7	6H-CC	48.98	7H-CC	58.38	53.68	4.70	4.70
PF	LO *Globorotalia nepenthes*	4.18	8H-CC	68.03	9H-1, 81	68.31	68.17	0.14	0.14
CN	LO *Discoaster quinqueramus*	5.6	10H-3, 81	80.81	10H-4, 81	82.31	81.56	0.75	0.75
CN	FO *Discoaster surculus*	7.5	15H-CC	125.70	16H-BCI	135.00	130.35	4.65	4.65
CN	FO *Discoaster quinqueramus*	8.5	17H-CC	144.80	19H-CC	163.98	154.39	9.59	9.59
CN	LO *Discoaster neohamatus*	9.4	19H-CC	163.98	20H-CC	173.44	168.71	4.73	4.73
CN	LO *Cyclicargolithus floridanus*	11.9	21H-CC	182.25	24H-CC	202.50	192.38	10.13	10.13
CN	Range *Cyclicargolithus floridanus*	11.9–13.6	29H-CC	241.75	29H-CC	241.75	241.75	0.00	0.00
			194-1192B-		194-1192B-				
CN	LO *Discoaster hamatus*	9.5	6H-CC	210.94	7H-BCI	219.90	215.42	4.48	4.48
CN	FO *Discoaster hamatus*	10.5	8H-CC	230.01	9H-BCI	239.00	234.51	4.50	4.50
PF	FO *Neogloboquadrina mayeri*	11.4	14X-CC	277.68	15X-BCI	296.80	287.24	9.56	9.56
CN	LO *Sphenolithus heteromorphus*	13.6	16X-CC	301.41	17X-BCI	316.00	308.71	7.29	7.29
PF	FO *Praeorbulina sicana*	16.4	21X-CC	344.27	22X-BCI	355.50	349.89	5.62	5.62
CN	Range *Sphenolithus heteromorphus*	13.6–18.2	22X-CC	347.00	22X-BCI	355.50	351.25	4.25	4.25

Notes: Source: PF = planktonic foraminifers, CN = calcareous nannoplankton. Datum: FO = first occurrence, LO = last occurrence. Core, section, interval: BCI = bottom of cored interval.

Table T7. Interpolated ages of lithologic unit boundaries and seismic reflectors, Site 1192.

Lithologic unit	Top of unit	
	Depth (mbsf)	Age (Ma)
I	0	0.6
IIA	2.4	0.7
IIB	103.1	6.5
III	258.1	10.9
IV	325.6	14.7
V	336.2	15.3
Seismic sequences and reflectors:		
Megasequence D	0	0.6
D-black	50	3.1
D-turquoise	81	5.4
Megasequence C	120	7.2
Megasequence B	240	10.5
B-turquoise	285	11.9
Megasequence A	Not drilled	
Basement	Not drilled	

Table T8. Headspace gas composition, Site 1192.

Core, section	Depth (mbsf)	C_1 (ppmv)
194-1192A-		
1H-5	6.00	11.8
3H-5	25.00	2.5
5H-5	35.50	2.6
6H-5	45.00	2.2
7H-5	54.50	2.0
8H-5	64.00	1.8
9H-5	73.50	2.0
10H-5	83.00	2.0
12H-5	93.50	2.3
13H-5	103.00	1.9
14H-5	112.50	1.9
15H-5	122.00	1.7
16H-5	131.50	2.0
17H-5	141.00	2.0
18H-5	150.50	1.8
19H-5	160.00	1.9
20H-5	169.50	2.1
21H-5	179.00	2.1
22H-5	188.50	2.7
24H-5	199.00	2.1
25H-5	208.50	2.2
26H-5	218.00	1.8
27H-5	227.50	2.7
29H-5	238.00	2.1
194-1192B-		
4H-5	187.90	2.1
5H-5	197.40	2.1
6H-5	206.90	1.9
8H-5	225.90	2.1
9X-5	235.40	2.2
10X-4	243.50	2.0
12X-3	261.20	2.1
15X-3	290.10	1.9
16X-3	299.80	2.1
17X-4	310.90	2.2
18X-4	320.50	2.0
19X-5	331.60	2.0
21X-5	342.20	2.3

Note: C_1 = methane.

Table T9. Interstitial water chemistry, Site 1192.

Core, section, interval (cm)	Depth (mbsf)	pH	Alk (mM)	Salinity	Cl⁻ (mM)	SO₄²⁻ (mM)	Na⁺ (mM)	Mg²⁺ (mM)	Ca²⁺ (mM)	K⁺ (mM)	NH₄⁺ (μM)	Sr²⁺ (μM)	Li⁺ (μM)	Mn²⁺ (μM)	Fe²⁺ (μM)
194-1192A-															
1H-4, 140–150	5.90	7.68	1.94	35.5	569	30.38	482	56.71	12.07	11.81	24	150	43.28	1.22	14.62
3H-4, 140–150	24.90	7.62	2.21	36.0	571	28.84	481	55.96	13.28	11.42	98	220	46.97	1.04	
5H-4, 140–150	35.40	7.64	2.24	36.0	570	28.43	483	53.69	13.61	11.09	138	235	40.81	0.67	
6H-4, 140–150	44.90	7.57	2.43	35.5	567	28.44	480	53.59	14.23	10.95	176				
7H-4, 140–150	54.40	7.56	2.34	35.5	567	27.20	479	52.25	14.62	11.03	219	331	42.91	0.44	14.62
8H-4, 140–150	63.90	7.37	2.41	35.5	565	25.27	482	48.53	14.05	10.36	261	427	65.62	0.63	
9H-4, 140–150	73.40	7.26	2.39	35.5	566	24.97	482	48.89	14.27	10.39	311	403	50.66	0.35	14.26
10H-4, 140–150	82.90	7.43	2.50	35.5	562	24.51	478	48.30	14.35	10.09	364	438	61.90	0.48	
12H-4, 140–150	93.40	7.48	2.52	35.5	566	23.53	484	46.81	14.26	9.67	334	497	58.90	0.29	38.84
13H-4, 140–150	102.90	7.39	2.76	35.5	566	23.35	484	46.73	14.36	9.64	466	620	87.72	0.48	
14H-4, 140–150	112.40	7.44	2.55	35.5	564	22.20	482	45.68	14.28	9.25	538	570	66.31	0.22	12.03
15H-4, 140–150	121.90	7.58	2.52	35.5	564	22.54	483	45.44	14.19	8.99	563	732	100.01	0.34	
16H-4, 140–150	131.40	7.38	2.31	35.5	561	22.17	480	45.01	14.16	9.00	546	515	61.15	0.24	6.62
17H-4, 140–150	140.90	7.49	2.33	35.0	561	21.37	479	44.69	14.42	8.70	586	467	49.93	0.13	
18H-4, 140–150	150.40	7.40	2.60	35.0	562	20.89	481	44.02	14.42	8.51	628	671	81.33	0.13	11.74
19H-4, 140–150	159.90	7.37	2.55	35.0	566	20.97	486	43.46	14.45	8.30	671	693	82.95	0.18	14.22
20H-4, 140–150	169.40	7.23	2.51	35.0	563	20.89	480	41.96	17.79	8.19	676	682	89.20	0.11	6.28
21H-4, 140–150	178.90	7.37	2.52	35.0	567	19.58	485	42.68	15.14	8.24	534	836	115.98	0.35	
22H-4, 140–150	188.40	7.63	2.59	35.0	564	19.33	484	42.17	14.53	8.04	756	704	95.60	0.17	9.67
24H-4, 140–150	198.90	7.45	2.59	34.5	565	18.94	486	41.29	14.45	7.88	779	877	131.94	0.21	
25H-4, 140–150	208.40	7.40	2.54	35.0	565	18.55	485	40.87	14.83	7.84	826	727	103.86	0.16	4.51
26H-4, 140–150	217.90	7.37	2.56	35.0	566	18.76	487	40.35	15.13	7.66	839	924	150.95	0.22	
27H-4, 140–150	227.40	7.38	2.44	34.5	565	17.90	485	39.79	15.32	7.75	871	725	108.01	0.18	3.91
29H-4, 140–150	237.90	7.54	2.20	34.5	563	17.99	480	40.74	16.14	7.85	876	951	170.81	0.21	
194-1192B-															
8H-4, 140–150	225.80	7.50	3.21	35.0	564	18.28	484	40.66	15.57	7.70	778	698	110.29	0.19	2.74
9X-4, 140–150	235.30	7.55	2.32	34.5	566	18.04	485	39.93	15.79	7.69	823	945	158.70	0.20	
10X-3, 140–150	243.40	7.58	2.31	34.5	567	18.13	482	40.97	16.70	7.78	880	695	115.58	0.18	3.47
12X-2, 140–150	261.10	7.91	1.89	35.5	566	16.74	481	40.24	16.12	7.86	922	829	144.75	0.23	
15X-2, 140–150	290.00	7.52	2.53	35.5	565	17.58	475	41.61	18.21	7.63	963	767	140.49	0.17	0.00
16X-2, 140–150	299.70	7.92	2.34	35.0	567	16.88	483	39.85	16.46	7.06	932	909	166.92	0.22	
17X-3, 140–150	310.80	7.64	2.93	34.5	568	16.35	482	39.63	17.77	7.12	998	732	132.68	0.28	0.51
18X-3, 140–150	320.40	7.61	2.43	34.5	568	15.86	481	39.19	17.81	7.07	1033	778	125.42	0.20	
19X-4, 140–150	331.50	7.56	2.79	34.5	568	14.99	483	37.46	18.05	6.40	942	828	141.29	0.15	0.03
21X-4, 140–150	342.10	7.52	2.91	35.0	570	15.50	485	38.58	17.57	6.66	914	805	131.24	0.26	1.69

Note: Alk = alkalinity.

Table T10. Carbon, nitrogen, sulfur, and hydrogen values and C/N and C/S ratios in sediments, Site 1192.

Core, section	Depth (mbsf)	IC (wt%)	CaCO$_3$ (wt%)	TC (wt%)	TOC (wt%)	Total N (wt%)	Total S (wt%)	Total H (wt%)	C/N ratio	C/S ratio
194-1192A-										
1H-2	2.25	10.94	91.2	—	—	—	—	—	—	—
1H-5	6.75	9.69	80.8	9.67	0.00	0.02	0.08	0.25	0.00	0.00
2H-2	11.75	9.41	78.4	—	—	—	—	—	—	—
3H-2	21.25	10.23	85.2	—	—	—	—	—	—	—
3H-5	25.75	10.20	85.0	10.10	0.10	0.02	0.09	0.23	4.17	3.10
5H-2	31.74	9.97	83.0	—	—	—	—	—	—	—
5H-5	36.24	10.17	84.8	10.30	0.13	0.06	0.06	0.20	2.17	2.17
6H-2	41.25	9.52	79.3	—	—	—	—	—	—	—
6H-5	45.75	9.48	79.0	9.70	0.22	0.08	0.00	0.10	2.75	
7H-2	50.74	8.73	72.7	—	—	—	—	—	—	—
7H-5	55.24	9.67	80.6	9.85	0.18	0.07	0.00	0.21	2.57	
8H-2	60.25	8.89	74.1	—	—	—	—	—	—	—
8H-5	64.75	9.65	80.4	9.84	0.19	0.06	0.18	0.23	3.17	1.06
9H-2	69.75	9.84	82.0	—	—	—	—	—	—	—
9H-5	74.25	9.28	77.3	9.50	0.22	0.07	0.30	0.29	3.14	0.73
10H-2	79.25	9.73	81.1	—	—	—	—	—	—	—
10H-5	83.75	9.56	79.7	9.65	0.09	0.07	0.23	0.26	1.29	0.39
12H-2	89.75	9.68	80.7	—	—	—	—	—	—	—
12H-5	94.25	10.23	85.2	10.50	0.29	0.03	0.12	0.25	11.60	2.42
13H-2	99.25	10.77	89.7	—	—	—	—	—	—	—
13H-5	103.75	10.34	86.2	10.50	0.12	0.02	0.35	0.17	6.00	0.34
14H-2	108.75	10.31	85.9	—	—	—	—	—	—	—
14H-5	113.25	10.78	89.8	10.80	0.02	0.02	0.19	0.17	1.00	0.11
15H-2	118.25	10.14	84.5	—	—	—	—	—	—	—
15H-5	122.75	10.55	87.9	10.70	0.15	0.06	0.00	0.19	2.50	
16H-2	127.75	10.23	85.2	—	—	—	—	—	—	—
16H-5	132.25	10.90	90.8	10.90	0.00	0.06	0.05	0.15	0.00	0.00
17H-2	137.25	10.64	88.6	—	—	—	—	—	—	—
17H-5	141.75	10.99	91.5	11.00	0.00	0.02	0.00	0.12	0.00	
18H-2	146.75	10.64	88.6	—	—	—	—	—	—	—
18H-5	151.25	10.82	90.2	10.90	0.03	0.06	0.17	0.15	0.50	0.18
19H-2	156.25	10.42	86.8	—	—	—	—	—	—	—
19H-3	157.10	10.82	90.1	10.80	0.00	0.02	0.49	0.12	0.00	0.00
19H-5	160.75	11.00	91.6	—	—	—	—	—	—	—
20H-2	165.75	10.28	85.6	10.20	0.00	0.08	0.13	0.22	0.00	0.00
20H-6	171.75	10.31	85.9	—	—	—	—	—	—	—
21H-2	175.25	10.32	85.9	10.50	0.13	0.03	0.00	0.16	4.33	
21H-5	179.75	10.34	86.2	—	—	—	—	—	—	—
22H-2	184.75	9.95	82.9	10.10	0.16	0.06	0.05	0.22	2.67	3.20
22H-5	189.25	10.21	85.0	—	—	—	—	—	—	—
24H-2	195.25	10.01	83.4	10.10	0.12	0.02	0.08	0.14	6.00	1.50
24H-5	199.75	10.75	89.6	—	—	—	—	—	—	—
25H-2	204.75	10.44	87.0	—	—	—	—	—	—	—
25H-5	209.25	10.40	86.6	—	—	—	—	—	—	—
26H-2	214.25	10.91	90.9	11.00	0.05	0.02	0.08	0.14	2.50	0.63
26H-5	218.75	10.65	88.7	—	—	—	—	—	—	—
27H-2	223.75	10.85	90.4	10.90	0.04	0.03	0.00	0.14	1.33	
27H-5	228.25	10.42	86.8	—	—	—	—	—	—	—
29H-2	234.25	10.75	89.5	10.80	0.05	0.03	0.09	0.16	1.67	0.56
29H-5	238.75	10.12	84.3	—	—	—	—	—	—	—
194-1192B-										
10X-2	241.25	10.64	88.6	10.68	0.04	0.02	0.29	0.16	2.00	0.14
10X-5	245.25	10.98	91.4	—	—	—	—	—	—	—
12X-2	260.45	9.44	80.2	9.88	0.44	0.02	0.10	0.22	29.33	2.50
12X-4	262.86	7.88	65.7	—	—	—	—	—	—	—
13X-CC	267.96	10.41	86.7	10.13	0.00	0.01	0.00	0.09	0.00	
14X-CC	277.61	10.18	84.8	—	—	—	—	—	—	—
15X-2	289.46	11.12	92.7	11.14	0.02	0.02	0.07	0.07	1.00	0.29
16X-1	297.55	10.59	88.2	—	—	—	—	—	—	—
17X-5	312.90	10.83	90.2	10.81	0.00	0.01	0.10	0.10	0.00	0.00
19X-2	327.85	8.20	68.3	—	—	—	—	—	—	—
19X-3	329.35	9.00	75.0	9.11	0.11	0.06	0.18	0.30	1.83	0.61
21X-2	338.45	10.27	85.6	—	—	—	—	—	—	—
21X-5	342.95	11.37	94.7	11.30	0.00	0.00	0.00	0.04	—	—

Notes: IC = inorganic carbon, TC = total carbon, TOC = total organic carbon, C/N = carbon/nitrogen, C/S = carbon/sulfur. — = not analyzed. C/S assigned to 194-1192B-12X-2 was determined by averaging values determined using TOC from CNS analysis and Rock-Eval pyrolysis.

Table T11. Results of Rock-Eval analyses on sediments, Site 1192.

Core, section	Depth (mbsf)	T_{max}	S_1	S_2	S_3	HI	OI	TOC (wt%)
194-1192A-								
1H-2	2.25	364	0.44	0.10	0.09	83	75	0.12
1H-5	6.75	379	0.21	0.10	2.33	100	2330	0.10
2H-2	11.75	407	0.13	0.22	1.48	169	1138	0.13
3H-2	21.25	406	0.10	0.18	1.18	200	1311	0.09
3H-5	25.75	401	0.13	0.18	1.53	150	1275	0.12
5H-2	31.74	418	0.23	0.38	1.89	211	1050	0.18
5H-5	36.24	417	0.15	0.32	1.98	168	1042	0.19
6H-2	41.25	398	0.17	0.37	2.08	148	832	0.25
6H-5	45.75	412	0.12	0.47	1.94	180	746	0.26
7H-2	50.74	398	0.16	0.36	2.31	180	1155	0.20
7H-5	55.24	420	0.14	0.46	2.26	242	1189	0.19
8H-2	60.25	399	0.18	0.35	2.19	125	782	0.28
8H-5	64.75	408	0.14	0.24	2.35	126	1236	0.19
9H-2	69.75	403	0.10	0.25	2.08	125	1040	0.20
9H-5	74.25	405	0.09	0.28	2.41	121	1047	0.23
10H-2	79.25	411	0.17	0.29	3.05	161	1694	0.18
10H-5	83.75	395	0.17	0.24	1.44	133	800	0.18
12H-2	89.75	412	0.12	0.37	1.43	160	621	0.23
12H-5	94.25	410	0.16	0.24	1.08	120	540	0.20
13H-2	99.25	410	0.11	0.19	1.01	172	918	0.11
13H-5	103.75	412	0.06	0.27	1.76	122	800	0.22
14H-2	108.75	405	0.16	0.28	1.51	164	888	0.17
14H-5	113.25	408	0.18	0.25	1.14	208	950	0.12
15H-2	118.25	406	0.14	0.33	1.32	206	825	0.16
15H-5	122.75	422	0.11	0.42	1.16	190	527	0.22
16H-2	127.75	414	0.20	0.45	1.23	250	683	0.18
16H-5	132.25	415	0.16	0.25	0.97	208	808	0.12
17H-2	137.25	411	0.06	0.26	1.66	288	1844	0.09
17H-5	141.75	422	0.05	0.33	1.15	366	1277	0.09
18H-2	146.75	410	0.06	0.27	1.18	245	1072	0.11
18H-5	151.25	410	0.05	0.23	0.95	230	950	0.10
19H-2	156.25	409	0.08	0.35	1.20	218	750	0.16
19H-3	157.10	400	0.06	0.22	1.07	84	411	0.26
19H-5	160.75	419	0.03	0.26	0.83	200	638	0.13
20H-2	165.75	412	0.08	0.39	1.34	216	744	0.18
20H-6	171.75	418	0.09	0.35	0.98	205	576	0.17
21H-2	175.25	412	0.07	0.30	0.77	187	481	0.16
21H-5	179.75	417	0.11	0.39	0.84	229	494	0.17
22H-2	184.75	410	0.10	0.33	0.93	194	547	0.17
22H-5	189.25	407	0.09	0.37	0.92	194	484	0.19
24H-2	195.25	409	0.11	0.23	5.30	164	3785	0.14
24H-6	199.75	435	0.09	0.31	3.44	258	2866	0.12
26H-2	214.25	417	0.10	0.23	1.75	230	1750	0.10
26H-5	218.75	418	0.13	0.28	1.70	186	1133	0.15
8H-2	222.15	418	0.04	0.21	0.74	233	822	0.09
27H-2	223.75	418	0.08	0.22	1.17	220	1170	0.10
8H-5	226.65	408	0.08	0.23	0.93	209	845	0.11
27H-5	228.25	421	0.13	0.33	1.96	183	1088	0.18
29H-2	234.25	414	0.12	0.29	1.70	241	1416	0.12
29H-5	238.75	401	0.08	0.21	0.99	161	761	0.13
194-1192B-								
10X-2	241.25	411	0.10	0.21	1.43	150	1021	0.14
10X-5	245.25	412	0.12	0.15	0.43	150	430	0.10
12X-2	260.45	397	0.11	0.09	0.15	150	250	0.06
12X-4	262.86	396	0.13	0.13	1.69	216	2816	0.06
13X-CC	267.96	406	0.09	0.12	1.08	267	1985	0.05
14X-CC	277.61	423	0.13	0.36	0.82	225	512	0.16
15X-2	289.46	412	0.06	0.19	0.55	237	687	0.08
16X-1	297.55	407	0.07	0.11	0.40	220	800	0.05
17X-5	312.90	413	0.05	0.18	1.15	225	1437	0.08
19X-2	327.85	402	0.14	0.29	1.52	103	542	0.28
19X-3	329.35	405	0.09	0.26	1.04	113	452	0.23
21X-2	338.45	410	0.09	0.23	0.59	191	491	0.12
21X-5	342.95	408	0.07	0.23	0.88	308	1116	0.08

Note: T_{max} = temperature of maximum hydrocarbon generation during pyrolysis in °C, S_1 = milligrams of free hydrocarbons per gram of rock, S_2 = milligrams of pyrolyzed hydrocarbons per gram of rock, S_3 = milligrams of carbon dioxide per gram of rock, HI = hydrogen index in milligrams of hydrocarbon per gram of TOC, OI = milligrams of carbon dioxide per gram of TOC, TOC = total organic carbon.